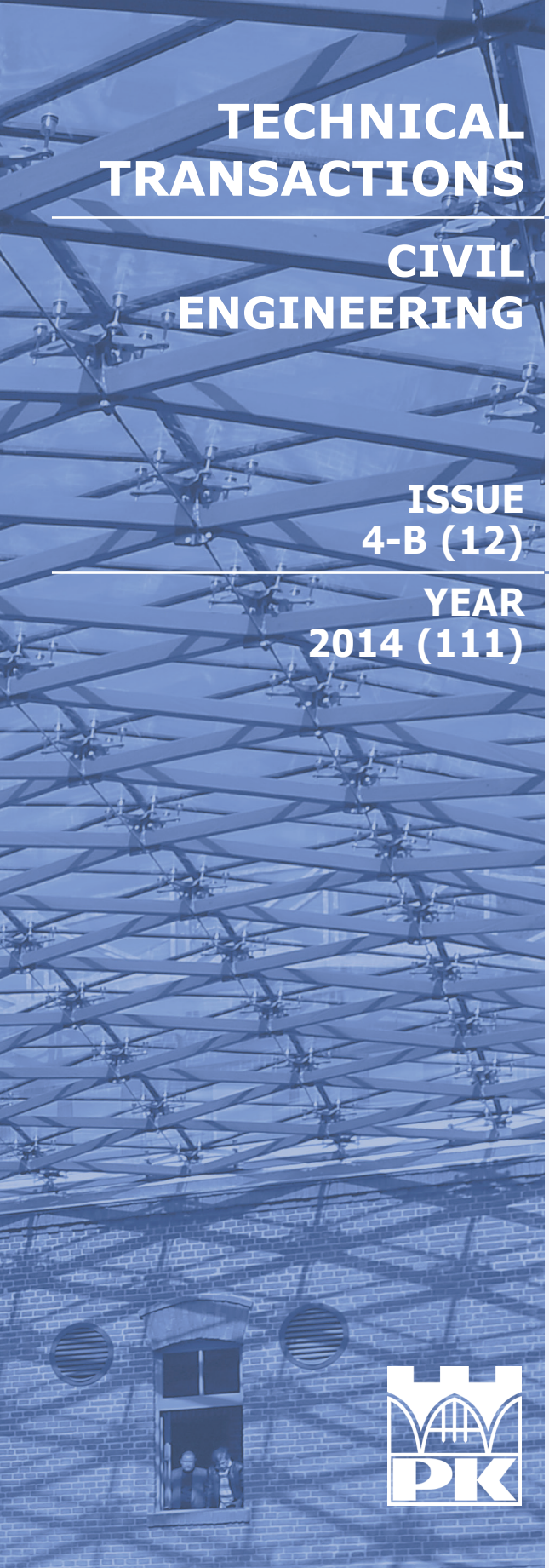

TECHNICAL TRANSACTIONS
CZASOPISMO TECHNICZNE

CIVIL ENGINEERING
BUDOWNICTWO

ISSUE 4-B (12)
ZESZYT 4-B (12)

YEAR 2014 (111)
ROK 2014 (111)

WYDAWNICTWO POLITECHNIKI KRAKOWSKIEJ

TECHNICAL TRANSACTIONS | CZASOPISMO TECHNICZNE

CIVIL ENGINEERING | BUDOWNICTWO

ISSUE 4-B (12) | ZESZYT 4-B (12)
YEAR 2014 (111) | ROK 2014 (111)

Pierwotną wersją każdego Czasopisma Technicznego jest wersja on-line
www.czasopismotechniczne.pl www.technicaltransactions.com

Civil Engineering Series
4-B/2014

Editorial Board

TECHNICAL TRANSACTIONS | CZASOPISMO TECHNICZNE
CIVIL ENGINEERING | BUDOWNICTWO
4-B/2014

BARBARA MARIA DEJA*

RENOVATION OF THE HISTORIC OLSZTYN VILLA CASABLANCA

RENOWACJA ZABYTKOWEJ OLSZTYŃSKIEJ WILLI CASABLANKA

Abstract

The paper outlines the details of the design and difficulties that had to be overcome in the course of the renovation and adaptation of a rich German factory owner's residence from 1912, which in 1988 was entered into the register of historic buildings of the Warmia and Mazury region.

Keywords: *renovation*, *adaptation*, *historic villa*

Streszczenie

W artykule przedstawiono szczegóły projektu i trudności związane z realizacją renowacji i adaptacji willi bogatego niemieckiego fabrykanta z 1912 roku, wpisanej w roku 1988 do rejestru zabytków województwa warmińsko-mazurskiego.

Słowa kluczowe: *renowacja*, *adaptacja*, *zabytkowa willa*

* Ph.D. Eng. Barbara Maria Deja, Department of Building Engineering and Building Physics, Faculty of Technical Sciences, University of Warmia and Mazury in Olsztyn.

1. Introduction

Among the historic monuments of the Old Town in Olsztyn there are three gothic buildings which are by far the oldest and the most important. The co-cathedral of St. Jacob the Apostle dates from the second half of the 14th Century. The castle of the Chapter of Warmia Bishopric was built between 1346 and 1353. The Upper Gate marks the area of the medieval town in the east. On the southern outskirts of the Old Town, stands a remnant of the medieval defensive wall. On the other side, to the north stands the Villa Casablanca at No. 5, Zamkowa Street. The villa was entered into the register of historic buildings of Warmia and Mazury province under the symbol A–1731 on the basis of the Provincial Heritage Monuments Protection Office decision of 14 September 1988.

The historic villa is located in a place of significant historic value within the borders of the castle free usage area, surrounded by a mill ditch at the end of the 19th Century, mentioned for the first time in the incorporation charter of 1353 [1]. This area lies within the borders of the Old Town which was entered into the register of provincial historic buildings (entry A-435) in accordance with the Provincial Heritage Monuments Protection Office decision of 17 September 1957. Again, it was entered into the register once more (entry C-160) as a cultural superimposition of the Old Town according to the dictates of the Provincial Heritage Monuments Protection Office's decision of 2 July 1992.

The villa (situated close to the bridge over the River Łyna, on the west side of an access road to the castle, surrounded by the garden and a large park) is located on the site of the 17th Century burgrave palace rebuilt for the first time in 1758 and subsequently, in the second half of the 19th Century [2].

This 19th Century building, known to us only from old photographs, had two floors – the ground floor and a usable attic, covered with a double-pitched roof [2].

By the end of the first decade of the 20th Century, it was a residence for high ranking German officers from the local garrison such as Major – General Alexander Menze and Major August von Schönebeck. Later on, the building was purchased by German entrepreneur Wilhelm Ernst Harich (owner of a printing house, a book store, a library, a stationery store, and the publisher of 'Allensteiner Zeitung') and was partially dissembled and extended. W.E. Harich lived in the villa from 1913 till 1940 [3]. The next owner (from 1945) was his daughter Else Loeffke, a widow of the chairman of a regional court in Olsztyn.

After the liberation of Olsztyn, the building was the residence for the governor of Olsztyn Province. After 1950, it was passed on to the Polish Army as a garrison club and library. From then on, the villa became known as Casablanca among local residents. After moving the garrison club to Saperska Street in the 1990s, the villa was left empty as a part of Military Property Agency's estate. In 2004, the building was bought by new owners (Olsztyn entrepreneurs) who decided to return it to its past greatness.

2. Description of the manufacturer's villa

The longitudinal axis of Harich's villa was laid in an east-west direction. In front of the northern façade, there is a small square divided by a lane of old lime trees (Zamkowa

Street). From this street ran the old access road to the castle (Fig. 1). The northern side of the building stands on a high escarpment that separates it from the park (Fig. 2).

The east elevation is directed towards the castle located just across the River Łyna, while on the west, it faces the garrison church (built in 1914) that is situated behind the park (Fig. 3).

Fig. 1, 2. The front and back elevations of Villa Casablanca, before the renovation in 2006

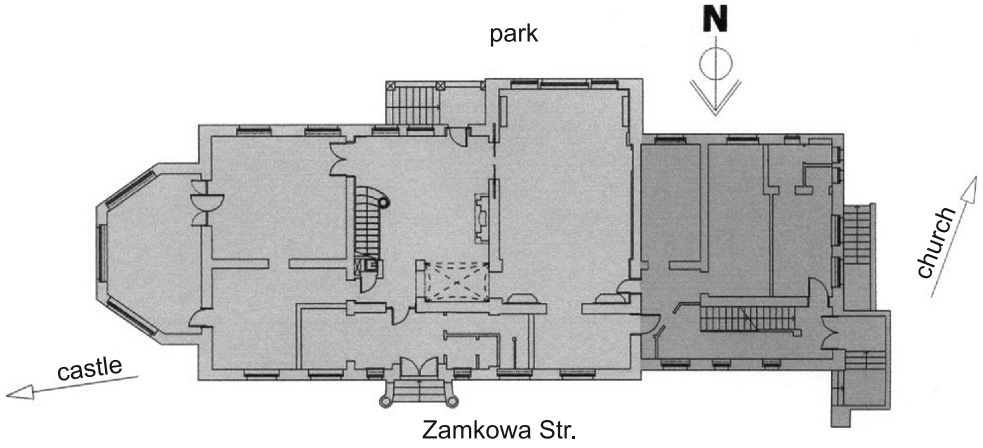

Fig. 3. Schematic view of the first floor and the building orientation

The present plan of the building was created by joining two parts – the 19th Century building plan based on a rectangle and a slightly lower wing based on a square adjoining it from the west of the building (Fig. 3).

As a result of the enlargement, in 1912 the residence became a three-storey building, including cellars beneath the entire building and a usable attic. From the east, the building was enriched with an avant-corps and a terrace, and from the south, with a loggia and an extended terrace [4].

The brick walls were put on an 80 cm high foundation made of field stones. Above the basement, under the terrace and loggias, a brick ceiling on steel beams was applied

(Fig. 4). The beam ceilings of the higher floors were made completely out of wood with a plastered soffit. The ceiling above the mansard loft in the higher wing of the building is made of wooden beams based on the external stud walls and on longitudinal steel binding joists, and additionally, on a central steel column (Fig. 5). An entresol in a fireplace ballroom and an entry hall are covered with a groined vault (Fig. 6), whereas the dining room on the representative ground floor is covered with a wooden, coffered ceiling (Fig. 7).

The entire building is covered with a mansard roof separately built on each part of the building – a hipped roof covers its central portion and a three-sloped roof covers the lower extension (Fig. 2). The wooden purlin roof braced by the stay-brace system is supported by two rows of wooden posts (Fig. 8).

Fig. 4, 5. The brick ceiling above the basement and the timber ceiling (above the attic) supported by steel binding joists and a steel column, 2011

The single and double-span rafters are supported by the purlins and the cap beam of a mansard roof. The roof is covered with plain ceramic tiles on wooden boarding. The roof has some dormer windows (Fig 1, 2).

The characteristic architecture of the beginning of the 20th Century, i.e. eclectic references to the past epoch styles are still seen in the interior arrangement [5]. The functions of the buildings, namely representative, residential and maintenance functions are clearly separated by the diverse interior arrangement. The residential and maintenance parts are located upstairs in the central part of the building and in the lower wing.

The presentable function of a building is the most explicit. On the transversal axis of the ground floor, there is a two-storey high, stately living room (Fig. 9). In the living room, there is a stone polychrome fireplace and lushly ornamented stairs (leading into the gallery – an orchestra balcony and a few steps further on, it opens to the living room entresol). There are doors to the terrace, garden and the rest of the representative rooms which are planned in enfilade.

The longitudinal walls of the fireplace living room are wood paneled, and the door lintels are ornamented with reliefs. The transversal walls are covered with a fabric and a stucco frieze with plant motifs on the upper portion. In the southern two-storey high wall there are wooden, stained glass windows equipped with an opening system and external roller blinds.


Fig. 6, 7. The groined vault covering the entresol in the fireplace ballroom and a coffered ceiling above the dining room on the ground floor, 2011

The living room has wooden radiator covers with a decorative grate and the glazed sliding door leading to the dining room, all of which are preserved. The walls of the dining room were laid with dark, carved oaken paneling. Mensal furniture composed into it (Fig. 7).


Fig. 8, 9. The timber roof structure and the view from the entresol over the two-storey fireplace ballroom with stained glass windows, 2011

On the ground floor, there is one more presentable interior (No. 4 in Fig. 3), on its flat ceiling there is a stuccowork ornament presenting acanthus leaves. The room opens itself to the view of the castle and the River Łyna, that can be admired from the three-sided avant--corps (Fig. 10).

On the second floor of the main part of the building, there are two rooms on the eastern side of the living room (both equipped with a door leading out to the terrace) and residential rooms on the western side accessible from the corridor leading to the staircase located in the lower wing of the building. In the attic, there is a spacious hall with a steel column supporting the ceiling and cubbyholes in the roof's slants.

Access between floors in the villa is provided by the staircase situated in the lower part of the building, one way brick stairs in the cellar and dog-legged ceramic stairs on steel beams on the rest of the floors.


Fig. 10, 11. The eastern Casablanca elevation before renovation (2006) and the main entrance after the renovation (2014)

The appearance of elevations was diversified much like the interior of the building [5]. The façade, rusticated in its corners, is the most distinguished feature. The main entrance, made as a portal, is closed at the top with a semi-circular arch (Fig. 11). The windows of the front façade are rectangular with a semi-circular arcade on the ground floor (Fig. 1). The window above the entrance door is especially richly decorated and has a small balcony. Stone stairs equipped with banisters finished with stone spheres lead up to the entrance to the building (Fig 11).

On the other elevations, one can find early modernistic solutions (commonly used no sooner than in the 1920s), such as: diversified sizes, proportions and window division and their unsymmetrical arrangement (Fig. 2), three-sided avant-corps with a terrace (Fig. 10), and diversified roof shapes [6].

3. The condition of the building and the restoration recommendations

The most extensive damage noticed by the present owners when taking the building over were caused by leaking insulation layers, the failure of the rain water drainage system and losses of roof sheeting (Fig. 12, 13).

The result of flooding was partial fungal infection of the roof structure (which were also infested with wood pests) and floor damage.

The dampness of the walls, escalated by recurrent freezing and thawing, caused numerous seam failures as well as the powdering and flaking of plaster. Areas of the walls striped of plaster were infested with micro-organisms. The destruction of the walls increased because of the cement plaster that was applied in the mid-twenties of the 20th Century being too permeable to water vapour [5].

Some parts of the plinth walls were also damaged due to rain water gathering caused by failure of the original sewer system. In the second half of the 20th Century, the plinth walls were fixed with terrazzo but it also did not help and finally went off especially around the main entrance and around the drain pipes (Fig. 14–16).


Fig. 12, 13. The condition of roofing and guttering before renovation, 2008

The cornice under the roof and the stuccowork details around the windows (covered with sealing cement, and few layers of emulsion paint) were constantly soaked with water which resulted in many seam failures and chipping. The terraces and the walls beneath lacked tight horizontal waterproofing. The most exposed elements of the elevations and the external stairs were also severely damaged by rain water (Fig. 16).



Fig. 14–16. The damage to walls caused by soaking, 2008

The windows of the attic and the maintenance areas of the building were almost completely destroyed, while the almost one hundred-year-old windows of both the ground (Fig. 17) and the first floor were accepted for restoration. Above the windows, there are the roller blind boxes, unfortunately, no remaining roller blinds were found.

The interior is quite well preserved with historic ceilings, stairs, panelling and fireplaces (Fig. 18). However, the stuccowork decoration of the representative chambers, the art nouveau window bars in the roof windows and the historic carved doors all needed thorough renovation.

Building restorers from Olsztyn carried out a comprehensive examination of Villa Casablanca in order to create the general renovation concept, with guidelines for the functionality and usability of the building's layout as well as a program of the methods and technology for the implementation of the conservatory [7].


Fig. 17, 18. The splendid window in the dining room (2006) and the historic fireplace during the restoration process, 2011

The most significant conclusion arising from the analyses of historic, artistic and utilitarian value of the building and its contemporary condition was the decision to start the renovation according to the Venice Charter requirements [8]. It should be carried out with all due respect to the original substance of the structure and building materials with the possibility of a modern conservatory and construction techniques where traditional techniques prove inadequate.

It was established (according to Article 5 of the Venice Charter) that implementation of a new utilitarian function in the building is useful and desirable. It would not only help to preserve the building, but would also bring considerable social benefits (a hotel with a restaurant located in the city centre). The range of adaptation cannot be unlimited because it cannot deprive the villa of its characteristic interior decor, its functionality and usability of the building's layout and its original elements [8].

A technological-executive program was prepared including detailed technological--executive solutions and works schedule related to conservatory procedures. After the approval of this program by the conservatory administration, it became the legal and methodological basis for the renovation of Villa Casablanca [9].

Solving the rain water drainage issue, the structural repair of the roof, the replacement of the roofing (new timber and tiles), the protection of terraces and balconies against damp, replacing old plaster and the terrazzo layer and rebuilding the main entrance stairs were considered the main tasks to fulfil.

At the same time, the restorers opted for removing some of the internal walls of the building (but not original walls that created an additional toilet in the main hall, and secondary division of the cellar) and the opening up of previously filled-in doors and windows. They also decided to restore all the original elements and colours of the villa's décor [5]. An additional task was to find a worthy place for the relocation of mazewas from the Jewish Cemetery that were used for strengthening the slope on the park side after the war [6].

4. The design of the villa adaptation into a conference centre/hotel complex

The architect behind the design of the renovation and adaptation of the historic Casablanca villa into a restaurant, club and conference centre all in one with guest rooms, is the Olsztyn architect, Anna Mikulska-Bąk [10].

According to the assumed concepts, the building has a cubature of 6154.0 m^3 and utility floor space of 1191.3 m^2. It consists of one usable cellar level and four above-ground storeys including three usable floors: the ground floor; the first floor; the attic. Additionally, there is a fourth floor of technical rooms located in the attic (Fig. 19).

Fig. 19. Longitudinal section of the Villa Casablanca, 2010. The red line indicates the cellar floor level before the deepening of the basement

In the basement level there is a restaurant of 159.40 m^2, a kitchen with technical and storage facilities and toilets for guests and staff. Under the existing terrace, a new room was designed which is equipped with the biggest air ventilation unit (the air intake and outlet

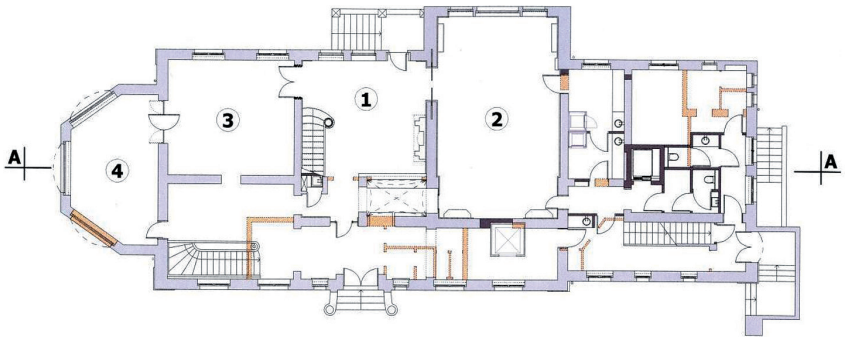

Fig. 20. A ground floor plan: 1 – fireplace ballroom; 2, 4 – conference halls; 3 – secretary office. Existing walls and ceilings – grey; walls devoted for demolition – orange; new walls and ceilings – black

for the gastronomy facilities are located in the retaining wall separating the terrace from the escarpment descending to the park).

The ground floor consists of: 48.40 m^2 fireplace ballroom; conference halls of 39.30 m^2 and 66.30 m^2; an office of 30.50 m^2 (rooms numbered as 1, 2, 3, 4, in the Fig. 20); sanitary and catering facilities for serving the conference halls.

The first floor is dedicated to two large conference halls of 65.90 m^2 and 40.90 m^2 each, a suite of 40.60 m^2, sanitary facilities, a terrace and a loggia.

On the first attic floor, under the mansard roof, the designer projected three luxury suites and a maintenance room with a total floor space of 182.70 m^2, while on the second floor of the attic, there is a boiler room, a ventilation room and a server room.

5. Range of restoration and modernisation works

The renovation of the Villa Casablanca combined with its functional modifications required changes to the original structure, which determined the necessity of applying an appropriate methodology to the proceedings [11].

The decision of locating a restaurant in the cellar required the removal of some of the walls and the lowering of the floor level, hence lowering of the foundations. In the foundation design (proceeded according to Eurocode 7 [12]) there were many elements that had to be considered, and namely the relocation of bearing walls and bigger load of the building as a result of the functional changes and the allocation of the ventilation channels under the floor of the cellar (Fig. 21).

Fig. 21, 22. The works of deepening the cellar, 2011

In order to make the usable height of the underground rooms greater than 1.0 m, the cellar walls were partially undercut and founded on the monolithic walls and the strip foundation (Fig. 22). Work was conducted with a high degree of diligence in order to avoid damaging the ceramic, segmental ceilings above the cellar.

The sectional strengthening of the foundation was made alternately from both sides of the walls. The excavated wall segments were cleaned of debris and the brims were hammered to the required level of the designed floor and finally, after setting up reinforcement bars,

they were filled with concrete of C16/20 class. The reinforcement of the foundation was conducted successively after reaching the required strength in the previously repaired foundation sections.

The foundations were covered with a damp proof course. The foundation walls and cellar walls were isolated with waterproof plaster and a cover against mechanical damage.

In the cellar and on the ground floor, the design assumed the demolition of parts of the load bearing walls and the replacement of them with a column-rafter system. The pillars were shaped in the grooves previously made in the walls, and they were designed as reinforced concrete columns (in accordance with Eurocode 2 [13], these were made with C 16/20 class concrete, and steel bars 34 GS), adjusting the dimensions of their cross-sections to the walls thickness. Steel double binding joists (designed acc. to Eurocode 3 [14]) were made of a rolled steel profile of varied dimensions depending on the length between the bearings, and on the designed doorways and window openings as well as on the load of the structure. The walls were demolished below the binding joist not earlier than after finishing placing all of the joists within one tract on all the floors.

One of the main renovation principles was to keep the historic ceilings: ceramic one supported by steel beams above the cellars and a wooden ceiling above the higher floors, including a coffered ceiling above one of the rooms on the ground floor.

Simultaneously, factors such as the increased load of the ceilings, ensuring proper fire protection and sound insulation, changes of the support conditions and breaking through ceilings in order to install lifts and a new chimney for a gas pizza oven should also be considered.

In the main part of the building, where the historic value of the ceiling is considerable and the strength of the wooden beams is insufficient (calculations made acc. to Eurocode 5 [15]), the cross-sections of the beams were reinforced by fixing additional timber elements on both sides of the beams (Fig. 23). The gaps between the beams were filled with mineral wool – additionally, fiberboard was used as sound insulation. Fire protection was guaranteed thanks to the paneling of the ceilings with fireproof materials (this protection was applied only from the upper side due to the need to preserve the original stuccowork of the ceilings).

In the lower part of the building, because of the installation of lifts and the demolition of a part of the bearing walls as well as large load changes, new R-C I-bars ceilings were designed (Fig. 24). These ceiling slabs are made of C16/20 class concrete reinforced with 34 GS steel, resting on the steel I-bars which were put in previously prepared chases in the old masonry bearing walls or new steel binding joists replacing some of the areas where the walls were demolished.

In the building, two service lifts have been installed (providing transit between the cellar and ground floor) and two passenger lifts. The panoramic lift that is situated in the main hall (Fig. 20) includes self-supporting, steel shaft construction. A foundation base plate was laid below the shaft.

The second passenger lift, situated in the lower wing of the building, was equipped with a monolith shaft (20–24 cm thick shaft walls made of C16/20 class concrete reinforced with mesh reinforcement of 34 GS steel) that goes through all the new monolith ceilings (Fig. 19, 20).


Fig. 23, 24. The timber ceiling beams strengthened by additional wooden elements from both sides, and a new R-C ceiling based on steel beams, 2011

The original, presentable, wooden staircase from the conference hall in the ground floor was restored (Fig. 25), as well as the ceramic stairs on steel beams in the maintenance area of the building. On the ground floor, to the left of the main entrance, a new staircase leading to the restaurant was made (Fig. 20).

The stained glass window in the ballroom (Fig. 26), as with most of the windows and interior doors (including a two-winged sliding door, hidden in the wall), was renovated. In the publication [16], there is a detailed description of the complex conservatory concerning the historic windows of Villa Casablanca.


Fig. 25, 26. The historic staircase and the stained glass window in the ballroom after the renovation, 2013

The ceiling above the ground floor, decorated with coves and friezes, was meticulously restored, as was the wall decorated with ornamental paintings. The wooden radiator covers were also reconstructed on the basis of preserved examples. In the ballroom (now a conference room), renovation of the polychrome fireplace and fragments of the decorative wall fabric covering was carried out.

The roof structure required only minor repairs, but the roofing was completely replaced (the colour of the new plain tiles perfectly matched the original).

The old, damaged plaster of the diverse structure covering the external walls, which was successively repaired by applying more new layers in the past, was removed, and after scrupulous stratigraphic studies, the original colour of the elevation was restored.

Fig. 27, 28. The front and southern Casablanca elevations after the renovation, 2014

The surroundings of the villa were cleaned up. The historic Jewish mazewas from the park side slope were moved to the funerary house at Zyndram of Myszkowice Street, and the slope was strengthened and planted with new greenery (Fig. 27). In front of the building, the street was cobblestoned, and a car park and a new descent to the square were built (Fig. 28).

The building and its surroundings (where the traffic was forbidden during the renovation) was ready for use in August 2013.

6. Difficulties related to the renovation execution

The renovation and adaptation of a historic buildings to a new utilitarian function is an interdisciplinary undertaking requiring the cooperation of specialists from many different branches of industry and science. It is also complicated due to the bothersome conservatory orders that were sometimes difficult to harmonize [7, 17] and the new design postulates that require a high – standard of work quality [11].

The main difficulties of the restoration of the Villa Casablanca in Olsztyn arose from the fact that the functions of this historic building completely changed, with numerous elements under conservatory protection and the necessity of ensuring the safety, durability, serviceability and reliability according to present norms and legal requirements [11]. Also significant was the fact that after many years of lack of maintenance and operation, the technical condition of the building was rather bad.

The new functional-utilitarian program required extra floor space for a restaurant, storerooms, ventilation and server control rooms. Locating them in the basement required the cellar to be deepened by the means of lowering the foundations of the building and the creating of an additional cellar under the avant – corps terrace.

Laying new foundations in an historic building is extremely difficult due to the danger of damaging the walls and the historic ceilings that in the course of exploitation, underwent

the process of ageing. Nevertheless, this approach is very often used in practice [18] because it allows some extra floor space to be obtained in a deepened cellar and gives an opportunity to create new foundations calculated with consideration to the new steady and changing loads of the building including climatic loads, according to the Eurocodes in force.

Harich's villa was a residential building with rooms of small floor spaces (apart from two representative lounges). The decision of adopting the building to gastronomic/conference functions (large rooms) required some of the load bearing walls to be demolished which could endanger the substance of the original structure.

An introduction of elevator shafts, the pizza oven chimney and mechanical ventilation ducts required making openings in the ceilings and creating fragments of new ceilings that were partially supported on existing load bearing walls. Procedures like these, especially in an old building, are not always problem – free. Sometimes they go wrong, the example of another Olsztyn historic building, the Dyplomat Hotel, suffered interference in the wall structure causing broad, local damage that brought repairs to a halt. The work was restarted after the immediate reinforcement of the walls [19].

7. Conclusions

The successful adaptation of the historic Villa Casablanca into a hotel with a restaurant and conference halls proved to be an opportunity to preserve the building and bring it back to its former splendor. As a result of this costly undertaking (with the enormous financial means of the investor as well as EU subsidies from the Regional Operational Program for Warmia and Mazury), the initial goals concerning the expected economic benefits, protection of the natural environment, social aspects, and cultural heritage were achieved [20].

First and foremost, the villa's adaptation saved a building of historic value, precious for the local community and for local art historians. The realization of the conservatory building works in this building was also a valuable experience for local companies specializing in such enterprises.

Due to the successful renovation, the whole surrounding area of the villa, previously bleak and neglected, was reshaped as a neat, pleasant spot.

Assigning the villa as a public utility building, not only made the building available for local residents and tourists, but also created additional employment. The fact that the building makes a profit for private investors is also important. The renovated Villa Casablanca (and its surroundings) is at present, one of the favourite meeting places for the inhabitants of Olsztyn.

References

[1] Rzempołuch A., *Architektura i urbanistyka Olsztyna 1353–1953*, Wydawnictwo UM, Olsztyn 2004, 109-112.

[2] Bętkowski R., *Olsztyn, jakiego nie znacie, 650 lat Olsztyna*, Wydawnictwo Imago Mundi, Olsztyn 2010, 188-189.

[3] Rzempołuch A., *Casablanca nad Łyną: O zabytkach inaczej*, Spotkania z zabytkami, nr 5, 2007, 21-23.

[4] Achremczyk S., Ogrodziński W. i inni, *Olsztyn 1353–2003*, Ośrodek Badań Naukowych i Towarzystwo Naukowe w Olsztynie, 2003, 272-273.
[5] Chodkowska W., *Dokumentacja historyczno-konserwatorska zabytkowej willi położonej w Olsztynie przy ul. Zamkowej 5*, 2004, 1-17.
[6] Dzieciątkowska J., *Proponowany program prac konserwatorskich elewacji willi „Casablanca" przy ul. Zamkowej w Olsztynie*, 2007, 1-13.
[7] Smólski J., Stępień P., *Kryteria konserwatorskie doboru rozwiązań inżynierskich w zabytkach architektury – w świetle doktryny i praktyki konserwacji*, Materiały IV Konferencji Naukowo-Technicznej Rew-Inż., 1998, Kraków 1998, 63-72.
[8] Karta Wenecka 1964, Narodowy Instytut Dziedzictwa, www.nid.pl, dostęp 15.07.2014 r.
[9] Ustawa z dnia 23.07. 2003 r. o ochronie zabytków i opiece nad zabytkami (Dz. U. z 2003 r. Nr 162, poz. 1568 z późn. zm.).
[10] Mikulska-Bąk A., *Przebudowa i remont zabytkowego budynku w Olsztynie przy ul. Zamkowej 5*, Projekt budowlany – architektura, 2012.
[11] Runkiewicz L., *Metodologia postępowania przy naprawach i wzmacnianiu w ramach odnowy obiektów zabytkowych*, Materiały VII Konferencji Naukowo-Technicznej Rew-Inż., 2006, Kraków 2006, 199-208.
[12] PN-EN 1997-1:2008. Eurokod 7. Projektowanie geotechniczne. Część 1: Zasady ogólne.
[13] PN-EN 1992-1-1:2008. Eurokod 2. Projektowanie konstrukcji z betonu. Część 1-1: Reguły ogólne i reguły dla budynków.
[14] PN-EN 1993-1-1:2005. Eurokod 3. Projektowanie konstrukcji stalowych. Część 1-1: Reguły ogólne i reguły dla budynków.
[15] PN-EN 1995-1-1: 2010. Eurokod 5. Projektowanie konstrukcji drewnianych. Część 1-1: Postanowienia ogólne. Reguły ogólne i reguły dotyczące budynków.
[16] Kowalczyk M., *Problematyka konserwacji zabytkowej stolarki okiennej na przykładzie budynku przy ul. Zamkowej 5 w Olsztynie*, Renowacje i zabytki, nr 4 (48), 2013, 80-85.
[17] Rozporządzenie Ministra Infrastruktury z dn. 12.04.2002 r. w sprawie warunków technicznych, jakim powinny odpowiadać budynki i ich usytuowanie. Dz. U. nr 75 z 2002 r. poz. 690, z późniejszymi zmianami.
[18] Janowski Z., Janowski M., *Problemy projektowe związane z adaptacją budynków zabytkowych na cele użyteczności publicznej*, Czasopismo Techniczne 2-B/2009, 139-150.
[19] Deja B.M., *Remont i adaptacja zabytkowej olsztyńskiej kamienicy na budynek hotelowy*, Czasopismo Techniczne 3-B/2011, 19-33.
[20] Radziszewska-Zielina E., Śladowski G., *Evaluation of historic building conversion options in the context of sustainable development*, Technical Transactions 1-B/2014, 153-164.

TECHNICAL TRANSACTIONS | **CZASOPISMO TECHNICZNE**
CIVIL ENGINEERING | BUDOWNICTWO
4-B/2014

KAZIMIERZ FURTAK*

FATIGUE BEARING STRENGTH OF CONNECTION WITH FLEXIBLE CONNECTORS

NOŚNOŚĆ ZMĘCZENIOWA ZESPOLENIA Z ŁĄCZNIKAMI WIOTKIMI

A b s t r a c t

The paper presents an analysis of the effect of load variations on the bearing strength of connection in steel–concrete elements with flexible connectors in the form of bolts. Data relating to the residual stresses from concrete slab shrinkage have been included in the analysis. The results of the author's experiments on the effect of variable loads on the bearing strength of the connection have been discussed following the author's experimental studies. Following the analysis of the results, it can be stated that the bearing strength of a connection with flexible connectors is significantly affected by the rigidity of the steel girder and slab (coefficient δ) together with the parameters of load cycles (κ, R) and the value of concrete shrinkage strain.

Keywords: *fatigue bearing strength*, *flexible connectors*, *variable loads*, *load cycles*, *shrinkage strain*

S t r e s z c z e n i e

W artykule poddano analizie wpływ zmienności obciążenia na nośność zespolenia w elementach typu stal–beton z łącznikami wiotkimi w formie sworzni. W analizie uwzględniono naprężenia własne od skurczu betonu płyty. Wpływ obciążeń zmiennych na nośność zespolenia uwzględniono na podstawie wyników własnych badań doświadczalnych. Na podstawie wyników przeprowadzonych analiz można stwierdzić, że istotny wpływ na nośność zespolenia z łącznikami wiotkimi ma stosunek sztywności dźwigara stalowego i płyty (współczynnik δ) oraz parametry cyklu obciążenia (κ, R), a także wartość odkształceń skurczowych betonu.

Słowa kluczowe: *nośność zmęczeniowa*, *łączniki wiotkie*, *obciążenia zmienne*, *liczba cykli*, *odkształcenia skurczowe*

* Prof. Ph.D. Eng. Kazimierz Furtak, Institute of Building Materials and Structures, Faculty of Civil Engineering, Cracow University of Technology.

1. Introduction

In calculating the connection bearing strength, the disintegrating forces from external loads operating in the reinforced concrete slab–steel girder contact plane are usually taken into account. These forces are compared with the bearing strength of the connection, identified with the bearing strength of the connectors. In such calculations, the forces operating in the connection plane are assumed to be constant and equal to the maximum ones. In actual reality, forces occur in the connection plane from residual stresses originating from concrete shrinkage and from the temperature difference between the concrete slab and the steel girder as well as from cement hydration heat [2, 3, 6]. Moreover, external loads can be time variable, which can lead to fatigue.

Residual stresses from concrete hydration occur only at the initial phase of concrete curing when its modulus of elasticity is still insignificant, thus, they do not have any major practical effect on fatigue strength. This is why they are usually disregarded in calculations. The stresses originating from the temperature difference between the concrete slab and the steel girder have also been neglected because in instances of seasonal temperature change, this difference arises very slowly in comparison to the usual load change rate. Besides, in the case of twenty-four hour changes, the effect can be either favourable or unfavourable.

The paper presents an analysis of the effect of load variations on the bearing strength of the connection in steel–concrete elements with flexible connectors in the form of bolts Residual stresses from concrete slab shrinkage are included in the analysis. The results of the author's experiments on the effect of variable loads on bearing strength of the connection are discussed following the author's experimental studies.

2. Effect of variable loads on connection bearing strength

The effect of variable loads on the bearing strength of the connection with flexible connectors has been determined on the basis of the results of the author's experiments carried out within a broader project on steel–concrete composite elements. The connectors used were 75 mm in length, d = 10 mm and 16 mm in diameter. Apart from the connectors' diameter, the other variables used in the tests included [3]: concrete compressive strength $\overline{f}_c$ and shear strength $\overline{f}_{ct}$ (concrete I: $\overline{f}_c = 34.80$ MPa, s_c = 1.71 MPa, $\overline{f}_{ct} = 2.36$ MPa, s_t = 0.12 MPa, concrete II: $\overline{f}_c = 45.96$ MPa, s_c = 2.16 MPa, $\overline{f}_{ct} = 3.08$ MPa, s_t = 0.15 MPa, concrete III: $\overline{f}_c = 61.10$ MPa, s_c = 2.63 MPa, $\overline{f}_{ct} = 4.10$ MPa, s_t = 0,19 MPa), maximum load $P_{\max}$ to ultimate strength P_n ($\kappa = P_{\max}/P_n$; κ = 0.60, 0.70, 0.80) ratio, and stress ratio $R = P_{\min}/P_{\max}$; R = 0.10, 0.20, 0.30), where $P_{\min}$ is the cycle maximum load. The measured value was the limit number of load cycles N resulting in fatigue failure. The tests were carried out on 72 elements.

On the basis of experimental results, the relation between the connection ultimate bearing strength R_{m} and fatigue strength R_{mN} can be adopted as:

$$R_{mN} = \kappa_s R_m \tag{1}$$

where κ_s is a coefficient dependent on the number and parameters of load cycles.

The value of coefficient κ_s can be calculated from the formula:

$$\kappa_s = 1.05 - 0.095(1 - R)\log N \tag{2}$$

where N is the number of load cycles leading to a loss of bearing strength due to changing loads.

Transformation of formula (2) leads to:

$$\log N = (1.05 - \kappa_s) / [0.095(1 - R)] \tag{3}$$

With formula (3) it is possible to compare the results of the author's experiments with the proposal of taking into account the effect of load variations in determining the bearing strength of a connection with flexible connectors. The following has been obtained [3]:

– for $\kappa = 0.60$ and $R = 0.10$; $N_t = 183.30 \cdot 10^3$ at $N_e = 191.57 \cdot 10^3$ (concrete II),
– for $\kappa = 0.70$ and $R = 0.20$; $N_t = 40.30 \cdot 10^3$ at $N_e = 47.69 \cdot 10^3$ and $N_e = 42.57 \cdot 10^3$ (concrete I), $N_e = 47.69 \cdot 10^3$ (concrete II) and $N_e = 51.37 \cdot 10^3$ (concrete III),
– for $\kappa = 0.80$ and $R = 0.30$; $N_t = 5.75 \cdot 10^3$ at $N_e = 5.99 \cdot 10^3$ (concrete II),

where N_t is a theoretical number of load cycles calculated from (3), while N_e is the limit number of cycles obtained in the experiment. The test results confirm the correctness of formula (2).

The results of experiments carried out by the author are convergent with the results obtained by other authors, including those in Fig. 1 [4] and Fig. 2. In these Figures, the difference of maximum and minimum shear stresses ($\Delta\tau = \tau_{max} - \tau_{min}$) depends on the number of load cycles N. A similar approach was adopted in EC4 [1] and publications [8–10].

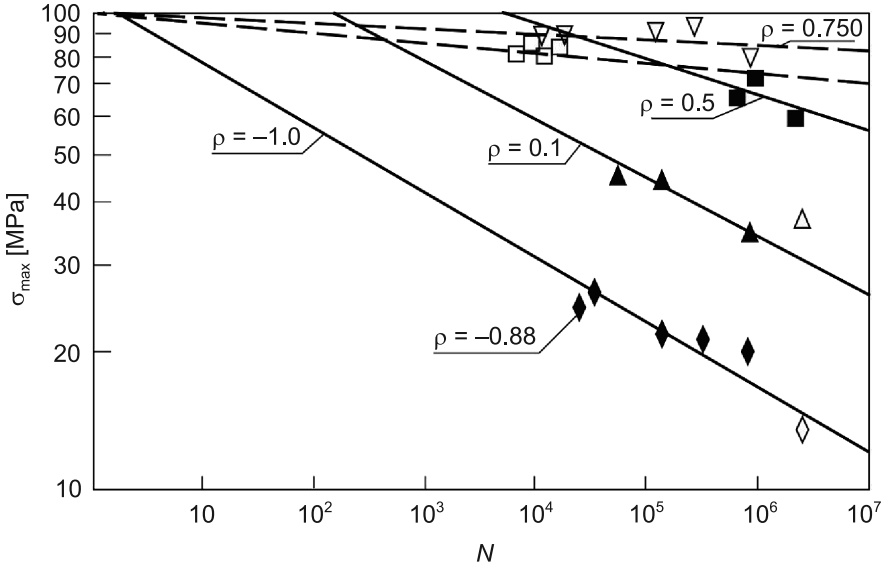

Fig. 1. Results of fatigue tests on flexible connectors [4]

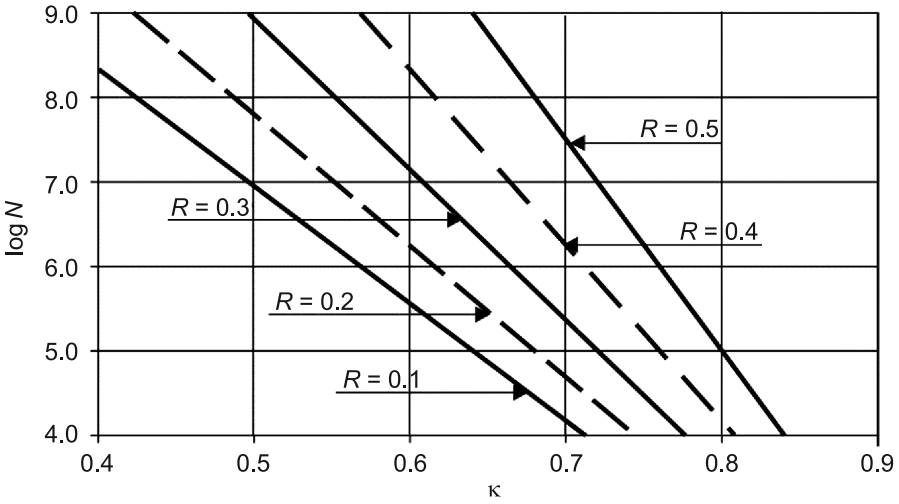

Fig. 2. Effect of parameters of load cycles (κ, *R*) on their limit number *N* (log*N*)

In the author's proposal formulae (2) and (3), fatigue bearing strength of the connection was made dependent on two parameters: the number of load cycles *N*; stress ratio *R*. The same parameters were decisive with regard to the difference between the maximum and minimum stresses in [4] and in Fig. 1. W EC4 [1] and in [8], inter alia, the difference in shear stress $\Delta\tau$ was made dependent only on the number of load cycles *N*.

Fatigue bearing strength dependence on a single parameter is profitable in structural design, which was demonstrated in EC4 [1]. In the analysis of the experimental results and theoretical solutions, it is more advantageous to introduce an additional parameter. This is why this approach was adopted in the present paper, which is justified by the test results quoted in [2, 4, 8–10].

The relationship between parameters κ and *R* and ΔP ($\Delta\tau$) is given by the formula:

$$\Delta P = P_{\max} - P_{\min} = P_{\max}(1-R) = \kappa(1-R)R_m \tag{4}$$

3. Effect of concrete shrinkage on stress state in connection plane

Following [2], maximum shear stresses from concrete shrinkage in the connection plane can be calculated from the formula:

$$\tau_{\max,s} = \frac{0.85\varepsilon_s E_c}{m(\delta+1)(1+\alpha\rho)} \operatorname{tg}h(ms_r) \tag{5}$$

where:

$\varepsilon_s(t)$ – free shrinkage strain,
$E_c(t)$ – concrete modulus of elasticity,
s_r – hypothetical crack spacing (calculated on the assumption that there is no external load acting on the composite element):

$$s_r = \frac{1}{m}\operatorname{arccos} h\frac{\varepsilon_{cs}(t)}{\varepsilon_{cs}(t)-\varepsilon_{ct,\lim}} \tag{6}$$

m – coefficient including slab reinforcement, approximately:

$$m = \sqrt{\frac{3.4\gamma_z}{A_c}} \tag{7}$$

γ_z – coefficient including reinforced concrete slab reinforcement, approximately:

$$\gamma_z = \frac{1+0.75\alpha\rho}{1+\alpha\rho} \tag{8}$$

α – modulus of elasticity of reinforcement E_a to modulus of elasticity of slab concrete ratio E_c ($\alpha = E_a/E_c$),

ρ – reinforced concrete slab reinforcement ratio,

A_c – reinforced concrete slab cross-section,

x – distance of the cross-section in question from the end of beam or cross-section with a crack

$$\varepsilon_{cs}(t) = \frac{\delta_c}{\delta_a+\delta_c}\varepsilon_s(t) \tag{9}$$

$$\delta = \frac{\delta a}{\delta c} \tag{10}$$

δ_a – generalised modulus of rigidity of steel girder

$$\delta_a = \frac{1}{E_a A_a} + \frac{z^2}{E_a I_a} \tag{11}$$

z – distance of centres of gravity of steel girder and reinforced concrete slab,

E_a – modulus of elasticity of steel,

A_a – cross-section of steel girder,

I_a – moment of inertia of steel girder relative to its axis of inertia,

$$\delta_c = \frac{1}{E_c A_c} \tag{12}$$

$\varepsilon_{ct,\lim}$ – limit concrete extension that can be calculated from the formula

$$E_{ct,\lim} = \frac{f_{ctm}}{E_c}\eta_\phi \tag{13}$$

where:

$$\eta_\phi = 1 + \frac{0.08\rho_r}{\phi^{1.5}} \tag{14}$$

f_{ctm} – mean concrete tensile strength [MPa],

E_{ct} – concrete modulus of tensile elasticity [MPa] adopted as equal to concrete modulus of compressive elasticity E_c,

ρ_r – reinforcement ratio [–] referring to effective area of cross-section of concrete in tension,

ϕ – diameter of reinforcement rods [m]; only in formula (14).

When $\varepsilon_{cs}(t) \leq \varepsilon_{ct,\lim}$ distance s_r should be adopted as equal to the distances between the cracks from external loads; when these do not occur calculation-wise, s_r is adopted as equal to the element length.

4. Analysis of connection bearing strength

The results of analysis as to the limit number of load cycles N ($\log N$) have been shown in Figures 1 and 2. The independent variables adopted were the operating maximum disintegrating force P_{max} to connection bearing strength R_m ($\kappa = P_{max}/R_m$) ratio and the stress ratio R ($R = P_{min}/P_{max}$; P_{min} – cycle minimum load, P_{max} – cycle maximum load).

The real degree of connection bearing strength being exhausted at maximum load is $\kappa \approx 0.6$, while the stress ratio is $R \approx 0.2$. This indicates that reaching the connection fatigue strength is real. This is valid if there are no factors causing a decrease of coefficient κ and an increase of coefficient R.

Figure 3 illustrates the dependence of maximum shrinkage stresses τ in the connection plane on shrinkage strains ε_s (free shrinkage) and on the value of parameter δ expressing the interrelationship between the steel girder rigidity and the reinforced concrete slab bonded with it. The values of strains τ at average values of free shrinkage ($\varepsilon_s \approx 2.0 \cdot 10^{-4}$)

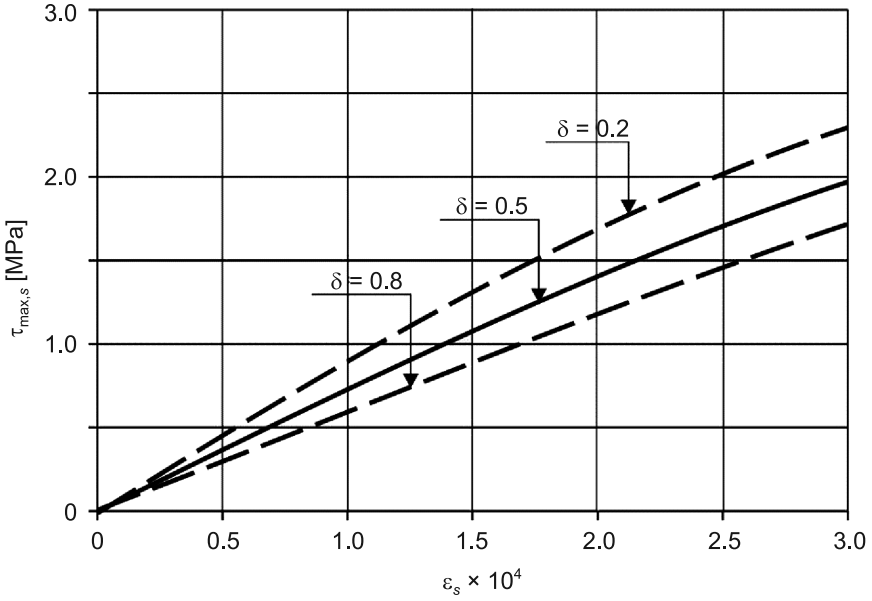

Fig. 3. Effect of concrete free shrinkage ε_s and rigidity of steel girder and connected reinforced concrete slab (δ) on shrinkage stresses τ in connection plane

are comparable with concrete adhesion to the steel girder ($\tau_p \approx 0.03 f_c$ [2]; f_c – concrete compressive strength). This indicates that concrete adhesion to the steel girder flange should not be taken into account when calculating the connection fatigue strength.

Shrinkage stresses are, in cross-sections of utmost effort, of opposite direction relative to disintegrating stresses from external loads. This indicates that they reduce the real value of coefficient κ, and in this way, increase the number of load cycles leading to fatigue strength being exceeded. A change of the value of κ can be described by an additional parameter λ equal:

$$\lambda = \kappa_{ws} / \kappa_w \tag{15}$$

where:

κ_{ws} – coefficient κ calculated with shrinkage stresses taken into account:

$$\kappa_{ws} = P_{\max} / R_{ms} \tag{16}$$

$$N_{ms} = R_m + R_s \tag{17}$$

κ_w – coefficient κ calculated disregarding shrinkage stresses:

$$\kappa_w = P_{\max} / R_m \tag{18}$$

$P_{\max}$ – cycle maximum load,
R_{ms} – connection bearing strength with concrete shrinkage included,
R_m – connection bearing strength disregarding concrete shrinkage,
R_s – disintegrating force in connection plane, from concrete shrinkage:

$$R_s = \tau_s A_p \tag{19}$$

A_p – connection surface investigated.

After transformations we obtain:

$$\lambda = 1 / (1 + R_s / R_m) \tag{20}$$

The plots for λ are shown in Fig. 4. They depend on the interrelationships between the steel girder rigidity and reinforced concrete slab represented by δ and on the value of free shrinkage ε_s. The higher ε_s, the lower the value of λ. The lower the value of δ, the higher λ. This indicates that the value of λ increases with increases of steel girder rigidity relative to the reinforced concrete slab cooperating with it.

A change in the value of κ results in a change in the limit number of cycles N which is followed by the fatigue failure of the connection (the connection fatigue strength becomes fully exhausted). The effect of concrete shrinkage on the limit number of cycles N (and log$N$ to be more precise) can be expressed by introducing factor μ, defined by formula:

$$\mu = \log N_{ms} / \log N_m \tag{21}$$

where:

N_{ms} – limit number of load cycles with concrete shrinkage included,
N_m – limit number of load cycles disregarded concrete shrinkage.

After transformations we receive:

$$\mu = (1 - \lambda\kappa_w) / (1 - \kappa_w) \tag{22}$$

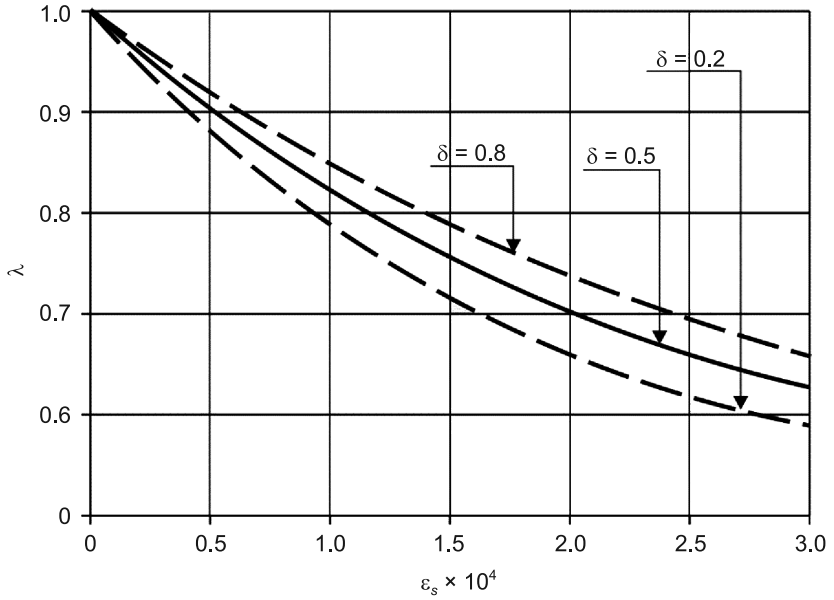

Fig. 4. Effect of concrete free shrinkage ε_s and rigidity of steel girder and connected reinforced concrete slab (δ) on coefficient λ

The value of μ depends on the value of free shrinkage ε_s and coefficient δ, as well as κ (cf. Figs. 5, 6 and 7). The higher the values of κ_s and κ, the higher the value of μ, and, consequently, the higher the fatigue durability. Additionally, the value of μ increases with the increase of the steel girder rigidity relative to the reinforced concrete slab rigidity.

5. Conclusions

It was proved in the paper that concrete shrinkage does have an effect on the connection static (ultimate) grammatical errors, meaning unclear and fatigue bearing strength. For ordinary conditions, the extreme shrinkage stresses are higher than the concrete adhesion to the steel girder flange. Therefore, this adhesion should not be taken into account in calculating the connection bearing strength.

The shrinkage stresses in the connection plane reduce the stresses from external loads. This indicates the possibility of allowing a higher external load. The reduction of stresses from external loads reduces the value of coefficient κ, which is equal to the cycle maximum load to bearing strength (of the connection) ratio.

With a decrease of the value of κ, the limit number of cycles at which the connection bearing strength becomes exhausted increases. Following the results analysis presented in Figures 5–7, it can be stated that when concrete shrinkage is disregarded, a fatigue hazard appears in calculations. When concrete shrinkage is taken into account, there is no such hazard.

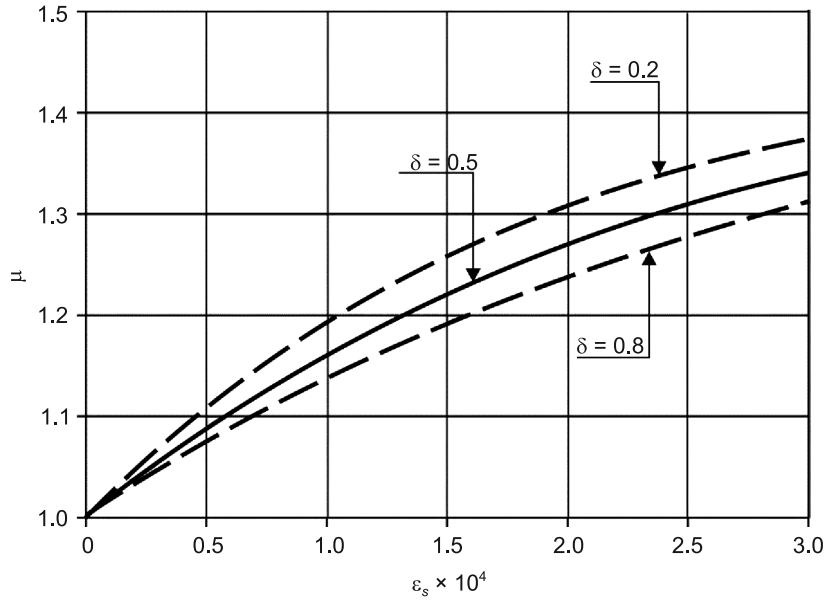

Fig. 5. Effect of concrete free shrinkage ε_s and rigidity of steel girder and connected reinforced concrete slab (δ) on coefficient μ at $\kappa = 0.5$

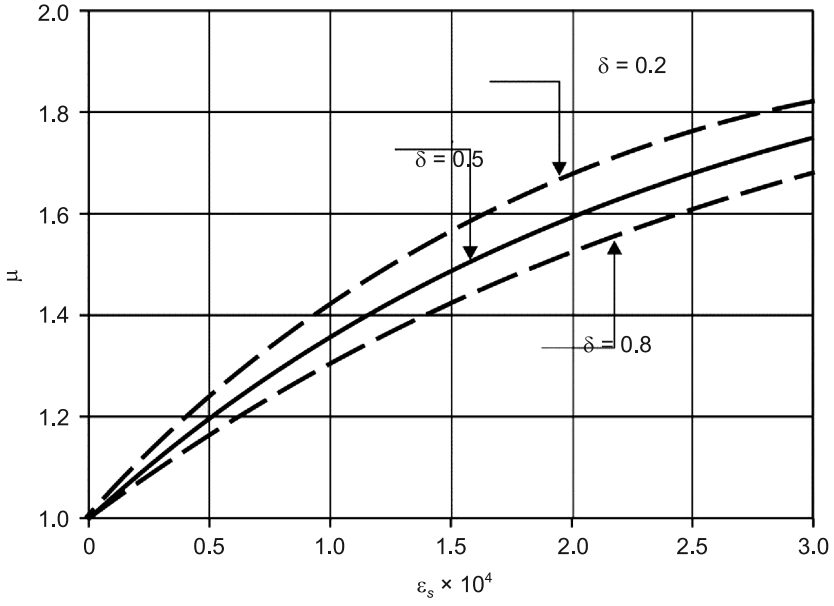

Fig. 6. Effect of concrete free shrinkage ε_s and rigidity of steel girder and connected reinforced concrete slab (δ) on coefficient μ at $\kappa = 0.5\mu$ and at $\kappa = 0.7$

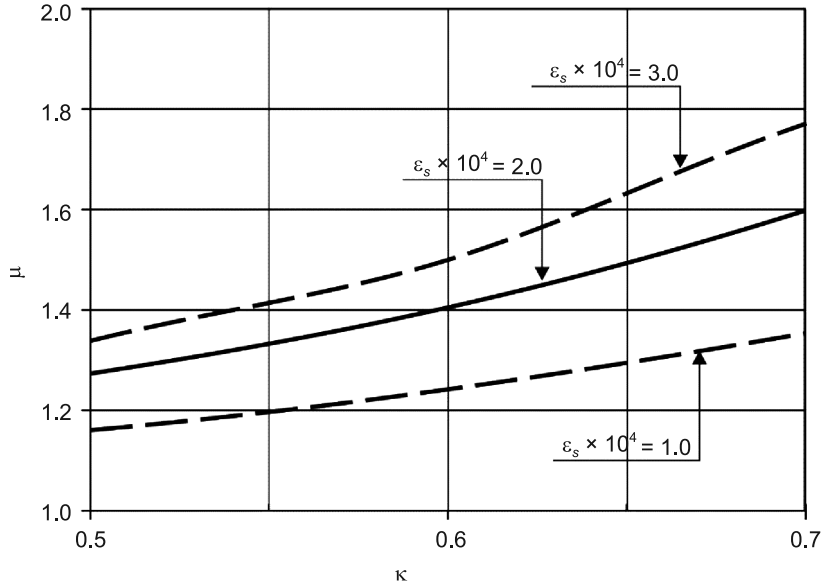

Fig. 7. Effect of concrete free shrinkage ε_s and coefficient κ on coefficient μ at $\delta = 0.5$

The proposal for calculating fatigue strength has been supported by the results of the experiments carried out by the author. Following the results analysis, it can be stated that the bearing strength of a connection made with strip connectors is significantly affected by the rigidity of the steel girder and slab (coefficient δ) together with the parameters of the load cycles (κ, R) and the value of the concrete shrinkage strain.

Final report of research project No. 7 T07E 025 14. Author K. Furtak.

References

[1] PN-EN1994-2: 2010: Eurocode 4 – Design of composite steel and concrete structures – Part 2: General rules and rules for Bridges.
[2] Furtak K., *Mosty zespolone* (*Composite bridges*), PWN, Warszawa–Kraków 1999.
[3] Furtak K., *Wpływ skurczu betonu i obciążeń zmiennych na nośność zespolenia w elementach typu stal – beton* (*Effect of concrete shrinkage and changing loads on connection bearing strength in steel–concrete elements*), Inżynieria i Budownictwo, 1–2/2009.
[4] Knowles P.R., *Composite Steel and Concrete Construction*, Butterworth and Co., Ltd. London 1973.
[5] Kuczma M., Kuczma B., *Steel-concrete composite beams with elasto-plastic connection* [In:] *Mathematical methods in continuum mechanics*, Technical University of Lodz Press. Lodz 2011.
[6] Łącki J., *Nośność zespolenia żelbetowej płyty z dźwigarem stalowym* (*Load capacity of connection reinforced concrete slabs with steel girder. PhD thesis*), praca doktorska, Kraków 2004.

[7] Madaj A., *Wytrzymałość zmęczeniowa łączników w stalowo-betonowych belkach zespolonych* (*Fatigue bearing strength of connectors in steel-concrete composite beams*), Prace IBDiM, nr 1–2/1997, Warszawa.
[8] Pechar J., Bureš J., Schindler A., *Kovové mosty*, SNTL, ALFA, Praha 1990.
[9] Roik K., Hannswille G., *Zur Zur Dauerfestigkeit von Kopfbolzendübeln bei Verbundträgern*, Der Stahlbau, 10/1983.
[10] Šimalová M., Bujňák J., *On determination of shear connection behavior by push test*, Transcom Conference University of Žilina, Žilina 1997.

TECHNICAL TRANSACTIONS | **CZASOPISMO TECHNICZNE**
CIVIL ENGINEERING | BUDOWNICTWO
4-B/2014

MARIAN GWÓŹDŹ*

DIFFERENTIATING THE RELIABILITY OF ALUMINUM STRUCTURES[1]

RÓŻNICOWANIE NIEZAWODNOŚCI KONSTRUKCJI ALUMINIOWYCH

Abstract

The design of aluminum structures, according to the modern generation of European standards, sets new requirements regarding the reliability management of such facilities before the authors of architectural and structural designs. Reliability problems should be formulated at an early stage of the investment process – the construction design, in a clear manner, requiring the authors of detailed designs and contracting companies to provide structures exhibiting the operating parameters in agreement with the expectations of the investor. The basics of substantive and formal requirements in this respect are set out in Eurocode PN EN 1990 and the European standards dealing with the manufacturing and erection of structures. Problems of modern reliability management for aluminum structures are referred to the case of large volume buildings subject to climate actions.

Keywords: *aluminum*, *reliability*, *consequence classes*, *structural classes*, *manufacturing classes*, *supervision level*, *inspection level*

Streszczenie

Projektowanie konstrukcji aluminiowych wg współczesnej generacji norm europejskich stawia przed autorami projektów architektoniczno-budowlanych nowe wymagania w zakresie zarządzania niezawodnością takich obiektów. Problemy niezawodności należy sformułować już na wczesnym etapie procesu inwestycyjnego – w projekcie budowlanym, w sposób jednoznaczny, zobowiązujący autorów projektów wykonawczych, a także firmy wykonawcze do dostarczenia konstrukcji o parametrach eksploatacyjnych zgodnych z oczekiwaniami inwestora. Podstawy merytoryczne i formalne w tym zakresie są sformułowane w Eurokodzie PN-EN 1990 oraz w europejskich normach wykonania konstrukcji. Problemy współczesnego zarządzania niezawodnością konstrukcji aluminiowych odniesiono do przypadków budynków kubaturowych poddanych oddziaływaniom klimatycznym.

Słowa kluczowe: *aluminium*, *niezawodność*, *klasy konsekwencji*, *klasy konstrukcyjne*, *klasy wykonania*, *poziom nadzoru*, *poziom inspekcji*

* Prof. Ph.D. D.Sc. Marian Gwóźdź, Institute for Building Materials and Structures, Faculty of Civil Engineering, Cracow University of Technology.

[1] The paper is a reprint of an article that appeared in Polish language under the title *Projektowanie konstrukcji aluminiowych. Różnicowanie niezawodności* in the journal Builder, No. 02/2014, 42-45.

1. Managing reliability in the design phase

In engineering approach to reliability problems used in the PN-EN 1990 [1] three level consequence classes have been introduced, denoted by CC1, CC2 and CC3 symbols respectively. Consequence classes are defined according to the risk to human life and health and economic consequences of structural damage or loss of fitness for purpose. CC consequence classes are associated with three corresponding structural reliability classes RC – RC1, RC2 and RC3, for which the code [1] sets the minimum required values of reliability coefficient β_u assigned to the ultimate limit states. See, among other works, [11] and [12].

Reliability diversification by the advanced mathematical method FORM [11] is based on full knowledge of the statistical parameters describing load and bearing capacity. At the present stage of the development of statistical methods, the design of building structures is permitted in three reliability classes (RC) by engineering load factors and bearing capacity method, and the FORM method allows for calibration of reliability measures in this method. For reliability class RC2 corresponding to consequence class CC2, partial coefficients are calibrated in the relevant branch Eurocodes. In particular, the basic coefficients for permanent and variable loads γ_F are specified in Annex A1 to the PN-EN 1990 [1], and bearing capacity factors γ_{Mi} for aluminum components in different parts of the Eurocodes PN EN 1999-1-1 [4] – PN EN 1999-1-5 [8].

A simple method of varying the reliability requirements for variable loads, according to [1], is an adjustment of the load factors γ_F, with K_{FI} correction factors listed in Table 1.

Table 1

Values of K_{FI} factors for actions according to PN-EN 1990

Correction factor	Reliability class		
	RC1	RC2	RC3
(1)	(2)	(3)	(4)
K_{FI}	0.9	1.0	1.1

In reliability theory, loads are described by functions that depend on the life of the structure. Therefore, designing a building requires the determination of the design life of the structure T_d, which is the time interval in which the structure, or part thereof, is to be used as intended with anticipated maintenance, without the need for major repairs.

The PN-EN 1990 [1] introduced a systematic breakdown of the useful design life into five categories, listed in Table 2. In most cases, building structures are designed assuming a 4th category design period, which corresponds to a 50-year long designed service life of a building. The PN-EN 1990 [1] stated explicitly recommended minimum values of reliability index β only for the ultimate limit state for the reference period $T = 1$ year and $T = 50$ years. The different service life periods T_d for buildings, according to Table 2, require an interpolation formula to determine the reliability index β corresponding to the accepted category of the designed service life. One may assume that for mutually independent random load peaks, the following relationship holds between reliability indicators for the reference period $T = n$ years and $T = 1$ year, expressed in terms of Laplace functions:

$$\Phi(\beta_n) = \Phi(\beta_1)^n. \tag{1}$$

Table 2

Designed Service Life categories according to PN-EN 1990

Category of Designed Service Life	Design life of the structure T_d in years	Sample structures
(1)	(2)	(3)
1	10	Temporary structures
2	10–25	Replaceable components
3	15–30	Agricultural structures and similar
4	50	Ordinary buildings
5	100	Monumental buildings, bridges

A practical example of the reduction of characteristic variable loads Q_{kn} at time $n \neq 50$ years is the application of appropriate reliability theory models to climate loads, described by the probability distributions of maximum values. In particular, the formula given in the standard PN EN 1991-1-5 [4] applies to thermal loads:

$$T_{k,n} = T_{k,50}\left\{k_i - k_j \ln\left[-\ln\left(1-\frac{1}{n}\right)\right]\right\} = T_{k,50}\eta_d, \tag{2}$$

where:

$T_{k,50}$ – characteristic values (maximum or minimum) of air temperature in the shade, with an annual probability of exceedance equal to 0.02,

k_i, k_j – multipliers specified in PN-EN 1991-1-5 [4]: $k_i = 0.781$ and $k_j = 0.056$ for the maximum temperature T_{max} while $k_i = 0.393$ and $k_j = -0.156$ for the minimum temperature T_{min} – respectively.

For snow load, the extrapolation formula given in the standard PN EN 1991-1-3 [2] holds:

$$s_{k,n} = s_{k,50}\frac{1-0.78v\left\{\ln\left[-\ln\left(1-\frac{1}{n}\right)\right]+0.577\right\}}{1+2.592v} = s_{k,50}\eta_d, \tag{3}$$

where:

$s_{k,50}$ – characteristic values of ground snow load according to [2],

v – coefficient of variation specified in the standard [2]: $v = 0.7$ for buildings located at a height of $H \leq 300$ m above sea level and $v = 0.8 \exp(-0.0006H)$ when $H > 300$ m above sea level.

The reduction formula for base wind speed according to PN-EN 1991-1-4 [3] is as follows:

$$v_{b,n} = v_b\sqrt{\frac{1-0.2\ln\left[-\ln\left(1-\frac{1}{n}\right)\right]}{1-0.2\ln[-\ln(0.98)}} = v_b\eta_d. \tag{4}$$

Table 3

Conversion coefficient values for climate loads

Return period n [years]	Conversion coefficient η_d			
	Action			
	s_k	v_b	T_{max}	T_{min}
(1)	(2)	(3)	(4)	(5)
10	0.70	0.90	0.91	0.74
15	0.77	0.93	0.93	0.81
25	0.87	0.96	0.96	0.89
30	0.90	0.97	0.97	0.92
50	1.00	1.00	1.00	1.00
100	1.13	1.04	1.04	1.11
300	1.33	1.10	1.10	1.28
500	1.42	1.12	1.13	1.36

Because of the complex structure of the formulas (2)–(4), the calculation of the characteristic climate loads for typical return periods is justified. One may present it in the form of the load conversion coefficient η_d for maximum loads having the return period of $n = 50$ years (see Table 3).

Reliability diversification of aluminum structures, an alternative to the complex calculations of probability level 2, may be done by reducing the load factors γ_F by the K_{Fi} reducing coefficients according to Table 1. The corresponding reduction factors K_{Ri} according to [1] may be used to reduce partial bearing capacity factors γ_{Mi} for sections and bars. In the current version of Eurocode PN EN 1999-1-1 [6] – PN EN 1999-1-5 [10], coefficients K_{Ri} have not been specified, because for the dominant variable loads with moderate scatter (load variation coefficients $v_F < 25\%$), the standardized values of coefficients K_{Fi} capture both the effect of reducing the loads and the strength of aluminum alloys. Climate loads, such as the snow load constitute an exception to this rule, since in Polish climate conditions, the snow load is characterized by high dispersion with variation coefficient values $v_F = 80 - 100\%$, cf [11].

A sample specification of reduction factors K_{Ri} for the strength of the AlCu4Mg2 alloy made in Poland is presented in Table 4. The values of K_{Ri} in columns (8)–(10) were calculated according to the following formula:

$$K_{Ri} = \frac{1 - 3.04 v_{\mathrm{Re}}}{1 - \beta_R v_{\mathrm{Re}}}. \tag{5}$$

Values of the partial reliability index $\beta_R = 0.8 \times 3.3 = 2.64$ for reliability class RC1, and $\beta_R = 0.8 \times 4.3 = 3.44$ for reliability class RC3 were adopted in the formula (5) according to [1]. Moreover, column (6) lists the central plastic bearing capacity factor $\overline{\gamma}_{M0}$ calculated as the ratio of average $\overline{R}_{02}$ and computational R_{ed} values (bottom quantiles calculated for the partial index β_R).

Table 4

Reliability measures $\overline{\gamma}_{M0}$ and γ_{M0}, reduction coefficients K_{Ri} specified on a statistical sample of AlCu4Mg2 alloy strength according to own research [11]

Product group	Thickness t [mm]	Yield limit R_{02} [MPa]					Reliability class		
							RC1	RC2	RC3
		$\overline{R}_{02}$	v_{Re}	β_R	$\overline{\gamma}_{M0}$	γ_{Mo}	K_{Ri}	K_{Ri}	K_{Ri}
(1)	(2)	(3)	(4)	(5)	(6)	(7)	(8)	(9)	(10)
Plates	2–10	308	0.059	3.04	1.24	1.00	0.972	1.000	1.030
	12–25	335	0.042		1.35	1.00	0.981	1.000	1.019
	26–40	335	0.037		–	–	0.984	1.000	1.017
	41–70	328	0.044		–	–	0.980	1.000	1.020
	2–80	322	0.062		1.29	1.00	0.971	1.000	1.031
Profile bars	2–20	378	0.093	3.04	1.42	1.00	0.963	1.000	1.055
Bars	to 30	373	0.098	3.04	–	–	0.947	1.000	1.059
	> 30	383	0.087		–	–	0.955	1.000	1.049
	16–130	381	0.090		–	–	0.953	1.000	1.053

Reliability diversification of aluminum structures, in addition to the specifications given above, may also be carried out by the system safeguards. The design supervision levels classification (DSL), cited in Table 5 exhibits such a character, indeed. The DSL is defined in PN-EN 1990 [1] for the design stage are linked to the reliability classes (RC) selected according to the importance of the structure. The diversification of project supervision within the design unit may further include the classification of designers and verifiers, depending on their expertise, skills and experience.

Table 5

Design supervision levels (DSL) according to the code PN-EN 1990 [1]

Design supervision level	Supervision characteristics	Minimum recommended requirements for checking calculations, drawings and specifications
(1)	(2)	(3)
DSL3 Referring to RC3	stringent	checked by an independent design entity
DSL2 Referring to RC2	standard	checked by the verifying authority of the design unit according to own procedure
DSL1 Referring to RC1	acceptable	self control: checked by the designer

2. Reliability management during manufacturing and erection of a structure

Ensuring the required reliability of aluminum structures involves at the stage of manufacturing and installation the need to develop a specification of the execution, which in accordance with PN EN 1090-3 [5], among others includes:

a) requirements relating to manufacturing classes,
b) technical requirements taking into account work safety,
c) quality plan,
d) functionality requirements.

Table 6

Dependencies taken into account when selecting Structure Execution Classes(EXC) [6]

Consequence Classes		CC1		CC2		CC3	
Service Classes		SC1	SC2	SC1	SC2	SC1	SC2
Manufacturing Classes	PC1	EXC1	EXC1	EXC2	EXC3	EXC3[a/]	EXC3[a/]
	PC2	EXC1	EXC2	EXC2	EXC3	EXC3[a/]	EXC4

[a/] EXC4 class is applied to special structures, whose destruction would result in extreme consequences; in particular when EXC4 class is required by national codes.

Four structure execution classes: EXC1, EXC2, EXC3 and EXC4 have been defined in Eurocode EN 1999-1-1 [6], starting with the least stringent (EXC1) to the most demanding (EXC4), see Table 6. Execution classes may be applied to an entire structure, to parts of the structure, and even to its details, therefore, within a single building, several execution classes (EXC) may occur.

According to the understanding adopted by the PN-EN 1090-3 [5], if the execution class is not specified in the design documentation, EXC2 class is assumed. Selection of execution classes (EXC) depends on the manufacturing category PC (non-welded components – PC1, welded components – PC2) and category of use (see Table 7), and is associated with the consequence classes CC defined in standard [1]. Manufacturing (PC) and Service (SC) classes take into account the risks associated with the manufacturing and service of the structure. The execution class (EXC) selection procedure includes in sequence:

a) Selection of consequence class (CC), taking into account the potential consequences of a structural disaster in the form of loss of life, economic and environmental degradation.
b) Determination of the manufacturing class (PC) and the service class (SC) (see Table 7).
c) Determination of the execution class (EXC) depending on the CC, PC and SC according to Table 6 (see PN-EN 1999-1-1 [6]).

The execution class (EXC) constitutes an essential element of structural reliability because it determines the requirements for enforcement actions formulated in the PN-EN 1090-3 (Table A.3 of the code [5]). In particular, requirements for design documentation, product design, processing and merging, welding, assembly and inspection, testing and corrective action are formulated there.

Table 7

Recommended criteria for service class (SC) according to code [6]

Class (SC)	Criterion
(1)	(2)
SC1	Aluminum structures and components designed against predominately static loads
SC2	Structures subject to repeated variable loads of intensity requiring implementation of the control procedure provided for components subject to fatigue (tolerated fatigue damage method according to [8])

Table 8

Inspection levels during erection of building structures according to the code PN-EN 1990 [1]

Inspection level	Characteristics	Requirements
(1)	(2)	(3)
IL3 referring to RC3	Stringent inspection	Third party inspection
IL2 referring to RC2	Standard inspection	Inspection according to own procedures of the erecting unit
IL1 referring to RC1	Acceptable inspection	Self inspection

The execution, as well as the design phase for a structure, is subject to control, which can be provided by organizing systematic inspections at various levels. Inspection levels (IL) at all stages of execution, including the production of building materials and products are defined in code PN EN 1990 [1], see Table 8. Inspection levels are associated with a Reliability Class (RC), cf paper [12], and may be implemented by means of appropriate quality management measures.

3. Conclusions

The Eurocodes constitute a new generation of standards leading to profound systemic changes at every stage of the investment cycle. Eurocode PN EN 1990 constitutes a normalized basis for the design stage and contains the formulation of basic elements of reliability management for building structures, including structures made of aluminum alloys. In the domain of manufacturing and erecting aluminum structures, code PN EN 1090--2 constitutes the basis for quality assurance. In contemporary developments, each structural design should include: building consequence class CC; reliability class RC; the design service life category; structure execution class EXC; supervision and inspection levels DSL and IL. It is also recommended, for buildings and their components sensitive to climate action, particularly for CC3 class buildings, to make precise forecasts of loads, derived from long-term meteorological observations, as well as differentiate reliability requirements in terms of computational strength for alloys.

References

[1] PN-EN 1990. Eurocode. Basics of structural design, PKN, Warsaw 2004.
[2] PN-EN 1991-1-3. Eurocode 1. Actions on structures. Part 1-3: General actions. Snow load, PKN, Warsaw 2005.
[3] PN-EN 1991-1-4. Eurocode 1. Actions on structures. Part 1-4: General actions. Wind loads, PKN, Warsaw 2008.
[4] PN-EN 1991-1-5. Eurocode 1. Actions on structures. Part 1-5: General actions. Thermal loads, PKN, Warszawa 2005.
[5] PN-EN 1090-3. Manufacturing and erection of steel and aluminum structures. Part 3: Technical requirements for aluminum structures, PKN, Warsaw 2012.
[6] PN-EN 1999-1-1. Eurocode 9. Design of aluminum structures. Part 1-1: General rules, PKN, Warsaw 2011.
[7] PN-EN 1999-1-2. Eurocode 9. Design of aluminum structures. Part 1-2: Calculation of structures due to fire conditions, PKN, Warsaw 2007.
[8] PN-EN 1999-1-3. Eurocode 9. Design of aluminum structures. Part 1-3: Structures subject to fatigue, PKN, Warsaw 2011.
[9] PN-EN 1999-1-4. Eurocode 9. Design of aluminum structures. Part 1-4: Structures made of cold formed plates, PKN, Warszawa 2012.
[10] PN-EN 1999-1-5. Eurocode 9. Design of aluminum structures. Part 1-1: Plates and shells, PKN, Warsaw 2012.
[11] Gwóźdź M., Machowski A., *Selected studies and calculations for building structures using probabilistic methods*, Cracow University of Technology Press (Monograph, 10 ed. sheets), Cracow 2011 (in Polish).
[12] Gwóźdź M., Kuchta K., *Reliability management for buildings according to PN-EN 1990*, Czasopismo Techniczne 2-A/2/2011.

TECHNICAL TRANSACTIONS | CZASOPISMO TECHNICZNE
CIVIL ENGINEERING | BUDOWNICTWO
4-B/2014

MICHAŁ PAZDANOWSKI*

RESIDUAL STRESSES AS A FACTOR OF RAILROAD RAIL FATIGUE

NAPRĘŻENIA RESZTKOWE JAKO CZYNNIK ZMĘCZENIA SZYN KOLEJOWYCH

Abstract

An analysis of the influence of residual stresses on material fatigue is presented in this paper. Residual stress distribution in railroad rails subjected to simulated service loads is considered. A mechanical model based on the plastic shakedown theory was used to determine residual stresses and the Dang Van fatigue criterion was applied.

Keywords: *residual stresses*, *material fatigue*, *Dang Van criterion*

Streszczenie

W artykule przedstawiono analizę wpływu naprężeń resztkowych wywołanych symulowanym obciążeniem szyn kolejowych kołami taboru kolejowego na zmęczenie materiału szyny. Do wyznaczenia rozkładu naprężeń resztkowych zastosowano model mechaniczny oparty na teorii plastycznego przystosowania, a jako kryterium zmęczeniowe przyjęto kryterium Dang Vana.

Słowa kluczowe: *naprężenia resztkowe*, *zmęczenie materiału*, *kryterium Dang Vana*

* Ph.D. Michał Pazdanowski, Institute for Computational Civil Engineering, Faculty of Civil Engineering, Cracow University of Technology.

1. Introduction

Railroad rails may catastrophically fail during service resulting in loss of human life and significant damage to rolling stock [1, 2]. The experimental investigations [3] revealed that residual stresses induced in a rail during manufacturing (roller straightening) and service (contact loads at the rail/wheel interface, exceeding the elastic bearing capacity of the rail material) may constitute an important factor affecting crack nucleation and growth.

In the current paper, the influence of residual stresses induced in a railroad rail during simulated service on the fatigue life of such a rail is given consideration.

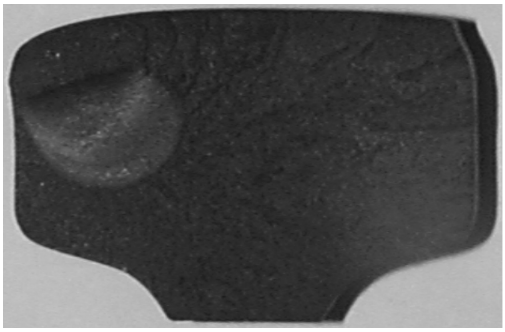

Fig. 1. Initiation and growth of fatigue crack in the head of rail subjected to service loads

Residual stresses in rails subjected to service conditions may be found through either numerical analysis [21], or through experimental investigations of specimens taken out of standard revenue tracks [22] or test tracks [23]. Experimental analysis is time consuming, costly and in the case of specimens taken out of revenue tracks, the loading history of a specimen may be impossible to ascertain. On the other hand, numerical analysis may be prohibitively time consuming when an exact elasto-plastic incremental analysis would have to be performed in order to find the final residual stress state in a rail after a significant number of loading cycles [21]. This obstacle may be avoided when one settles for an estimate of residual stress distribution in a rail subjected to ***simulated*** service loads computed using the mechanical model based on the elasto-plastic shakedown theorem initially proposed in [4, 5]. Although the application of this mechanical model yields only an estimate of residual stresses induced by simulated service loads, numerous tests have shown that this estimate is of reasonably good quality [6].

Multiaxial high cycle fatigue criteria for metals may be divided into three main groups [7]: critical plane approaches, such as Findley [10], Matake [11], McDiarmid [12], Dietmann [13]; approaches based on stress invariants, such as Marin [14], Crossland [15], Kakuno-Kawada [16], Deperrois [17]; approaches based on stress averages within the elementary volume, such as Grubisic and Simburger [18], Liu and Zenner [19], or Dang Van [20]. According to [7], criteria belonging to the group of approaches based on the stress averages within material volume yield results closest to experiments for so called ‘hard’ metals (which include steels). Therefore, the simplest of these, the Dang Van [20] criterion, was used in further analysis.

2. Residual stress evaluation method

The residual stress calculation method based on shakedown theorems [9], in its simplest form may be stated as the following minimization problem [5]:
find:

$$\min_{\sigma_{ij}^r} \int_V (\sigma_{kl}^r - \sigma_{kl}^0)^T \cdot C_{ijkl} \cdot (\sigma_{ij}^r - \sigma_{ij}^0) \cdot dV \tag{1}$$

subject to:

$$\sigma_{ij,j}^r = 0 \ - \text{ for each point in } V \tag{2.1}$$

$$\sigma_{ij}^r \cdot n_j = 0 \ - \text{ for each point on } \delta V \tag{2.2}$$

$$\Phi(\sigma_{ij}^r + \sigma_{ij}^E(t)) \leq \sigma_y \ - \text{ for each point in } V \tag{2.3}$$

where:

- $\sigma_{ij}^r, \sigma_{kl}^r$ – time independent residual stresses induced in the considered body by the actual loading program,
- $\sigma_{ij}^0, \sigma_{kl}^0$ – initial residual stresses existing in the considered body prior to the application of current loading program,
- σ_{ij}^E – time dependent elastic stresses induced in the body by current loading program changing in time,
- s_y – material yield limit,
- C_{ijkl} – elastic compliance matrix,
- n_j – vector perpendicular to the body boundary.

Formula (1) denotes the total complementary energy of residual stresses while formulas (2.1) and (2.2) denote the internal equilibrium conditions and zero static boundary conditions of those stresses. Formula (2.3) denotes the yield condition, which has to be satisfied in every moment of time. Of course, all the constraints (2) have to be satisfied in every point of the considered body.

3. The Dang Van fatigue criterion

The Dang Van fatigue criterion may be counted among the fatigue criteria based on the mesoscopic scale approach, i.e. the scale of metal grains of a metallic aggregate [7]. Thisfatigue criterion is based on an average measure of the plastic strain accumulated in all the flowing crystals within an elementary volume of the material.

This criterion condenses the history of six stress tensor components into the load path defined by two components, and thus simplifies fatigue damage calculations [8]. The criterion combines hydrostatic pressure σ_H and momentary maximum shearing stress τ_a calculated according to the Tresca criterion:

$$\tau_a(t) = \frac{1}{2} \cdot \left[s_{\mathrm{I}}^{v}(t) - s_{\mathrm{III}}^{v}(t) \right] \tag{3}$$

evaluated for the part of stress deviator tensor which varies in time; this part is defined as:

$$s_{ij}^{v}(t) = s_{ij}(t) - s_{ij}^{c} = [\sigma_{ij}(t) - \delta_{ij} \cdot \sigma_H(t)] - s_{ij}^{c} \tag{4}$$

where s_{ij}^{c} constitutes the solution of the following minimax problem:

$$s_{ij}^{c} = \min_{s_{ij}^{*}} \max_{t} (s_{ij}(t) - s_{ij}^{*}) \cdot (s_{ij}(t) - s_{ij}^{*}) \tag{5}$$

i.e. such value of the time independent stress deviator s_{ij}^{*} for which the maximum of the norm (5) reaches the lowest value. Shear stress and hydrostatic pressure are then combined linearly to yield an equivalent scalar:

$$\tau_{eq,DV} = \max_{t} (\tau_a(t) + \alpha \cdot \sigma_H(t)) \tag{6}$$

which in turn may be used to estimate the fatigue damage [8].

The constant α is determined as follows:

$$\alpha = 3 \cdot \left(\frac{\tau_D}{\sigma_D} - \frac{1}{2} \right) \tag{7}$$

where τ_D and σ_D represent fatigue limits in torsion and tension-compression, respectively. According to the Dang Van criterion, time independent residual stresses do not affect the momentary maximum shear stress τ_a (3), but affect only the hydrostatic stress term σ_H [8].

4. Service load simulation program

The contact load acting on the rail crown has been simulated by biparabolic pressure distribution spanned over the rectangular contact area applied at seven evenly distributed discrete contact locations shown in Fig. 2, where location 1 is centered on the rail's longitudinal axis of symmetry while location 7 is offset by 25 mm to the left of this axis. Peak pressure p_0 and patch dimensions $a \times b$ have been determined using elastic Hertz contact formulae to compute the contact ellipse area for the given contact load, and later on, to determine a rectangle with equivalent area and biparabolic pressure distribution balancing this contact load. For the purpose of current calculations, 132RE rail (US type) made of steel exhibiting the following material data have been assumed: 206 GPa Young Modulus, 483 MPa yield limit, 0.3 Poisson's ratio. Three values of wheel load have been considered, namely: 147 kN, 160 kN, 173 kN. These values correspond to standard wheel loads on heavy haul rail lines in North American practice.

A 3D Finite Element Method computational model was used to find the necessary momentary elastic stress distributions σ_{ij}^{E} (2.3), while a 2D Meshless Finite Difference Method computational model was applied to determine the rail longitudinal axis independent distributions of residual stresses σ_{ij}^{r}.

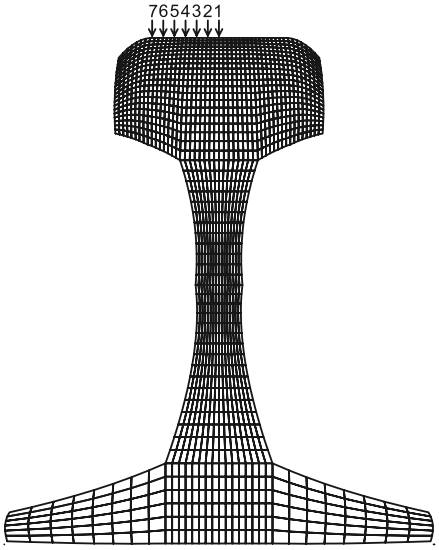

Fig. 2. Load application points on the rail crown and mesh used during numerical analysis

Table 1

Peak residual and elastic hydrostatic stress levels introduced in rail

Location (Fig. 2)	Load [kN]	Compression [MPa]		Tension [MPa]	
		residual σ_H^r	elastic σ_H^r	residual σ_H^r	elastic σ_H^r
2	147	–107.900	–496.460	78.733	–197.260
4		–130.622	–438.299	80.716	–197.779
6		–140.146	–432.423	97.209	–188.910
2	160	–120.254	–407.357	79.491	–209.653
4		–126.147	–423.772	81.502	–211.301
6		–140.023	–459.753	108.147	–192.702
2	173	–142.589	–446.350	107.429	–187.212
4		–147.962	–371.866	116.255	–187.289
6		–171.047	–369.222	153.002	–165.418

The distribution of hydrostatic residual stress σ_H^r (directly affecting the Dang Van fatigue criterion) in the railhead for all three considered values of wheel load applied at the rightmost load application point depicted in Fig. 2 is presented in Fig. 3. For better readability, tensile and compressive parts of this stress are depicted separately on the right and left, respectively. Peak residual hydrostatic pressure levels introduced by each of the considered

loading scenarios at selected loading locations are presented in Table 1. and compared to the highest elastic (momentary) hydrostatic pressure levels introduced by simulated wheel load introduced at the same locations in the railhead.

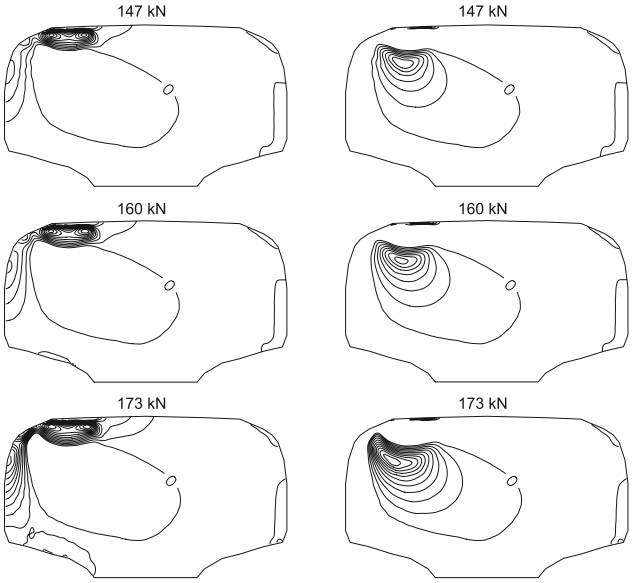

Fig. 3. Hydrostatic residual stress σ_H^r decomposed into positive (compression – at left) and negative (tension – at right) parts. Contour interval 14 MPa

Locations of peak hydrostatic residual stresses σ_H^r (compressive component denoted by ○, and tensile component denoted by ●) as well as von Mises equivalent residual stresses σ_0^r (denoted by □) corresponding to load application points indicated in Fig. 2 are depicted in Fig. 4.

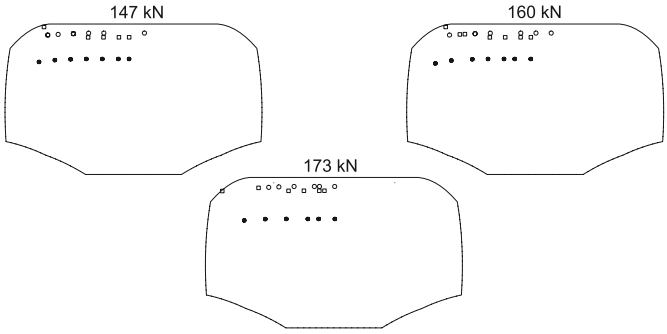

Fig. 4. Location of extreme values of hydrostatic residual stress and von Mises equivalent residual stress induced by contact loads applied at locations indicated in Fig. 2

5. Conclusions

Initial calculations performed so far indicate that the residual stress levels due to simulated contact loads may reach levels on a par with actual (momentary) elastic stresses created by these loads, and thus should be included in fatigue calculations. Values of these stresses tend to increase substantially (by up to 23.5% in compression and up to 30.1% in tension for the results presented in Table 1) as the load application area shifts away from the center of the railhead. When the load application area gets very close to the gauge side of the rail an additional stress concentration zone occurs at the gauge side of railhead. This phenomenon may additionally be aggravated should two point contact load occur (for instance on a curved track). Thus, two point contact loads will be subjected to analysis in further work.

The results presented in the 5th column of Table 1 are of special interest from the practical point of view, as the tensile stresses have an adverse influence on the fatigue life of the body subject to cyclic loads. The residual hydrostatic tension for loading scenarios considered so far reaches a level of almost 32% of the material yield limit, thus indicating that these stresses significantly affect rail fatigue life, and the safety of railroad operation.

The location of extreme residual hydrostatic stresses below the running surface of the rail remains fairly stable, regardless of the load application point location, though the depth of extreme stresses seems to be affected by the load magnitude for tensile stresses only.

At the locations indicated in Fig. 4 by ●, the residual hydrostatic pressure for higher wheel loads is on par with the elastic hydrostatic pressure. The positive sign of this pressure (tension) indicates substantially increased risk of rail failure fatigue in this zone.

References

[1] Steel R.K., et al, *Catastrophic web cracking of railroad rail: A discussion of the unanswered questions*, AAR, 1990.

[2] Zerbst U., Lunden R., Edel K.-O., Smith R.A., *Introduction to the damage tolerance behaviour of railway rails – a review*, Engineering Fracture Mechanics, vol. 76, 2009, 2563-2601.

[3] Groom J.J., *Determination of residual stresses in rails*, Batelle Columbus Laboratories, Rpt. No. DOT/FRA/ORD 83-05 Columbus OH, 1983.

[4] Orkisz J., Harris A., *Analysis of residual stresses at shakedown, a hybrid approach*, Theoretical and Applied Fracture Mechanics, vol. 9, 1988, 109-121.

[5] Orkisz J., et al., *Discrete analysis of actual residual stresses resulting from cyclic loadings*, Computers and Structures, vol. 35, 1990, 397-412.

[6] Pazdanowski M., *On estimation of residual stresses in rails using shake-down based method*, Archives of Transport, vol. 22(3), 2010, 319-336.

[7] Papadopulos I.V., Davoli P., Gorla C., Filippini M., Bernasconi A., *A comparative study of multiaxial high-cycle fatigue criteria for metals*, International Journal of Fatigue, vol. 19(3), 1997, 219-235.

[8] Bernasconi A., Davoli P., Filippini M., Foletti S., *An integrated approach to rolling contact sub-surface fatigue assessment of railway wheels*, Wear, vol. 258, 2005, 973-980.

[9] Martin J.B., *Plasticity – fundamentals and general results*, The MIT Press, 1975.

[10] Findley W.N., *A theory for the effects of mean stress on fatigue of metals under combined torsion and axial load or bending*, Journal of Engineering for Industry, vol. 11, 1959, 301-306.

[11] Matake T., *An explanation on fatigue limit under combined stress*, Bull JSME, vol. 20(141), 1977, 257-263.
[12] McDiarmid D.L., *A general criterion for high cycle multiaxial fatigue failure*, Fatigue and Fracture of Engineering Materials and Structures, vol. 14, 1990, 429-453.
[13] Dietmann H., Bhonghibhat T., Schmid A., *Multiaxial fatigue behaviour of steels under in-phase and out-of-phase loading, including different waveforms and frequencies* [in:] D. Kussmaul, D.L. McDiarmid, D. Socie (Eds.): *Fatigue under biaxial and multiaxial loading*, MEP, London 1991, 449-464.
[14] Marin J., *Mechanical behavior of engineering materials*, Prentice-Hall, Englewood Cliffs, N.J., 1962.
[15] Crossland B., *Effect of large hydrostatic pressure on the torsional fatigue strength of an alloy steel* [in:] *Proceedings of the international conference on fatigue of metals*, IME London 1956, 138-149.
[16] Kakuno H., Kawada Y., *A new criterion of fatigue strength of a round bar subjected to combined static and repeated bending and torsion*, Fatigue and Fracture of Engineering Materials and Structures, vol. 2, 1979, 229-236.
[17] Deperrois A., *Sur le calcul de limites d'endurance des aciers*, PhD thesis, Paris 1995.
[18] Grubisic V., Simburger A., *Fatigue under combined out-of-phase multiaxial stresses* [in:] *Fatigue, Testing and Design*, Proc. SEE Conf., vol. 2, London 1976, 1-28.
[19] Zenner H., SimburgerA., Liu Z., *On the fatigue limit of ductile metals under complex multiaxial loading*, International Journal of Fatigue, vol. 22, 2000, 137-145.
[20] Dang Van K., Griveau B., Message O., *On new multiaxial fatigue criterion: theory and application* [in:] *Biaxial and multiaxial fatigue*, MEP, London 1989, 479-496.
[21] Ringsberg J.W., Lindback T., *Rolling contact fatigue of rails including numerical simulations of the rail manufacturing process and repeated wheel rail contact loads*, International Journal of Fatigue, vol. 25, 2003, 547-558.
[22] Groom J.J., *Determination of residual stresses in rails*, Batelle Columbus Laboratories, Rpt. DOT/FRA/ORD-83-05, Columbus, OH, 1983.
[23] Lo K.H., Mummery P., Buttle D.J., *Characterization of residual principal stresses and their implications on failure of railway rails*, Engineering Failure Analysis, vol. 17, 2010, 1273-1284.

TECHNICAL TRANSACTIONS | **CZASOPISMO TECHNICZNE**
CIVIL ENGINEERING | BUDOWNICTWO
4-B/2014

EDYTA PIĘCIORAK*

THE INFLUENCE OF SUPPORT WIDTHS OF TRAPEZOIDAL SHEETS ON LOCAL TRANSVERSE RESISTANCE OF THE WEB ACCORDING TO PN-EN 1993-1-3

WPŁYW SZEROKOŚCI PODPARCIA BLACH TRAPEZOWYCH NA NOŚNOŚĆ POPRZECZNĄ ŚRODNIKA WG PN-EN 1993-1-3

Abstract

This paper comments on the calculations algorithm and presents examples of the determination of local transverse resistance of the web for trapezoidal sheets according to the rules given in the standard PN-EN 1993-1-3 [4]. The calculations were carried out for different support widths and thicknesses of the stiffened and unstiffened webs of trapezoidal sheets. The results obtained in the calculations show a distinctly positive influence of the increase of the support widths on the local transverse resistance of the web of trapezoidal sheets.

Keywords: *trapezoidal sheet*, *local transverse forces*, *local transverse resistance of the stiffened and unstiffened web*, *effective bearing length*

Streszczenie

W artykule przedstawiono wraz z komentarzem algorytm oraz przykłady wyznaczania nośności poprzecznej środnika blachy trapezowej wg PN-EN 1993-1-3 [4]. Obliczenia przeprowadzono dla różnych szerokości podparcia i różnych grubości blach trapezowych z usztywnieniami i bez usztywnień środnika. Otrzymane wyniki pokazały wyraźnie korzystny wpływ zwiększenia szerokości podparcia blachy trapezowej na nośność poprzeczną środnika.

Słowa kluczowe: *blacha trapezowa, obciążenie skupione*, *nośność poprzeczna środnika nieusztywnionego i z usztywnieniem*, *efektywna długość strefy docisku*

* Ph.D. Eng. Edyta Pięciorak, AGH University of Science and Technology, Faculty of Mining and Geoengineering, Department of Geomechanics, Civil Engineering and Geotechnology.

1. Introduction

Technical catalogue prepared by particular producers are usually used in the process of designing trapezoidal sheets. They help to avoid tedious calculations [1] in order to determine their carrying capacities. The choice of a trapezoidal sheet is made through comparison of its uniformly distributed design loads in ULS (ultimate limit state) and characteristic loads in SLS (serviceability limit state) with the limit values of the loading given in the tabular form. While choosing trapezoidal sheets, it is important to pay attention to the minimum width on the support, because the limit load values given in the technical catalogue are given under the condition it is sufficient [2, 3, 7]. However, the technical catalogue may only be a supplementary tool for designing the sheets under consideration. Rather, the standard PN-EN-1993-1-3:2008 [4] should be applied for a roof covering in certain instances. According to its guidelines, in the case of webs of trapezoidal sheets, unstiffened transversally within the cross-section at the end supports as well as at the internal supports, the check of the patch load acting on the webs neglected, though the widths of the supports are of great importance for the local transverse resistance of the sheets.

This paper presents the algorithm and examples of the determination of the local transverse resistance of unstiffened and stiffened webs for a trapezoidal sheet 92 mm high. The influence of support widths changing from 10 mm to 200 mm on the local transverse resistance of the web of trapezoidal sheets with thicknesses from 0.75 mm to 1.5 mm is visible.

2. The resistance of a trapezoidal sheet loaded by local transverse forces

2.1. The local transverse resistance of an unstiffened web of a trapezoidal sheet

To avoid crushing, crippling or buckling in a web subjected to a support reaction or other local transverse force applied through the flange, the transverse force F_{Ed} shall satisfy, according to (6.13) in [4]:

$$F_{Ed} \leq R_{w,Rd} \tag{1}$$

where

F_{Ed} – the transverse force,
$R_{w,Rd}$ – the local transverse resistance of the web, according to (6.18) in [4]:

$$R_{w,Rd} = \alpha \cdot t^2 \sqrt{f_{yb} \cdot E} \left(1 - 0.1\sqrt{\frac{r}{t}}\right)\left[0.5 + \sqrt{0.02\frac{l_a}{t}}\right]\left(2.4 + \left(\frac{\phi}{90}\right)^2\right) / \gamma_{M1} \tag{2}$$

where

r – the internal radius of the corners (see Fig. 1),
t – the design core thickness of the steel material before cold-forming, exclusive of metal and organic coatings (see Fig. 1),
ϕ – the angle of the web relative to the flanges [degrees] (see Fig. 1),
l_a – the effective bearing length for the relevant category,

α – the coefficient for the relevant category,
f_{yb} – the basic yield strength,
γ_{M1} – the partial factor.

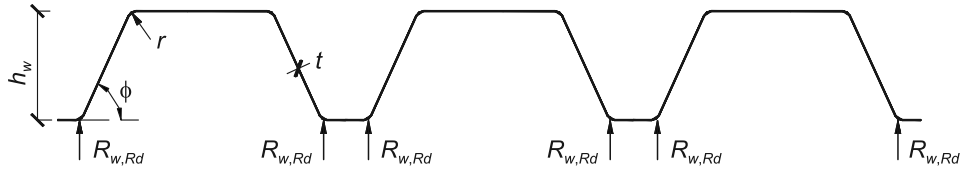

Fig. 1. Example of a cross-section for a trapezoidal sheet with a few unstiffened webs [4]

The local transverse resistance $R_{w,Rd}$ of an unstiffened web should be determined as specified in (2), provided that both of the following conditions are satisfied, according to (6.17) in [4]:

$$c \geq 40 \text{ mm} \tag{3}$$

$$\left(\frac{r}{t}\right) \leq 10 \tag{4}$$

$$\left(\frac{h_w}{t}\right) \leq 200 \sin\phi \tag{5}$$

$$45^{\circ} \leq \phi \leq 90^{\circ} \tag{6}$$

where

c – the distance from the support reaction to a free end (see Fig. 2, 3),
h_w – the web height between the midlines of the flanges (see Fig. 1).

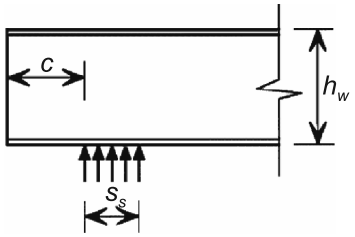

Fig. 2. Category 1 – reaction at the end support with $c \leq 1{,}5h_w$ clear from a free end [4]

The values of l_a and α should be obtained depending on category 1 and 2. The relevant category (l or 2) should be based on the clear distance c from the local load distributed on the distance s_s to a free end (see Fig. 2, 3).

The maximum value for l_a = 200 mm. When the support is a cold-formed section with one web or a round tube, a value of 10 mm should be taken for s_s. The value of the effective bearing length l_a should be obtained as follows, after formulas 6.19 in [4]:

for category 1:

$$l_a = 10 \text{ mm} \tag{7}$$

for category 2:

$$l_a = s_s \quad \text{for} \quad \beta_v \leq 0.2 \tag{8}$$

$$l_a = 10 \text{ mm} \quad \text{for} \quad \beta_v \geq 0.3 \tag{9}$$

l_a = interpolated linearly between the values of l_a for 0.2 and 0.3 for $0{,}2 < \beta < 0{,}3$ (10)

where

s_s – the length of stiff bearing,

and

$$\beta_v = \frac{|V_{Ed,1}| - |V_{Ed,2}|}{|V_{Ed,1}| + |V_{Ed,2}|} \tag{11}$$

in which $|V_{Ed,1}|$ and $|V_{Ed,2}|$ are the absolute values of the transverse shear forces on each side of the local load or the support reaction, and $|V_{Ed,1}| \geq |V_{Ed,2}|$.

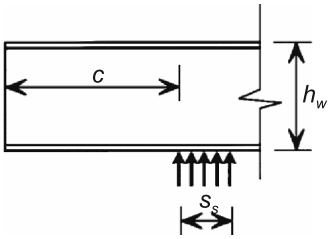

Fig. 3. Category 2 – reaction at the end support with $c > 1{,}5h_w$ clear from a free end [4]

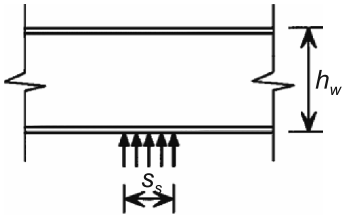

Fig. 4. Category 2 – reaction at the internal support [4]

The value of coefficient α should be obtained as follows:
for category 1:

$$\alpha = 0{,}075 \text{ for sheeting profiles} \tag{12}$$

for category 2:

$$\alpha = 0{,}015 \text{ for sheeting profiles} \tag{13}$$

The analytical calculations were carried out with use of Mathcad 14 [5] and the graphs were presented with the use of Microsoft Excel 2010 [6].

Example 1

Calculate the local transverse resistance of the unstiffened web of a 92 mm high trapezoidal sheet. The cross-section of the trapezoidal sheet is presented in Fig. 5.

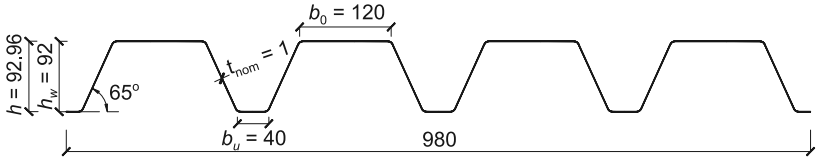

Fig. 5. The cross-section of a trapezoidal sheet 92 mm high

Calculation of the design thickness of the trapezoidal sheet

After formula (3.3c) in [4]:

$$t = t_{\text{cor}} = t_{\text{nom}} - t_{\text{metallic}} = 1.0 - 0.04 = 0.96 \text{ mm}$$

where:

- t – design core thickness of steel material before cold forming,
- t_{nom} – nominal sheet thickness after cold forming inclusive of zinc and other metallic coating, t_{nom} = 1.0 mm,
- t_{cor} – the nominal thickness minus zinc and other metallic coating,
- t_{metallic} – the thickness of the metallic coating (for the usual Z275 zinc coating, t_{zinc} = 0.04 mm).

Verification of the condition of the geometrical proportions of the trapezoidal sheet

After Table 5.1 in [4]:

For the upper flange:

$$\frac{b}{t} = \frac{120}{0.96} = 125 < 500$$

where according to Fig. 5: $b = b_0$ = 120 mm, as calculated: t = 0.96 mm.

For the bottom flange:

$$\frac{b}{t} = \frac{40}{0.96} = 41.67 < 500$$

where according to Fig. 5: $b = b_u$ = 40 mm, as calculated: t = 0.96 mm.

For the web:

$$45^{\text{o}} \le \phi = 65^{\text{o}} \le 90^{\text{o}}$$

$$\frac{h}{t} = \frac{92.96}{0.96} = 96.83 < 500 \cdot \sin(\phi) = 453.15$$

where according to Fig. 5: h = 92.96 mm, ϕ = 65°, as calculated: t = 0.96 mm.

Conclusion: Appropriate geometrical proportions a trapezoidal sheet allow the use of standard PN-EN-1993-1-3 [4].

Verification (obtained from 2–5) of the condition for a trapezoidal sheet during calculation of the local transverse resistance of the web

$$c \geq 40 \text{ mm}$$

$$\frac{r}{t} = \frac{6.5}{0.96} = 6.77 \leq 10$$

$$\frac{h_w}{t} = \frac{92}{0.96} = 95.83 \leq 200 \sin\phi = 181.26$$

$$45^o \leq \phi = 65^o \leq 90^o$$

where after Fig. 5: $h_w = 92$ mm.

Calculation of the local transverse resistance of the web

Category 1 – local load applied with $c \leq 1.5h_w = 1.5 \cdot 92 = 138$ mm clear from a free end (see Fig. 2).

After formula (2):

$$R_{w,Rd} = 0.075 \cdot 0.96^2 \sqrt{320 \cdot 2.1 \cdot 10^5} \left(1 - 0.1\sqrt{\frac{6.5}{0.96}}\right)\left[0.5 + \sqrt{0.02\frac{10}{0.96}}\right]\left(2.4 + \left(\frac{65}{90}\right)^2\right) \Big/ 1.0$$

$$R_{w,Rd} = 1.17 \text{ kN}$$

where

$\alpha = 0.075$ – for sheeting profiles (category 1),
$t = 0.96$ mm,
$f_{yb} = 320$ MPa,
$E = 210$ GPa,
$r = 6.5$ mm,
$l_a = 10$ mm – for category 1,
$\phi = 65$ deg,
$\gamma_{M1} = 1.0$.

Category 2 – reaction at the end support with $c > 1.5h_w = 1.5 \cdot 92 = 138$ mm clear from a free end (see Fig. 3) and reaction at the internal support (see Fig. 4), $\beta_v \geq 0.3$.

After formula (2):

$$R_{w,Rd} = 0.15 \cdot 0.96^2 \sqrt{320 \cdot 2{,}1 \cdot 10^5} \left(1 - 0.1\sqrt{\frac{6.5}{0.96}}\right)\left[0.5 + \sqrt{0.02\frac{10}{0.96}}\right]\left(2.4 + \left(\frac{65}{90}\right)^2\right) \Big/ 1.0$$

$$R_{w,Rd} = 2{,}343 \text{ kN}$$

where:

a = 0.15 – for sheeting profiles (category 2),
$l_a = 10$ mm – for category 2 and $b_v \geq 0.3$; the other values as above.

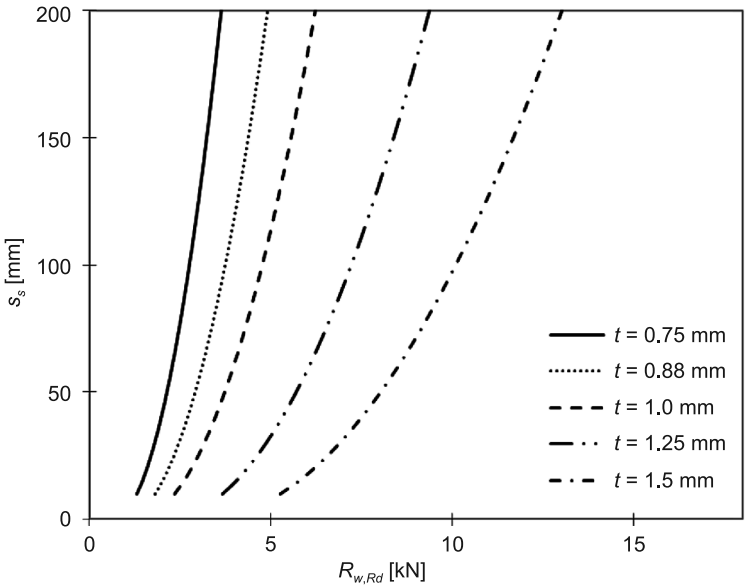

Fig. 6. Relation $s_s - R_{w,Rd}$ for the trapezoidal sheet 92 mm high, with an unstiffened web of thickness t = 0.75 mm – 1.5 mm

Figure 6 presents the way in which support widths s_s = 10 mm – 200 mm influence on the local transverse resistance of the unstiffened web of the trapezoidal sheet 92 mm high (category 2) of thickness from 0.75 mm to 1.5 mm.

2.2. The local transverse resistance of stiffened web of the trapezoidal sheet

For cross-sections with stiffened webs, the local transverse resistance of a stiffened web may be determined by multiplying the corresponding value for a similar unstiffened web by the factor $\kappa_{a,s}$, according to (6.22) in [4]:

$$F_{Ed} \leq R_{w,Rd} \cdot \kappa_{s,a} \tag{14}$$

where

$$\kappa_{a,s} = 1.45 - 0.05 \cdot \frac{e_{\max}}{t} \tag{15}$$

but

$$\kappa_{a,s} \leq 0.95 + 35000 \cdot t^2 \cdot \frac{e_{\min}}{(b_d^2 \cdot s_p)} \tag{16}$$

where (see Fig. 7):

$e_{\max}$ – the larger eccentricity of the folds relative to the system line of the web,
$e_{\min}$ – the smaller eccentricity of the folds relative to the system line of the web,
b_d – the developed width of the loaded flange,
s_p – the slant height of the plane web element nearest to the loaded flange.

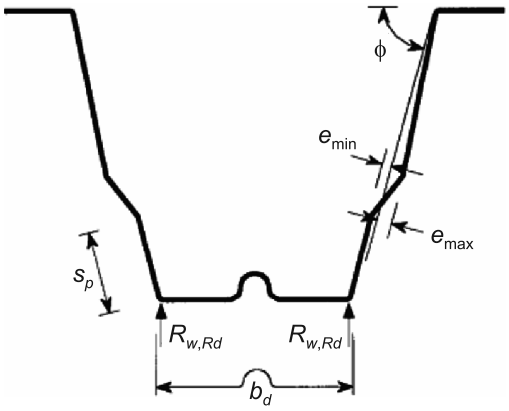

Fig. 7. Stiffened webs [4]

The local transverse resistance of a stiffened web may be determined as specified in (2) for cross-sections with longitudinal web stiffeners folded in such a way that the two folds in the web are on opposite sides of the system line of the web joining the points of intersection of the midline of the web with the midlines of the flanges (see Fig. 7), that satisfy the condition:

$$2 < \frac{e_{\max}}{t} < 12 \tag{17}$$

Example 2

Calculate the local transverse resistance of stiffened web of trapezoidal sheet 92 high. The cross-section of trapezoidal sheet are presented in Fig. 8.

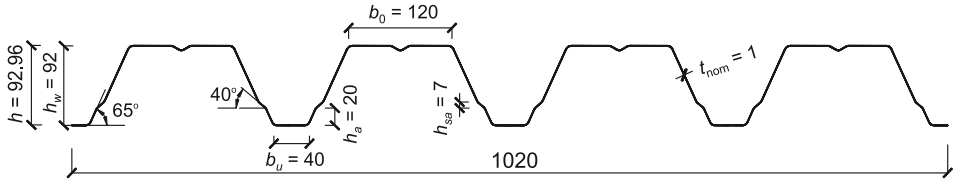

Fig. 8. The cross-section of a 92 mm high trapezoidal sheet

Calculation of the design thickness of the trapezoidal sheet

According to example 1.

Verification of the condition of the geometrical proportions of the trapezoidal sheet

According to example 1.

Verification (obtained from 2–5) of the condition of the trapezoidal sheet during calculation of the local transverse resistance of the web

According to example 1.

Calculation of the local transverse resistance of the unstiffened web

Category 1 – local load applied with $c \le 1.5h_w = 1.5 \cdot 92 = 138$ mm clear from a free end (see Fig. 2).

According to example 1: $R_{w,Rd} = 1.17$ kN

Category 2 – reaction at the end support with $c > 1.5h_w = 1.5 \cdot 92 = 138$ mm clear from a free end (see Fig. 3) and reaction at internal support (see Fig. 4), $\beta_v \ge 0.3$.

According to example 1: $R_{w,Rd} = 2.343$ kN

Calculation of the local transverse resistance of the stiffened web

After formula (17):

$$2 < \frac{e_{\max}}{t} = \frac{3.24}{0.96} = 3.375 < 12$$

After formula (15):

$$\kappa_{a,s} = 1.45 - 0.05 \cdot \frac{e_{\max}}{t} = 1.45 - 0.05 \cdot \frac{3.24}{0.96} = 1.281$$

where according to Fig. 7: $e_{max} = 3.24$ mm, as calculated: $t = 0.96$ mm.

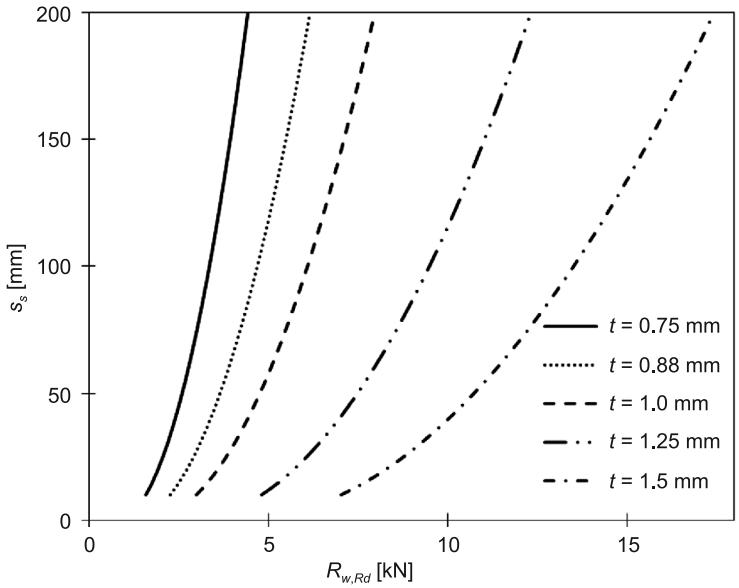

Fig. 9. Relation s_s - $R_{w,Rd}$ for the trapezoidal sheet 92 mm high, with an stiffened web from thickness $t = 0.5$ mm – 1.5 mm

After formula (16):

$$\kappa_{a,s} \le 0.95 + 35000 \cdot t^2 \cdot \frac{e_{\min}}{(b_d^2 \cdot s_p)} = 0.95 + 35000 \cdot (0.96)^2 \cdot \frac{1.0}{(40^2 \cdot 22.07)} = 1.864$$

$$\kappa_{a,s} = 1.281 \leq 1.864$$

where according to Fig. 7: $e_{\min}$ = 1.0 mm, $b_d = b_u$ = 40 mm, s_p = 22.07 mm, as calculated: t = 0.96 mm.

For cross-sections of a trapezoidal sheet 92 mm high with stiffened webs, the local transverse resistance of the stiffened web should be determined from:

$$R_{w,Rd} \cdot \kappa_{a,s} = 1.17 \cdot 1.281 = 1.5 \text{ kN} \quad \text{(category 1)}$$

$$R_{w,Rd} \cdot \kappa_{a,s} = 2.343 \cdot 1.281 = 3.0 \text{ kN} \quad \text{(category 2)}$$

Figure 9 presents the path in which support widths s_s = 10 mm – 200 mm influence on the local transverse resistance of the stiffened web of trapezoidal sheet 92 mm high (Category 2) of thickness from 0.75 mm to 1.5 mm.

3. Conclusions

The analysis of the influence of the support width s_s for the 92 mm high trapezoidal sheet showed an increase of the local transverse resistance of the web in the case of the modification of the support width s_s from 10 mm to 200 mm. The values and increase [%] of the local transverse resistance of the unstiffened and stiffened webs for different thickness t and support width s_s are given in Table 1.

Table 1

The values of the local transverse resistance Rw,Rd [kN]of the unstiffened and stiffened webs for the 92 mm high trapezoidal sheet

t [mm]	Web without stiffening			Web with stiffening		
	s_s = 10 mm	s_s = 200 mm	Increase $R_{w,Rd}$ [%]	s_s = 10 mm	s_s = 200 mm	Increase $R_{w,Rd}$ [%]
0.75	1.302	3.629	179	1.591	4.435	179
0.88	1.808	4.908	171	2.273	6.169	171
1.0	2.343	6.224	166	3.001	7.973	166
1.25	3.663	9.367	156	4.821	12.327	156
1.5	5.257	13.022	148	7.039	17.436	148

By comparison of the relation $s_s - R_{w,Rd}$ for the 92 mm high trapezoidal sheet with the unstiffened web (see Fig. 6) and with the stiffened web (see Fig. 9), it is possible to determine the influence of the stiffening of the web on its local transverse resistance. The stiffening of the web of the 92 mm high trapezoidal sheet results in an increase of transverse resistance in relation to the unstiffened web by about 22% for t = 0.75 mm, 26% for t = 0.88mm, 28% for t = 1.0 mm, 32% for t = 1.25 mm and 34% for t = 1.5 mm.

Moreover, the thicknesses of both the unstiffened and stiffened webs of the trapezoidal sheet have an important influence on its transverse resistance. An increase of the thickness t from 0.75 mm to 0.88 mm causes an increase the local transverse resistance

of the web by about 35% (with the unstiffened web) and by about 39% (the stiffened web). A further increase from 0.75 mm to 1.0 mm results in an increase the local transverse resistance of the web at about 71% (unstiffened web) and at about 80% (stiffened web). With an increase of thickness from 0.75 mm to 1.25 mm, the increase is approx. 158% (unstiffened web) and approx. 179% (stiffened web), and from 0.75 mm to 1.5mm it is approx. 259% (unstiffened web) and at about 293% (stiffened web).

This publication was supported by project 11.11.100.197/AS.

References

[1] Bródka J., Broniewicz M., Giżejowski M., *Kształtowniki gięte. Poradnik projektanta*, Polskie Wydawnictwo Techniczne, 2007.
[2] Pięciorak E., *Elementy z kształtowników i blach profilowanych na zimno*, XXVII Ogólnopolskie Warsztaty Pracy Projektanta Konstrukcji, tom II, Szczyrk, 7–10 marca 2012,147-208.
[3] Pięciorak E., Piekarczyk M., *Determination of Effective Cross-Section for Trapezoidal Sheet in Bending According to PN-EN 1993-1-3 Standard*, Czasopismo Techniczne, Budownictwo, R. 109, z. 3-B, 2012, 113-137.
[4] PN-EN 1993-1-3:2008 Eurocode 3. Design of Steel Structures. Part 1-3. General Rules. Supplementary Rules for Cold-Formed Members and Sheeting.
[5] Program Mathcad 14.
[6] Program Microsoft Excel 2010.
[7] Winter G., Pian R.H.J., *Crushing Strength of Thin Steel Webs*, Cornell University Engineering Experimental Station Bulletin, No 35, Part 1, 1946.

TECHNICAL TRANSACTIONS | **CZASOPISMO TECHNICZNE**
CIVIL ENGINEERING | BUDOWNICTWO
4-B/2014

IZABELA TYLEK*, KRZYSZTOF KUCHTA*

MECHANICAL PROPERTIES OF STRUCTURAL STAINLESS STEELS

WŁAŚCIWOŚCI MECHANICZNE KONSTRUKCYJNYCH STALI NIERDZEWNYCH

A b s t r a c t

In the paper, the mechanical properties of structural stainless steels referred to in EN 1993-1-4 [6] used in the design of building structures and civil engineering works, are described. Some information about stainless steel behaviour at elevated temperatures is also given.

Keywords: *stainless steel*, *mechanical properties*, *EN 1993-1-4*, *EN 1993-1-2*

S t r e s z c z e n i e

W artykule opisano właściwości mechaniczne konstrukcyjnych stali nierdzewnych objętych normą EN 1993-1-4 [6], stosowanych w projektowaniu budowlanych obiektów inżynierskich. Podano również informacje na temat zachowania stali nierdzewnych w podwyższonych temperaturach.

Słowa kluczowe: *stal nierdzewna*, *właściwości mechaniczne*, *EN 1993-1-4*, *EN 1993-1-2*

* Ph.D. Assist. Prof. Izabela Tylek, Ph.D. Assist. Prof. Krzysztof Kuchta, Institute of Building Materials and Structures, Faculty of Civil Engineering, Cracow University of Technology.

1. Introduction

The most important distinguishing feature of stainless steels is their greatly increased corrosion resistance in comparison to carbon steels. This is the result of applying chromium (Cr) as the main alloying component to a minimum quantity of 10.5% and limiting carbon (C) content to a maximum of 1.2%. The different chemical composition causes the formation of microstructures that usually do not occur in carbon steels and have a great influence on the physical and mechanical properties of stainless steel.

The paper describes mechanical properties (that are not material constants) of structural stainless steels covered by the European Standard EN 1993-1-4 [6].

2. Types, grades and designation of stainless steel

The main criterion of stainless steel classification is the microstructure, it is this that distinguishes different steels: ferritic; austenitic; austenitic-ferritic (so called duplex steels); martensitic; precipitation hardening. In building structures, designed according to EN 1993-1-4 [6], only ferritic, austenitic and austenitic-ferritic stainless steels with nominal yield strength f_y up to and including 480 N/mm^2 may be applied. Within the given microstructure, stainless steels can be additionally divided into grades of different chemical composition and physical, mechanical and technological properties.

The chemical compositions of particular grades of stainless steel are given in EN 10088 [12–16]. The composition ranges of main alloying elements for structural stainless steels listed in Table 2.1 EN 1993-1-4 [6] are given in Table 1.

Table 1

Chemical composition ranges for structural stainless steels

Type of stainless steel	Chemical composition [wt%]			
	C (max)	Cr	Ni	Mo
Ferritic	0.03–0.08	10.50–18.00	0–1.00	–
Austenitic	0.02–0.08	16.50–21.00	6.00–26.00	0–7.00
Austenitic-ferritic	0.03	21.00–24.00	3.50–6.50	0.10–3.50

For the reason of description conciseness, the most popular in engineering practice is the stainless steel numbering designation system [11]. The structure of steel number is as follows: 1.*xxyy*, where: 1 – material group number (steel), *xx* – steel group number, *yy* – sequential number of steel grade:

- 1.40*yy* – stainless steels with less than 2.5% nickel (Ni), without molybdenum (Mo), niobium (Nb) and titanium (Ti),
- 1.41*yy* – stainless steels with less than 2.5% nickel (Ni), with molybdenum (Mo) but without niobium (Nb) and titanium (Ti),
- 1.43*yy* – stainless steels with min. 2.5% nickel (Ni), without molybdenum (Mo), niobium (Nb) and titanium (Ti),

– 1.44*yy* – stainless steels with min. 2.5% nickel (Ni), with molybdenum (Mo) but without niobium (Nb) and titanium (Ti),
– 1.45*yy* – stainless steels with special additions.

Cold worked hardened stainless steels should be additionally marked by specifying one of the following parameters: C*nnn* – cold worked hardened with a minimum tensile strength of *nnn* MPa [10]; CP*nnn* – cold worked hardened with a minimum 0.2% proof strength of *nnn* MPa [10] or hardness (no specifications for the designation of hardness levels of cold worked hardened steels in [10]). Some details are given in Table 2.

Table 2

Nominal values of the yield strength f_y and the ultimate tensile strength f_u, for work hardened structural stainless steels to EN 10088 [6]

Type of stainless steel	0.2% proof strength level in the cold worked condition	f_y [N/mm^2]	Tensile strength level in the cold worked condition	f_u [N/mm^2]
Austenitic steels	CP350	350	C700	700
	CP500	500	C850	850
	CP700	700	C1000	1000

3. Mechanical properties of stainless steel

Supplementary provisions for the design of buildings and civil engineering works that extend and modify the application of EN 1993-1-1 [3], EN 1993-1-3 [5], EN 1993-1-5 [7] and EN 1993-1-8 [8] to austenitic, austenitic-ferritic and ferritic stainless steels are given in EN 1993-1-4 [6]. Indicated in [6] differences between mechanical and physical properties of carbon and stainless steels are important for structural safety. They include principal material properties (E, f_y) and also refer to stainless steel behaviour (e.g. σ–ε curve, behaviour during cold working or at elevated temperatures). These differences cannot be ignored during formulating and checking conditions of the ultimate and serviceability limit states in all design situations mentioned in EN 1990 [2].

3.1. Stress-strain behaviour

Stainless steels are characterized by a completely different stress-strain (σ–ε) curve than carbon steels. Unlike carbon steel, the stress-strain relationship of stainless steel is nonlinear (even in the elastic stage of material behaviour) with no explicit yield stress. Additionally, stainless steel σ–ε curves do not show a plateau before strain hardening which is typical of carbon steel (Fig. 1).

Nonlinearity of σ–ε curve is characterized by coefficient *n* defined as [1, 6]:

$$n = \frac{\log(0.05)}{\log(R_{p0.01} / f_y)} = \frac{\ln(20)}{\ln(f_y / R_{p0.01})} \tag{1}$$

where

$R_{p0,01}$ – the 0.01% proof stress,
f_y – the 0.02% proof stress.

According to [6], n may take the values from the range of 5–14 (see Table 4), the larger the coefficient n, the more the nonlinearity of the σ–ε curve. It means that the nonlinear elastic range of stainless steel behaviour, usually ignored in case of carbon steels, should be taken into account in the modelling of material behaviour, especially in the calculation of serviceability limit states (SLS) [6].

Stainless steels may be much more ductile than carbon grades which manifests as an ability to achieve large plastic strains in the range between yield strength and ultimate tensile strength. For example, elongation of austenitic stainless steel may be over 45%, while for structural carbon steel, it is around 25%.

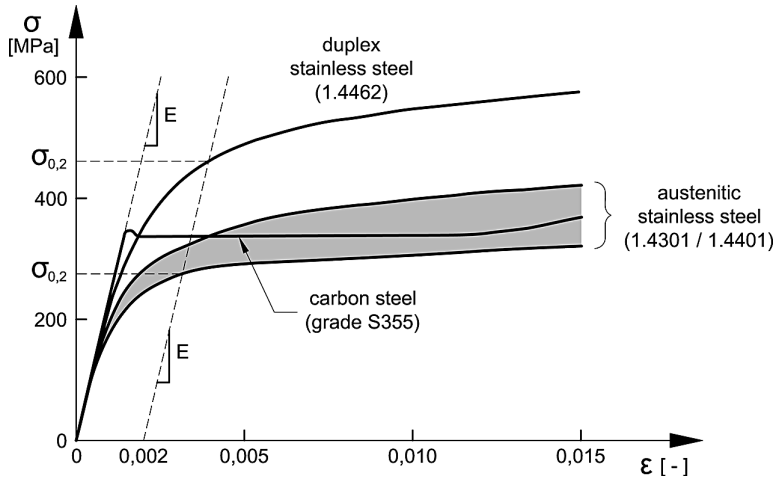

Fig. 1. Typical experimental stress-strain curves [1]

Plastic processing of stainless steel causes its work hardening which results in an increase in the yield strength, the ultimate strength and the hardness of the material. Further information about stainless steel work hardening is given in p. 3.4 of this paper. On the basis of numerous research investigations, it was shown that, in most cases, both cold and hot rolled material is characterized by higher strength in a direction transverse to the direction of rolling than in a longitudinal direction (see Table 3). It also has been found that stainless steel σ–ε curves do not show symmetry in case of compression and tension; in the annealed condition, σ–ε curves tend to be more nonlinear in tension than in compression [22]. Comparison of experimental values of mechanical properties of selected austenitic (1.4404) and austenitic-ferritic (1.4462) stainless steel grades allows us to notice that relative differences between values of the 0.2% proof strength due to anisotropy and asymmetry of stress-strain relationship do not exceed 5%. Anisotropy and asymmetry of stainless steel is the probable reason for increasing, in comparison with carbon steel, values of partial factors $\gamma_{M0} = 1{,}1$ and $\gamma_{M1} = 1{,}1$ recommended by EN 1993-1-4 [6]. Simultaneously, in design

Table 3

Representative values of stress-strain characteristics for materials in the annealed condition [22]

Stainless steel grade	Direction and character of stress	0.2% proof strength [N/mm^2]	Modulus of elasticity [kN/mm^2]	$\sigma_{0.01}/\sigma_{0.2}$	Index *n*
1.4404	LT	277	193	0.65	6.9
	LC	285		0.71	8.6
	TT	286	198	0.70	8.5
	TC	297		0.74	10.0
1.4462	LT	518	199	0.57	5.4
	LC	525		0.56	5.2
	TT	544	207	0.54	4.8
	TC	540		0.59	5.7

LT – Longitudinal tension,
LC – Longitudinal compression,
TT –Transverse tension,
TC – Transverse compression.

Table 4

Values of coefficient n according to [6]

Steel grade	Coefficient *n*	
	Longitudinal direction	Transverse direction
1.4003	7	11
1.4016	6	14
1.4512	9	16
1.4301	6	8
1.4306		
1.4307		
1.4318		
1.4541		
1.4401	7	9
1.4404		
1.4432		
1.4435		
1.4539		
1.4571		
1.4462	5	5
1.4362		

calculations, the values of yield strength (the 0.2% proof strength) f_y and ultimate tensile strength f_u should be assumed constant for a particular grade, independently of the direction of rolling and loading [6].

For the design of stainless steel structures, especially in the case of material in the annealed condition, nonlinear stress-strain curve with strain hardening according to Annex C of EN 1993-1-4 [6] may be used to describe material behaviour. This spline function is a modification of the well-known Ramberg-Osgood formula:

$$\varepsilon = \begin{cases} \dfrac{\sigma}{E} + 0.002\left(\dfrac{\sigma}{f_y}\right)^n & \text{for} \quad \sigma \le f_y \\ 0.002 + \dfrac{f_y}{E} + \dfrac{\sigma - f_y}{E_y} + \varepsilon_u\left(\dfrac{\sigma - f_y}{f_u - f_y}\right)^m & \text{for} \quad f_y < \sigma \le f_u \end{cases} \tag{2}$$

where

- n – the coefficient depending on rolling direction according to (1); it also may be taken from Table 4 or calculated from measured values,
- E_y – the tangent modulus of stress-strain curve at the yield strength, defined as $E_y = E/(1 + 0.002n\, E/f_y)$,
- ε_u – the ultimate strain, corresponding to the ultimate strength f_u; it may be obtained from approximation $\varepsilon_u = 1 - f_y/f_u$, but $\varepsilon_u \le A$ where A is the elongation after fracture defined in [13–16],
- m – the coefficient that may be determined as $m = 1 + 3.5\, f_y/f_u$.

Figure 2 shows nonlinear stress-strain curves for a longitudinal (solid lines) and a transverse (dashed lines) rolling direction, determined from formula (2), for the most popular grades of ferritic, austenitic and duplex stainless steels. To better demonstrate differences between stress-strain relationships for different rolling directions in the elastic range, stress-strain curves from Fig. 2 were drawn for limited range of strains (Fig. 3).

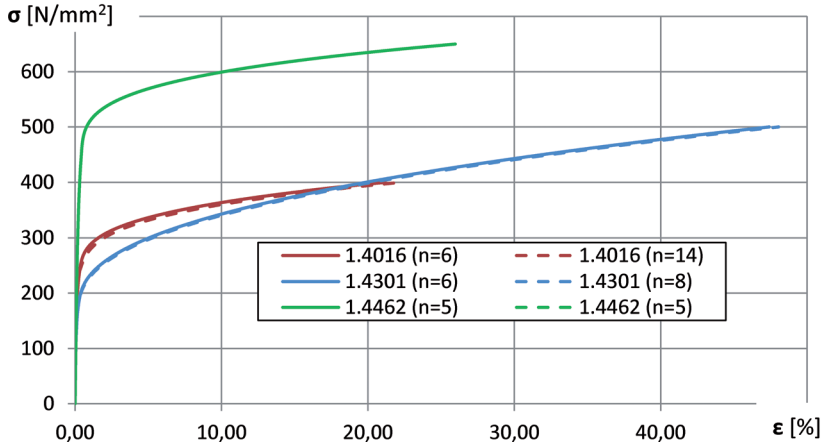

Fig. 2. Stress-strain curves for different types of stainless steel

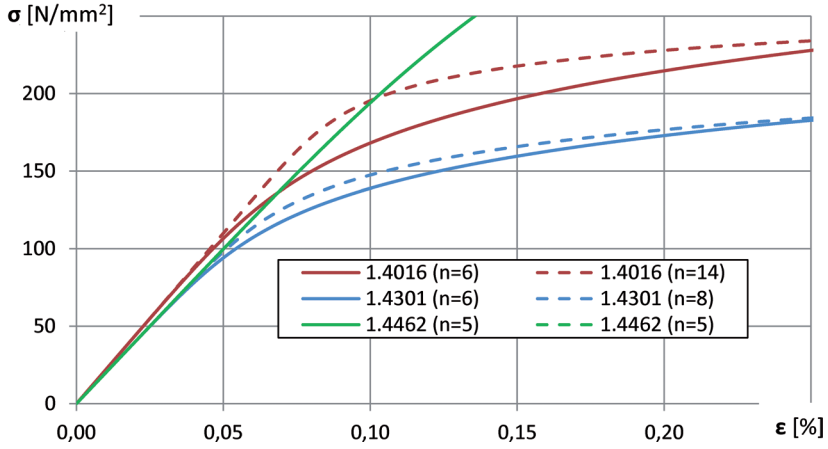

Fig. 3. Stress-strain curves for different types of stainless steel (limited strain range)

3.2. Influence of chemical composition and microstructure on mechanical properties of stainless steel

Mechanical properties of structural stainless steels significantly depend on their microstructure [1, 20, 21, 22] that is a derivative of both the chemical composition of the alloy and its heat treatment.

Austenitic and ferritic stainless steels have quite low yield strength: 175–300 MPa and 240–260 MPa, respectively, while in the case of the most common carbon steels it is 235(215) MPa for S235 grade and 355(335) for S355 grade, depending on element thickness.

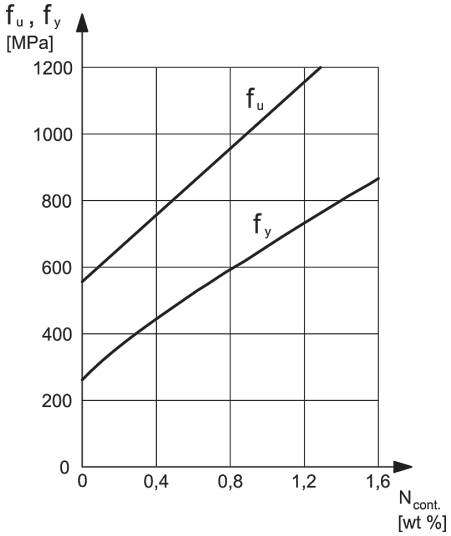

Fig. 4. Effect of nitrogen on the strength of austenitic stainless steels [17]

Austenitic-ferritic stainless steels are characterized by the highest yield strength from among all stainless steel types (even more than two times higher than for some austenitic grades).

The increasing of yield strength and tensile strength of austenitic stainless steels is mostly related to their high content of carbon (C) and nitrogen (N) which are alloying elements that improve these properties. If the nitrogen (N) content is increased from 0.05% to 0.20%, an increase of yield strength from 270MPa to 340MPa will be achieved [17]. Figure 4 shows the influence of nitrogen (N) content on yield strength and ultimate tensile strength of austenitic steels.

The strength of ferritic stainless steels increases with increasing carbon (C) content in the alloy; the influence of chromium (Cr) content on the strength of this type of stainless steel in negligible. At the same time, attainment of good ductility of ferritic steel requires a very low content of carbon (C) and nitrogen (N). High content of chromium (Cr) reduces ductility of ferritic stainless steels.

Table 5

Mechanical properties of stainless steel in the annealed condition at room temperature [16]

Type of stainless steel	Grade of stainless steel	Hardness HB[1)] max	0.2% proof strength $R_{p0,2}$ [MPa] min.	Tensile strength R_m [MPa]	Elongation after fracture A [%] (long.)
Ferritic	1.4003	100	260	450–600	20
	1.4016	100	240	400–630	20
Austenitic	1.4307	215[2)]	175	500–700[2)]	45
	1.4306	215[2)]	180	460–680[2)]	45
	1.4311	230[2)]	270	550–760[2)]	40
	1.4301	215[2)]	190	500–700[2)]	45
	1.4541	215[2)]	190	500–700[2)]	40
	1.4404	215[2)]	200	500–700[2)]	40
	1.4406	250[2)]	280	580–800[2)]	40
	1.4401	215[2)]	200	500–700[2)]	40
	1.4571	215[2)]	200	500–700[2)]	40
	1.4432	215[2)]	200	500–700[2)]	40
	1.4435	215[2)]	200	500–700[2)]	40
	1.4439	250[2)]	280	580–800[2)]	35
	1.4539	230[2)]	230	530–730[2)]	35
	1.4547	260[2)]	300	650–850[2)]	35
	1.4529	250[2)]	300	650–850[2)]	40
Austenitic--ferritic	1.4462	270	450	650–880	25
	1.4362	260	450	600–830	25

[1)] Only for guidance

[2)] The maximum HB-values may be raised by 100 HB or the tensile strength value may be raised by 200 MPa and the minimum elongation value may be lowered to 20% for sections and bars of ≤ 35 mm thickness having a final cold deformation and for hot formed sections and bars of ≤ 8 mm thickness.

Table 5 summarizes the basic mechanical properties of a max. 160 mm thick section made of structural stainless steels.

According to Table 5, the 0.2% proof strength $R_{p0,2}$ is about 25–50% of the tensile strength R_m for structural austenitic steels, 40–60% for structural ferritic steels and 50–75% for structural austenitic-ferritic steels.

The effect of alloying elements and microstructure on the strength of austenitic and austenitic-ferritic stainless steel may be estimated (with an uncertainty of approximately 20 MPa) from the following regression equations [20]:

$$R_{p0.2} = 120 + 210\sqrt{\mathrm{N} + 0.02} + 2\mathrm{Mn} + 2\mathrm{Cr} + 14\mathrm{Mo} + 10\mathrm{Cu} + (6.15 - 0.054\delta)\,\delta + \\ + (7 + 35(\mathrm{N} + 0.2))d^{-1/2} \quad [\mathrm{MPa}] \tag{3}$$

$$R_{p1.0} = R_{p0.2} + 40 \quad [\mathrm{MPa}] \tag{4}$$

$$R_m = 470 + 600\,(\mathrm{N} + 0.02) + 14\mathrm{Mo} + 1.5\delta + 8d^{-1/2} \quad [\mathrm{MPa}] \tag{5}$$

where

N, Mn, etc. – the level of the alloying elements [wt %],
δ – the ferrite content [%],
d – the grain size [mm].

Ferritic and austenitic-ferritic stainless steels have good ductility of similar orders of magnitude. Excellent ductility characterizes austenitic stainless steels, their elongation is about two times larger than in the case of ferritic or duplex structural steels and can reach 35–45% (Table 5).

The hardness of iron alloys, including stainless steels, is dependent on their chemical composition which is shown in Fig. 5.

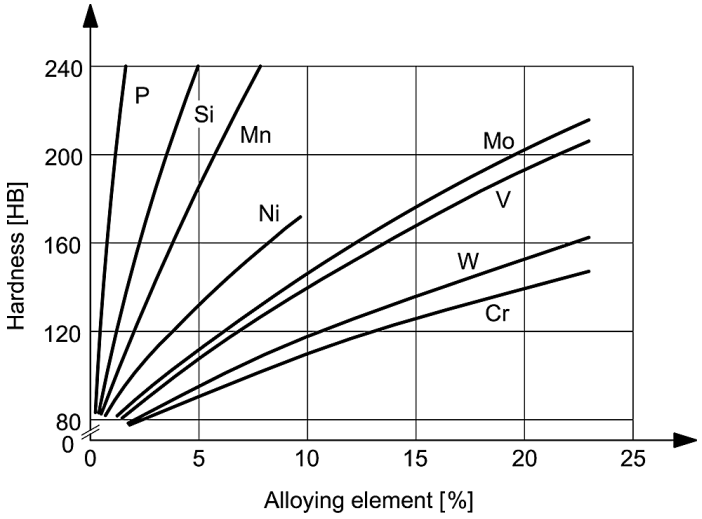

Fig. 5. Influence of substitutional elements on hardness of iron alloys [21]

The hardness of stainless steel differs between steel types (Table 5); the lowest value is for ferritic grades (~100 HB) and the highest – for austenitic-ferritic grades (250–260 HB).

3.3. Strain rate sensitivity

Strain rate sensitivity is more distinct in the case of stainless steels than in the case of carbon steels. Figure 6 illustrates the strain rate effect on the stress-strain curves of selected stainless steel grades.

It can be seen that higher values of strength and lower rupture strain are achieved at higher strain rates. In the design of blast walls made of stainless steel, where predominant loading is accompanied by a high strain rate, the design strength is customarily multiplied by a strain rate enhancement factor to utilize the increase in strength at higher strain rates [22].

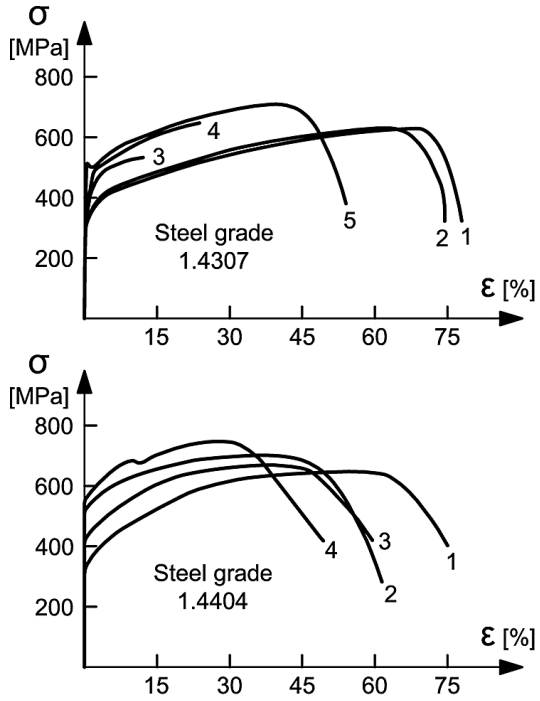

Curve	Strain rate [sec^{-1}]
1	10^{-4}
2	10^{-2}
3	50
4	140
5	502

Curve	Strain rate [sec^{-1}]
1	$0{,}4 \times 10^{-2}$
2	15
3	44
4	420

Fig. 6. Strain rate effect on grades 1.4307 and 1.4404 [22]

It should be also noted that the obtained results are influenced by the loading procedure. Constant stress rates usually give higher value of proof stresses than constant strain rates. The influence of the strain rate disappears at temperatures above 200°C – this is shown in Fig. 7 for stainless steel grade 1.4401.

The minimum values of stainless steel strength given in EN 10088 [13–16] are determined on the basis of tensile testing according to ISO 6892-1 [18]. In this international standard, two methods of testing speeds are available - based on strain rates (method A) and

based on stress rates (method B). During discussions concerning the speed of testing in the preparation of ISO 6892:1998, it was decided to recommend the use of strain rate control in future revisions [18].

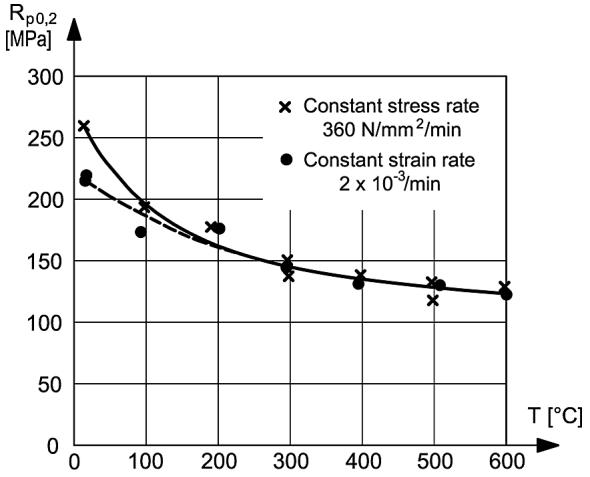

Fig. 7. Effect of loading procedure on the 0.2% proof stress [22]

The recommendations of method A given in [18] are aimed at minimizing the effect of strain rate variations and thus minimizing the measurement uncertainty of the test results. During determination of the upper yield strength R_{eH} or proof strength properties R_p (plastic extension) and R_t (total extension), the strain rate should be kept as 0.00025 s^{-1} (recommended) with a relative tolerance of ±20%, up to and including the determination of R_{eH} or R_p or R_t [18]. For the determination of the lower yield strength R_{eL}, maintaining the same value of strain rate is recommended until discontinuous yielding has ended [18]. To determine the tensile strength R_m and percentage elongation after fracture A, after determination of the required yield/proof strength properties, the strain rate shall be changed to 0.0067 s^{-1} (recommended) with a relative tolerance of ±20% [18].

3.4. Effect of cold working and heat treatment

One of the properties of stainless steel is its ability to harden to a higher rate than carbon steel. Structural stainless steel consistent with [6], i.e. steels with a ferritic, austenitic or austenitic-ferritic microstructure can only be hardened (i.e. made stronger) by cold working and cannot be strengthened by heat treatment. It was noticed that, because of work hardening, Bauschinger's effect occurs also for stainless steels [1, 22]. In general, cold working may cause increases of proof strengths and also ultimate tensile strength and a decrease of elongation. Figure 8 shows how cold working affects proof strengths, ultimate tensile strength and elongation after fracture of austenitic stainless steel grade 1.4307 and austenitic-ferritic grade 1.4462.

Cold working also intensifies the anisotropy and asymmetry of the stainless steel stress-strain relationship. The degree of asymmetry and anisotropy depends on the steel grade, the

level of cold working and the manufacturing route. Figure 9 compares stress-strain curves for stainless steel grade 1.4318, cold worked to strength level C850 (R_m = 850 – 1000 MPa) [13, 15], illustrating the differences caused by the change of direction and the character of the acting load.

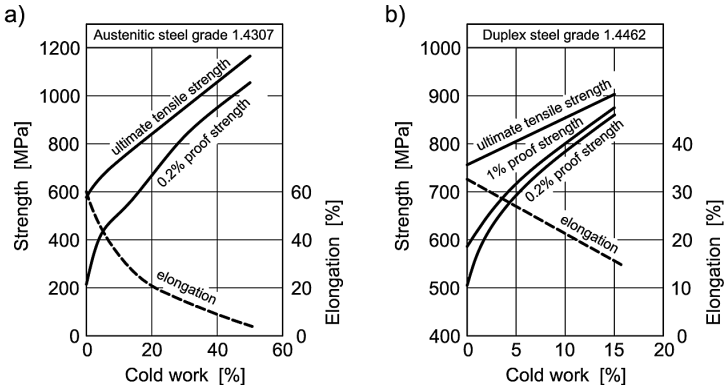

Fig. 8. Effect of cold working on a sample of stainless steel: a) austenitic grade 1.4307 b) austenitic-ferritic grade 1.4462 [22]

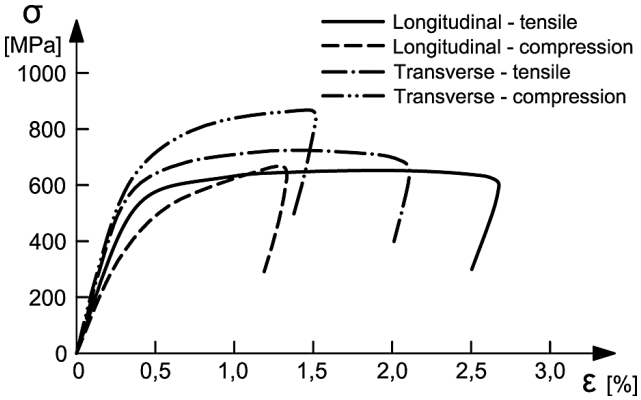

Fig. 9. Typical stress-strain curves for austenitic stainless steel grade 1.4318, cold worked to strength level C850 for transverse compression [23]

The work hardening of stainless steel may be caused by cold rolling (most often it is an intended effect) or by the fabrication process of the structural member (most often it is an unintended effect), or a combination of both. The 0.2% proof strength for the cold formed corners of the cross-section is around 20%-100% (usually 50%) higher than for flat parts of the cross-section [22, 23]. This is a local effect depending on the cross-section geometry. It has also been found that the degree of work hardening depends on the manufacturing methods. For example, if a rectangular hollow section is cold formed from annealed material in two stages (first the circular hollow section is fabricated and then it is shaped into a rectangular hollow section) a moderate increase in the strength of the flat parts and

a large increase in the strength of the corners is observed. In cases where the rectangular hollow section is fabricated by direct bending from a flat sheet, the strength of the flat parts is essentially unchanged, while the strength increase in the corners is large (but not as large as the enhancement with the indirect fabrication method) [22].

The stainless steel rate of work hardening (strength enhancement) depends on the steel microstructure and the alloy composition. For ferritic stainless steels, the work hardening is limited, while the rate of the work hardening of austenitic and austenitic-ferritic stainless steels is larger. Nickel (Ni), manganese (Mn), nitrogen (N), copper (Cu) and carbon (C) tend to reduce the rate of the work hardening, while most other alloying elements will increase it.

Rules for the use of stainless steel in the work hardened condition are given in Annex B of EN 1993-1-4 [6]. These rules may be applied only if the properties of work hardened steel are maintained during the fabrication and execution of the structure and during the whole design life of the structure. In the design of stainless steel structures [6], increased nominal values of yield strength f_y and ultimate tensile strength f_u may be adopted only for material delivered in the cold worked conditions specified in EN 10088 (type of process route 2H) [13–16]. Rules given in EN 1993-1-4 [6] are applicable only for material up to grade C700 and CP350, i.e. for work hardened structural stainless steel with an ultimate tensile strength f_u not higher than 700 MPa or with a yield strength f_y not higher than 350 MPa. In the case of higher grades, rules of [6] may only be applied if the structure is designed with cross-section resistance without local or global instability. In all other cases, stainless steel structures should be designed by testing according to Section 7 of [6]. Taking advantage of work hardening during the fabrication of structural components also requires verification by full size tests in accordance with [6].

Welding or heat treatment of cold worked stainless steel makes it partially or fully annealed. Steel microstructure gets back to its original form and steel strength decreases to original value (before cold working). Heat treatment like annealing or softening also reduces stainless steel anisotropy. Stainless steels are generally supplied in an annealed (softened) condition and mechanical properties given in EN 10088 [13–16] relate to steel in this condition. According to recommendations of EN 1993-1-4 [6], welding or heat treatment of products made of work hardened stainless steel should not be done unless it can be proved by testing that the execution of the structure will not reduce the mechanical properties below the values to be adopted.

3.5. Toughness

Toughness of stainless steel is diverse and changes with the steel microstructure and temperature. In Fig. 10, toughness of different stainless steel types and their changes with temperature are compared. As mentioned before, martensitic steels are not permitted for use in the design of building structures [6] due to, among other things, their low toughness (Fig. 10). It can be seen that, for all stainless steel types, toughness increases as the temperature increases and the largest quantitative differences relate to the low-temperature range.

Ferritic and austenitic-ferritic stainless steels are characterized by a change of behaviour from tough to brittle at a specific temperature (the so-called transition temperature) from the range of around –60°C to 0°C. Such a phenomenon is not observed in the case of austenitic stainless steels. The transition temperature of ferritic steels increases with increases

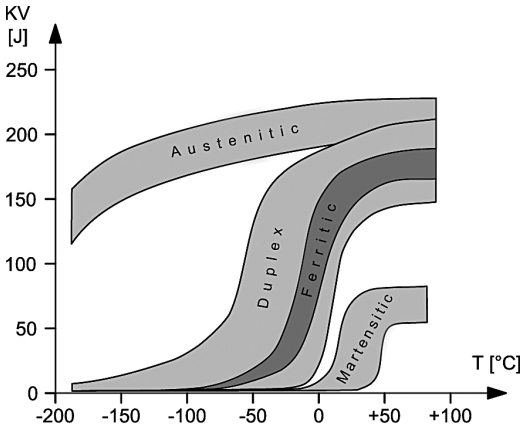

Fig. 10. Toughness for different types of stainless steels, where KV is the impact energy (Charpy V-Notch) [20]

in the carbon (C) and nitrogen (N) contents (steel becomes brittle at higher temperatures). The toughness of ferritic stainless steels is also strongly dependent on the grain size and metallurgical purity of the alloy. Coarse-grained ferritic stainless steels at room temperature often have very low toughness (at the level of 10 J/cm^2), therefore, after proper finishing of plastic processing, ferritic stainless steels should not be heated up to temperatures of fast grain growth, i.e. higher than 900°C. In the case of austenitic-ferritic stainless steels, a higher transition temperature is the effect of an increase in the ferrite content. Transition temperature of this stainless steel type is usually below –50°C and the lower value of impact strength is about 30 J. Austenitic stainless steels have very good toughness at all temperatures and because of a lack of toughness transition, are preferable for low temperature applications [19, 20].

3.6. Fatigue

Fatigue is the process of initiation and propagation of cracks in structure caused by cyclic loading. Initiation and propagation of fatigue cracks depend on stress amplitude, number of load cycles and its duration. Number of load cycles to structure failure (lifetime) increases with decreasing load amplitude (Fig. 11).

In table 6, fatigue properties (S_0 – load amplitude), determined for ferritic, austenitic and austenitic-ferritic stainless steels and a lifetime of 10^6–10^7 load cycles, with their tensile strength R_m are compared.

Analyses were conducted at two levels of loading asymmetry cycle coefficient ($R = 0$ and $R = -1$).

Stainless steel fatigue strength may change dependent on environment conditions. Figure 12 shows how an aggressive environment may affect the fatigue strength of stainless steel; lower pH denotes more aggressive conditions (equivalent grades according to EN 10027-2 [11] are given in brackets). Fatigue strength was determined at 40°C for rotating bending stress at 100 Hz. Tests were made in air and in 3% NaCl at various pH levels [20]. The fatigue strength of all the analyzed grades decreases with environment aggressiveness.

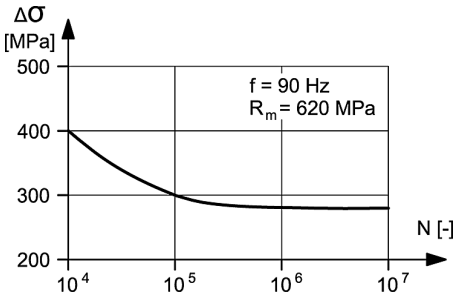

Fig. 11. S-N curve (Wöhler curve) for austenitic stainless steel grade 316HMo (equivalent grade: 1.4435) [20]

Table 6

Fatigue properties of stainless steels, relationship between tensile strength and fatigue strength [20]

Type of stainless steel	S_0/R_m		Permissible stress level
	Stress ratio		
	$R = -1$	$R = 0$	
Ferritic	0.70	0.47	Yield strength*)
Austenitic	0.45	0.30	Yield strength*)
Austenitic-ferritic	0.55	0.35	Yield strength*)
*) the value depends on stainless steel grade			

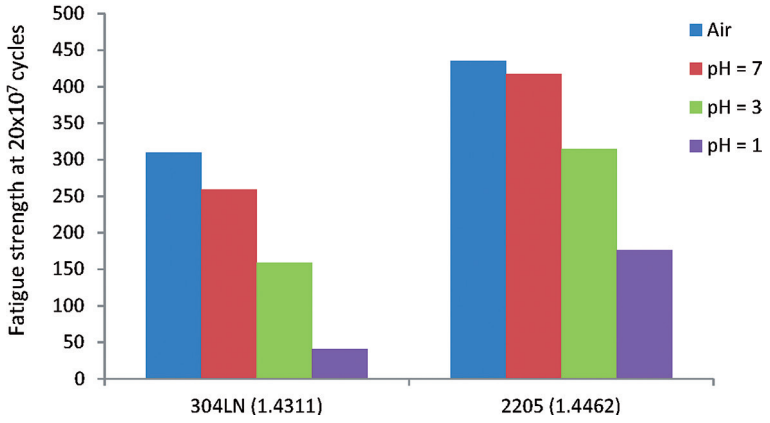

Fig. 12. Effect of environment aggressiveness on fatigue strength for selected stainless steel grades [20]

Proper detailing of structural elements helps prevent stress concentration and increases stainless steel fatigue strength. For that reason, sharp changes in cross-section, misalignments and eccentricities, partial penetration welds, intermittent welding and fillet welds should be avoided.

According to EN 1993-1-4 [6] fatigue strength of stainless steel structures should be determined on the basis of recommendations given in EN 1993-1-9 [9].

3.7. Properties of stainless steel at elevated temperatures

Steel is a non-combustible material, but in some cases, the effect of elevated temperatures on its mechanical properties must be taken into account. Behaviour of stainless steel structure at elevated temperatures is essential in the design for accidental situation of fire exposure.

Recommendations for structural fire design are given in EN 1993-1-2 [4]. The methods presented in [4] are also applicable to stainless steel members and sheeting within the scope of EN 1993-1-4 [6]. Properties of stainless steel at elevated temperatures are specified in Annex C of [4]. The stress-strain relationship for this type of steel at elevated temperatures is presented in Fig. 13.

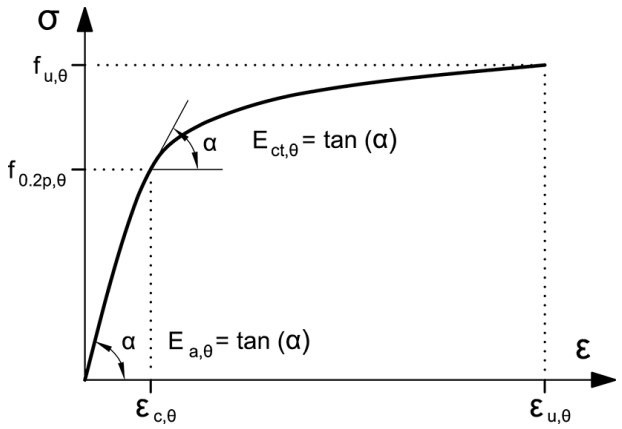

Fig. 13. Stress-strain relationship for stainless steel at elevated temperatures [4]

Symbols used in Fig. 13 are as follows:

$f_{u,\theta}$ – tensile strength,
$f_{0.2p,\theta}$ – the proof strength at 0.2% plastic strain,
$E_{a,\theta}$ – the slope of the linear elastic range,
$E_{ct,\theta}$ – the slope of proof strength,
$\varepsilon_{c,\theta}$ – the total strain at proof strength,
$\varepsilon_{u,\theta}$ – the ultimate strength.

Important parameters in the design of stainless steel structures exposed to fire are reduction factors applied to the stress-strain relationship for steel at elevated temperatures.

These reduction factors are defined as follows [4]:

– reduction factor for the modulus of elasticity (slope of linear elastic range at temperature θ, relative to slope at 20°C)

$$k_{E,\theta} = E_{a,\theta} / E_a, \tag{6}$$

– reduction factor for the yield strength (proof strength at temperature θ, relative to yield strength at 20°C)

$$k_{0.2p,\theta} = f_{0.2p,\theta} / f_y, \tag{7}$$

– reduction factor for the tensile strength (tensile strength at temperature θ, relative to tensile strength at 20°C)

$$k_{u,\theta} = f_{u,\theta} / f_u. \tag{8}$$

Analogously, as in the case of carbon steel, the reduction factor for the effective yield strength can also be determined:

$$k_{y,\theta} = f_{y,\theta} / f_y. \tag{9}$$

Stainless steel effective yield strength $f_{y,\theta}$ may be calculated using the correction factor $k_{2\%,\theta}$ given in Annex C of EN 1993-1-2 [4]:

$$f_{y,\theta} = f_{0.2p,\theta} + k_{2\%,\theta}(f_{u,\theta} - f_{0.2p,\theta}). \tag{10}$$

Reduction factors for the slope of the linear elastic range $k_{E,\theta}$ according to (6) and for effective yield strength $k_{y,\theta}$ according to (9), determined for stainless steel selected grades (1.4330 – ferritic, 1.4301 – austenitic, 1.4462 – duplex) and for carbon steel, are compared in Fig. 14–15 (20–1200°C) and in Table 7 (600–1100°C).

Table 7

Reduction factors for the determination of stiffness and strength at elevated temperatures [4]

Steel temp. [°C]	Reduction factor for the slope of the linear elastic range $k_{E,\theta} = E_{a,\theta}/E_a$				Reduction factor for the effective yield strength $k_{y,\theta} = f_{y,\theta}/f_y$			
	1.4003	1.4301	1.4462	carbon steel	1.4003	1.4301	1.4462	carbon steel
600	0.7600	0.7600	0.7600	0.3100	0.575	0.718	0.647	0.470
700	0.7100	0.7100	0.7100	0.1300	0.270	0.590	0.441	0230
800	0.6300	0.6300	0.6300	0.0900	0.167	0.424	0.325	0.110
900	0.4500	0.4500	0.4500	0.0675	0.142	0.237	0.133	0.060
1000	0.2000	0.2000	0.2000	0.0450	0.110	0.110	0.043	0.040
1100	0.1000	0.1000	0.1000	0.0225	0.055	0.050	0.022	0.020

As it can be seen, reduction of stainless steel modulus of elasticity depends on steel temperature. In comparison with value of Young's modulus at 20ºC, this reduction varies from 24% at 600°C to 90% at 1100°C. It should be noted, that reduction of carbon steel modulus of elasticity is higher – 69% at 600°C and 97.75% at 1100°C. Effective yield strength of stainless steel at a temperature of 600ºC is equal to 57.5%–71.8% of yield strength value at a temperature of 20°C. At a temperature of 1100°C effective yield strength decreases to 2.2%–5.5% of its value at a temperature of 20°C. In the case of carbon steel, reduction of effective yield strength in temperature range 600°C to 900°C is greater than in the case of stainless steel. In temperature range 1000–1100°C effective yield strength reduction is greater for carbon steel and duplex stainless steel than for

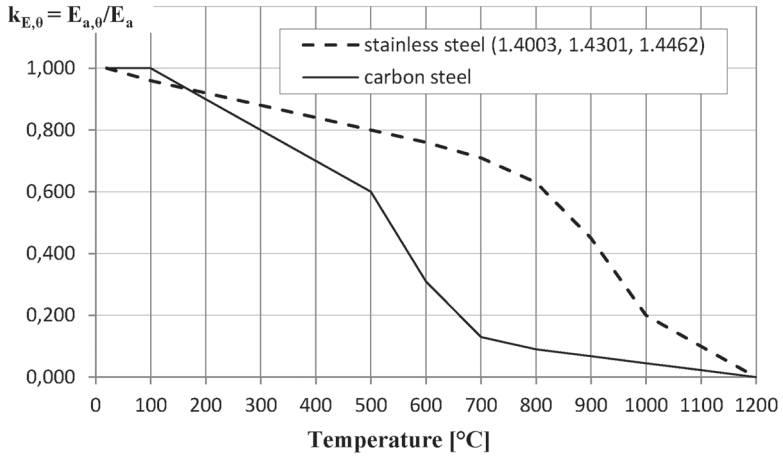

Fig. 14. Reduction factor $k_{E,\theta}$ for the slope of linear elastic range

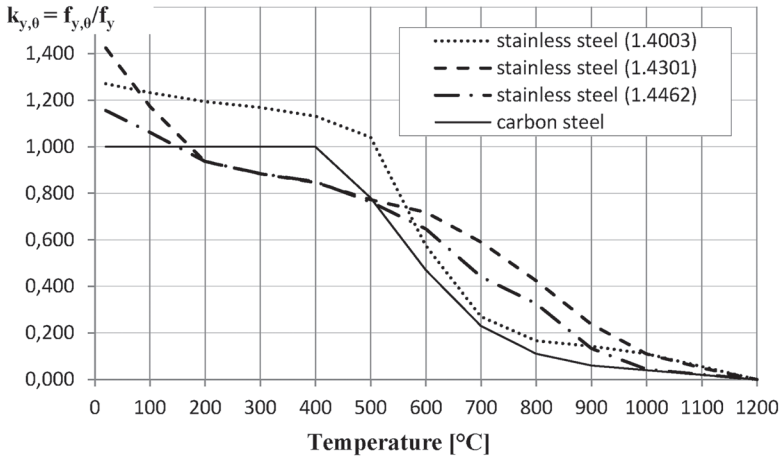

Fig. 15. Reduction factor $k_{y,\theta}$ for the effective yield strength

ferritic and austenitic stainless steels. Summarizing, in the structural design for accidental situation of fire exposure, reduction of stiffness at temperatures above 200°C and reduction of resistance at temperatures above 500°C is lower for analyzed stainless steel grades than for carbon steel.

The strength of stainless steel at elevated temperatures is also described by its creep strength, which is its ability to resist distortion over a long-term exposure to high temperature. Creep strength is usually measured by creep-rupture strength, i.e. the stress value that causes specimen rupture after 100 000 hours of exposure (basic value). If deformation is of greater concern, then the design may be based on creep deformation strength, i.e. the stress value that causes specimen strain of 1% after 100 000 hours of exposure. Figure 16 shows how the strengths of stainless steels change with increasing temperature.

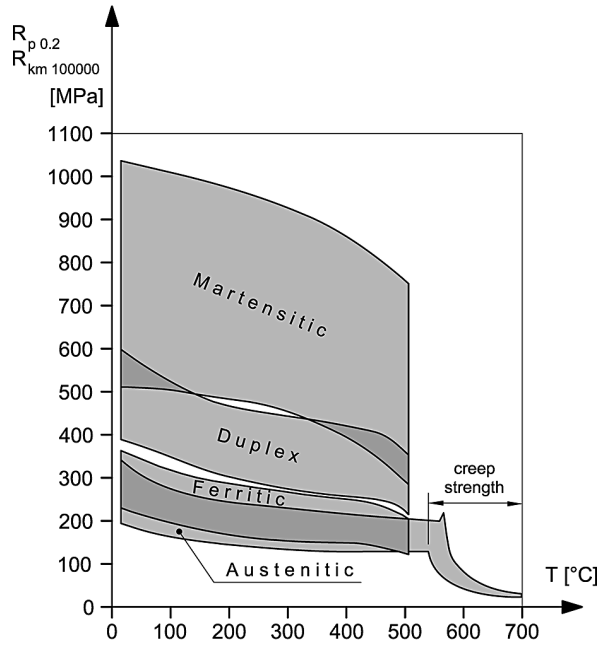

Fig. 16. Elevated temperature strength of stainless steels, including nonstructural type – martensitic [20]

Ferritic stainless steels keep quite high strength up to temperatures of around 500°C, but at higher temperatures where deciding is creep strength – low for this type of stainless steel – their application is usually limited. Furthermore, at temperatures above 350°C, embrittlement of these steels may occur.

Austenitic-ferritic stainless steels at temperatures of up to 500°C have higher strength than all other stainless steels, but their creep strength is low (Fig. 16). The disadvantage of this stainless steel type, as in the case of ferritic grades, is the risk of embrittlement at temperatures above 350°C, so this is usually the upper limit of their service temperature.

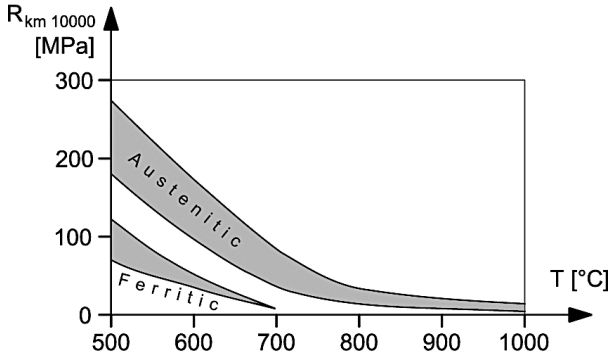

Fig. 17. Creep strength of ferritic and austenitic stainless steels [20]

The strength of most austenitic structural stainless steels at temperatures 0–500°C is lower than in the case of other stainless steels (Fig. 16) while at higher temperatures, they are characterized by superior creep strength – Fig. 16 and Fig. 17.

The coefficient of thermal expansion α, the thermal conductivity k, and the specific heat c, are physical not mechanical properties. The response of the mechanical model of stainless steel structure strongly depends on these thermal quantities, they are briefly described below.

The coefficient of thermal expansion α and thermal conductivity k are the properties that take significantly different values depending on the microstructure of stainless steel, they also distinguish stainless steel from carbon steel.

Values of coefficient of thermal expansion α between 20°C and 100°C for ferritic and austenitic-ferritic stainless steel are similar to that of carbon steel, but austenitic structural grades may have an almost 40% higher coefficient of thermal expansion than carbon steel [12]. High thermal expansion of austenitic stainless steels is the reason for large thermal stresses and distortions. The thermal elongation of austenitic stainless steel referred to in EN 1993-1-4 [6], may be determined according to Annex C of EN 1993-1-2 [4]; it monotonically increases with increasing steel temperature.

The thermal conductivity k of stainless steel is lower than the thermal conductivity of carbon steel which is related to a high chromium content in stainless steels. At temperature of 20°C the lowest thermal conductivity has austenitic stainless steel (12––15 W/m·K). The highest thermal conductivity at the same temperature has ferritic stainless steel (25 W/m·K) [12]. By comparison, carbon steel thermal conductivity k at 20°C is about 53 W/m·K. The thermal conductivity of stainless steel increases with increasing temperature [4].

The specific heat c of ferritic stainless steels (430–460 J/kg·K) is similar to those of carbon steels (440 J/kg·K), while most austenitic and duplex grades have around 15% larger specific heat [12]. Stainless steel specific heat is a monotonically increasing function of temperature; its value may be calculated according to Annex C of EN 1993-1-2 [4].

4. Conclusions

Stainless steels may have different mechanical properties depending on their chemical content and microstructure. In the design of buildings and civil engineering works, only ferritic, austenitic and austenitic-ferritic (duplex) stainless steels are approved for use [6]. Austenitic stainless steels are the most common type. These steels are characterized by good strength and ductility and can be harden by cold working. Ferritic stainless steels do not have as good ductility as austenitic grades, but the strength of some ferritic grades (Table 2.1 of [6]) is higher than that of austenitic ones. Austenitic-ferritic (duplex) stainless steels combine properties of austenitic and ferritic steels. They have higher strength than austenitic grades, but lower ductility. Ferritic and duplex stainless steels can be hardened only by cold working.

Differences between the behaviour and properties of carbon and stainless steels are specified in EN 1993-1-4 [6] and should be taken into account in the design of building

structures. One of these differences refers to the stress-strain curve: for stainless steel, it is nonlinear, even in the elastic stage of material behaviour, with no explicit yield stress and not showing a plateau before strain hardening. Another characteristic is that the modulus of elasticity depends upon the steel grade.

Mechanical, physical and technological properties of stainless steel, its behaviour during cold working and heat treatment, or at elevated temperatures, defines the scope of applications of this kind of steel. In comparison with popular carbon steel grades (S235 and S355), structural stainless steels are generally characterized by higher strength, higher ductility, a higher work hardening rate, lower thermal conductivity, and most of all, higher corrosion resistance. Unfortunately, with all these advantages, stainless steel is about four times more expensive than carbon steel. The high price of stainless steel may be compensated by lower steel consumption due to higher strength, lower costs of structure maintenance due to lack of anticorrosive coatings and the long life cycle of structure. Therefore, choosing between cheaper carbon steel and more expensive stainless steel should be preceded by a wider analysis of the total investment costs and not only the costs of building materials.

References

[1] Baddoo N.R., Burgan B.A., *Structural design of stainless steel*, SCI Publication P291, The Steel Construction Institute, Ascot, 2001.
[2] EN 1990:2002. Eurocode – Basis of structural design.
[3] EN 1993-1-1:2005. Eurocode 3 – Design of steel structures – Part 1-1: General rules and rules for buildings.
[4] EN 1993-1-2:2005. Eurocode 3 – Design of steel structures – Part 1-2: General rules – structural fire design.
[5] EN 1993-1-3:2006. Eurocode 3 – Design of steel structures – Part 1-3: General rules – Supplementary rules for cold-formed members and sheeting.
[6] EN 1993-1-4:2006. Eurocode 3 – Design of steel structures – Part 1-4: General rules – Supplementary rules for stainless steels.
[7] EN 1993-1-5:2006. Eurocode 3 – Design of steel structures – Part 1-5: Plated structural elements.
[8] EN 1993-1-8:2005. Eurocode 3 – Design of steel structures – Part 1-8: Design of joints.
[9] EN 1993-1-9:2005. Eurocode 3 – Design of steel structures – Part 1-9: Fatigue.
[10] EN 10027-1:2005. Designation systems for steels – Part 1: Steel names.
[11] EN 10027-2:1992. Designation systems for steels – Part 2: Numerical system.
[12] EN 10088-1:2005. Stainless steels – Part 1: List of stainless steels.
[13] EN 10088-2:2005. Stainless steels – Part 2: Technical delivery conditions for sheet/plate and strip of corrosion resisting steels for general purposes.
[14] EN 10088-3:2005. Stainless steels – Part 3: Technical delivery conditions for semi-finished products, bars, rods, wire, sections and bright products of corrosion resisting steels for general purposes.
[15] EN 10088-4:2009. Stainless steels – Part 4: Technical delivery conditions for sheet/plate and strip of corrosion resisting steels for construction purposes.
[16] EN 10088-5:2009. Stainless steels – Part 5: Technical delivery conditions for bars, rods, wire, sections and bright products of corrosion resisting steels for construction purposes.
[17] International Molybdenum Association, *Practical guidelines for the fabrication of high performance austenitic stainless steels*, London 2010.

[18] ISO 6892-1:2009. Metallic materials – Tensile testing – Part 1: Method of test at room temperature.
[19] Kaliszewski E., Czyżowicz S., *Podstawowe wiadomości o stalach odpornych na korozję*, (online) homepage, http://www.n-s.pl/betolit/betolit/porady/stal.pdf (date of access: 2014-01-30).
[20] Leffler B., *Stainless steel and their properties*, (online) homepage: www.hazmetal.com, (date of access: 2014-01-30).
[21] McGuire M.F., *Stainless steel for design engineers*, ASM International, Ohio, 1st Edition, 2008.
[22] The European Stainless Steel Development Association Euro Inox and The Steel Construction Institute, *Design manual for structural stainless steel – Commentary (Second Edition)*, 2003.
[23] The European Stainless Steel Development Association Euro Inox and The Steel Construction Institute, *Design manual for structural stainless steel (Third Edition)*, 2006.

TECHNICAL TRANSACTIONS | CZASOPISMO TECHNICZNE
CIVIL ENGINEERING | BUDOWNICTWO
4-B/2014

IZABELA TYLEK*, KRZYSZTOF KUCHTA*

PHYSICAL AND TECHNOLOGICAL PROPERTIES OF STRUCTURAL STAINLESS STEEL

WŁAŚCIWOŚCI FIZYCZNE I TECHNOLOGICZNE KONSTRUKCYJNYCH STALI NIERDZEWNYCH

A b s t r a c t

The paper summarizes microstructures and, associated with them, the physical and technological properties of structural stainless steel covered by EN 1993-1-4 [4]. Recommendations of the code [4] concerning the modelling of stainless steel properties are also described.

Keywords: *stainless steel*, *physical and technological properties*, *EN 1993-1-4*

S t r e s z c z e n i e

W artykule opisano struktury wewnętrzne i związane z nią właściwości fizyczne i technologiczne konstrukcyjnych stali nierdzewnych zgodnych z EN 1993-1-4 [4]. Podano również zalecenia zwarte w [4], dotyczące modelowania właściwości stali nierdzewnej.

Słowa kluczowe: *stal nierdzewna*, *właściwości fizyczne i technologiczne*, *EN 1993-1-4*

* Ph.D. Assist. Prof. Izabela Tylek, Ph.D. Assist. Prof. Krzysztof Kuchta, Institute of Building Materials and Structures, Faculty of Civil Engineering, Cracow University of Technology.

1. Introduction

Stainless steels, due to their appropriate chemical composition, are resistant to corrosion. Their diverse chemical composition and relatively high content of chemical components (e.g. by comparison with alloy steels) [7–11] cause that different microstructures may arise during alloy solidification. Physical and technological properties of the alloy strongly depend on its microstructure. Usually, the stainless steel microstructure contains one or two principal phases which determine the physical, mechanical and anticorrosive properties of steel. It should be noted that, if there is no proper control of the alloy chemical composition or the production technology, phases other than principal may occur in stainless steel microstructure. These additional phases may have a negative impact on properties of stainless steel. There are some methods that allow for determining which stainless steel phases will exist for a given alloy composition and temperature so it can be pointed out what kind of thermal treatments are needed to obtain the required microstructure of stainless steel. For complicated alloy systems, it is very difficult to determine analytically which phase may occur for given chemical composition and temperature. For this reason, most published phase diagrams enabling the calculations of existing phases are experimentally derived [15].

Stainless steel may be marked in accordance with two designation systems, one of which being the numbering system consistent with [6], according to which:

- 1.40*xx* – stainless steels with less than 2.5% nickel (Ni), without molybdenum (Mo), niobium (Nb) and titanium (Ti),
- 1.41*xx* – stainless steels with less than 2.5% nickel (Ni), with molybdenum (Mo) but without niobium (Nb) and titanium (Ti),
- 1.43*xx* – stainless steels with at least 2.5% nickel (Ni), without molybdenum (Mo), niobium (Nb) and titanium (Ti),
- 1.44x*x* – stainless steels with at least 2.5% nickel (Ni), with molybdenum (Mo) but without niobium (Nb) and titanium (Ti),
- 1.45*xx* – stainless steels with special additions.

Two last numbers (*xx*) specify subsequent grades within the group of stainless steels.

In this paper, microstructure and physical and technological properties of structural stainless steels covered by European Standard EN 1993-1-4 [4] are described.

2. Chemical composition and microstructure of stainless steel

The term ‘stainless steel’ concerns a chemically diverse group of iron-base (Fe) alloys. In these kinds of alloys, the main element of chemical composition, besides iron (Fe), is chromium (Cr) that provides appropriate corrosion resistance. According to EN 10088-1 [7], stainless steel should contain at least 10.5% of chromium and not more than 1.20% of carbon (C). Proper alloy chemical composition guarantees formation of appropriate microstructure of stainless steel and, related with it, required physical, mechanical and technological properties of stainless steel. Chemical compositions of structural stainless steel is given in Fig. 1 and in Fig. 2 [7].

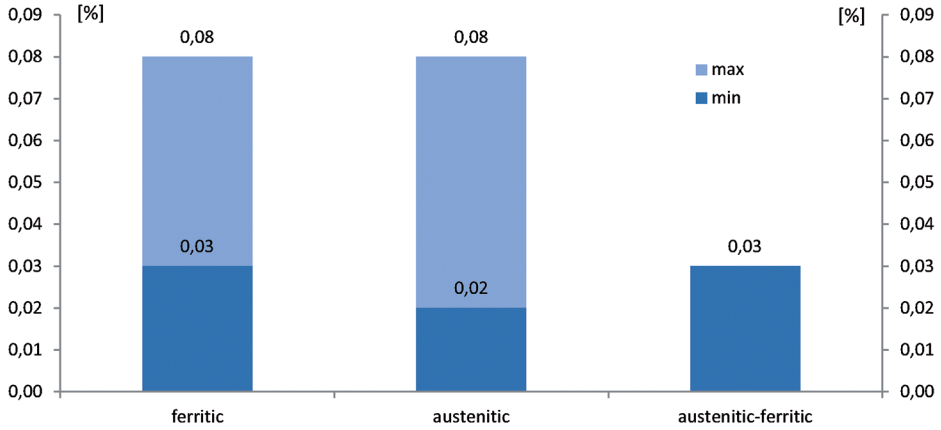

Fig. 1. The range of maximum carbon (C) content for different stainless steel categorie

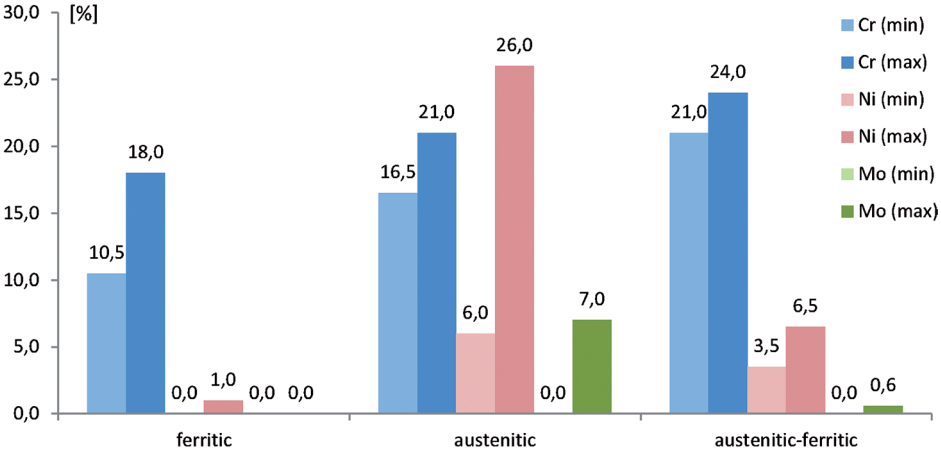

Fig. 2. The range of main alloying element content for different stainless steel categories

During alloy solidification, the diverse chemical composition of stainless steel causes the possible occurrence of three principal phases: martensite; ferrite; austenite. The content of these phases in steel microstructure determines the properties of the particular categories and grades of stainless steel [13–15], is described below. According to the current European Standard for the design of buildings and civil engineering works made of stainless steel [4], as structural steels, only steels with a ferritic, austenitic or austenitic-ferritic microstructure can be used. Austenitic-ferritic steels are also called duplex steels.

The principal property of stainless steels, according to the definition included in [7], is their resistance to corrosion resulting from high (min. 10.5%) chromium (Cr) content. The chromium (Cr) content enables the formation of a thin passive film on the element surface, protecting stainless steel elements from corrosion. Chromium (Cr) is also the main alloying element that promotes the ferritic microstructure of stainless steel. Silicon (Si),

aluminum (Al), molybdenum (Mo), wolfram (W), niobium (Nb) and titanium (Ti) have a similar influence on stainless steel microstructure. Additionally, titanium (Ti) enhances toughness and corrosion resistance and silicon (Si) increases the oxidation resistance of ferritic stainless steel. The formation of a stable ferritic microstructure is not favoured by the presence of carbon (C) and nitrogen (N), their content in ferritic stainless steels is limited to 0.025% (C) and 0.015% (N) [7]. Moreover, the presence of carbon (C) and nitrogen (N) strongly decreases toughness and corrosion resistance of this category of stainless steel.

The main alloying element that promotes the austenitic microstructure of stainless steel is nickel (Ni). Its content in austenitic stainless steel, according to [7], is not less than 3.0%, while for structural grades specified in Table 2.1 of EN 1993-1-4 [4] – min. 6.0%. Nickel (Ni) increases the ductility and toughness of stainless steel, enhances corrosion resistance in acid environments and resistance to stress corrosion, but it also reduces the rate of work hardening during cold deformation. Other elements that promote an austenitic microstructure are carbon (C) and copper (Cu). Carbon (C) increases strength, but may decrease resistance to corrosion. According to [7], in austenitic stainless steels, the content of carbon (C) is limited to 0.020%. Copper (Cu) increases corrosion resistance in some acid environments. Nitrogen (N) is another austenite former – it also enhances resistance to localized corrosion, especially in the presence of molybdenum (Mo). Manganese (Mn) can have an influence on the balance between austenite and ferrite in stainless steel microstructure. Depending on alloy temperature, it may be an austenite former (at low temperatures) or a ferrite former (at high temperatures). Manganese (Mn) improves hot ductility it is used to deoxidize molten steel and, as it increases the solubility of nitrogen (N), it is also used to obtain a higher nitrogen content and enhance strength and resistance to corrosion. The addition of titanium (Ti), as well as the addition of niobium (Ni), increases resistance to the intergranular corrosion of austenitic stainless steels, it also improves mechanical properties at high temperatures.

With regard to stainless steel microstructure, alloying elements can be divided into ferrite and austenite stabilizers, which are those which promote a ferritic microstructure and those which promote an austenitic microstructure [13], see Table 1.

Table 1

Classification of alloying elements

Ferrite stabilizers	Austenite stabilizers
Iron (Fe)	Nickel (Ni)
Chromium (Cr)	Nitrogen (N)
Molybdenum (Mo)	Carbon (C)
Silicon (Si)	Manganese (Mn)
Niobium (Nb)	Copper (Cu)
Aluminum (Al)	
Titanium (Ti)	
Wolfram (W)	

Based on this classification, a Schaeffler-Delong diagram, which illustrates the effect of the alloying elements on stainless steels microstructure, was developed (Fig. 3).

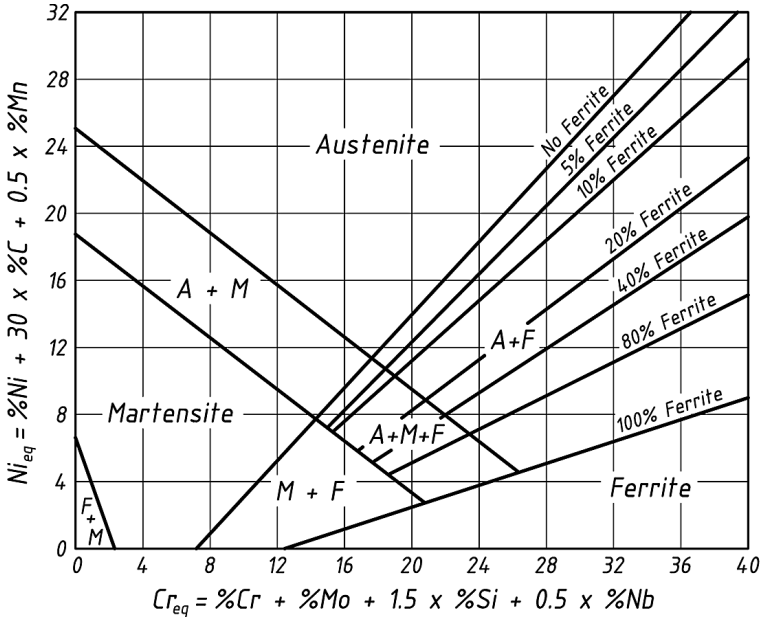

Fig. 3. Schaeffler-Delong constitution diagram for stainless steel [15]

If the austenite stabilizers ability to promote the formation of austenite is related to that for nickel, and the ferrite stabilizers likewise compared to chromium, it becomes possible to calculate the total ferrite and austenite stabilizing effect of the alloying elements in the steel [14]. This gives the so called chromium Cr_{eq} and nickel Ni_{eq} equivalents, defined as below [15]:

$$Cr_{eq} = \%Cr + \%Mo + 1.5\%Si + 0.5\%Nb, \tag{1}$$

$$Ni_{eq} = \%Ni + 30\%C + 0.5\%Mn. \tag{2}$$

Chromium equivalent Cr_{eq} (1), presented on the horizontal axis of the Schaeffler-Delong diagram, shows how to select an appropriate content of chromium (Cr), molybdenum (Mo), silicon (Si) and niobium (Nb) to obtain a chromium-like effect. Nickel equivalent Ni_{eq} (2), presented on the vertical axis of the Schaeffler-Delong diagram, performs the same function for nickel (Ni) and austenite formers. On the basis of the Schaeffler-Delong diagram, for the given values of Cr_{eq} and Ni_{eq}, some information about the joint effect of alloying elements on the microstructure of stainless steel can be found.

Originally, the Schaeffler-Delong diagram was developed for weld metal, but it transpires that it can also provide useful information for wrought and heat treated material. It should be noted that the Schaeffler-Delong diagram presented in Fig. 3 is not the only one which has been published. In specialist literature, several different diagrams with slightly different equivalents, phase limits or general layout can be found. They are the results of conducted research and discussions [14].

3. Influence of stainless steel microstructure on its properties

Both principal phases of structural stainless steel, i.e. ferrite and austenite, differ in properties, and their percentage in microstructure has a definite influence on steel properties.

Ferrite is a solid solution of carbon (C) in alpha iron (α-Fe) with a body-centered cubic (BCC) crystal structure (Fig. 4a). It is relatively soft and plastic, it has higher electrical and thermal conductivity and lower thermal expansion than austenite. The strength of ferrite decreases with temperature to a greater degree than happens in the case of austenite but in spite of this, ferritic stainless steel is great high-temperature material.

Austenite is a solid solution of carbon (C) in gamma iron (γ-Fe) with a face-centered cubic (FCC) crystal structure (Fig. 4b). It has good toughness, even in low temperatures. Austenite has lower stacking fault energies than ferrite which results in higher work-hardening rates. Ferrite and austenite alloys with a similar content of alloying elements have a similar yield strength, but austenitic alloys are more ductile and have higher work-hardening rates and higher tensile strengths [15]. Austenite, in contrast to ferrite, is nonmagnetic.

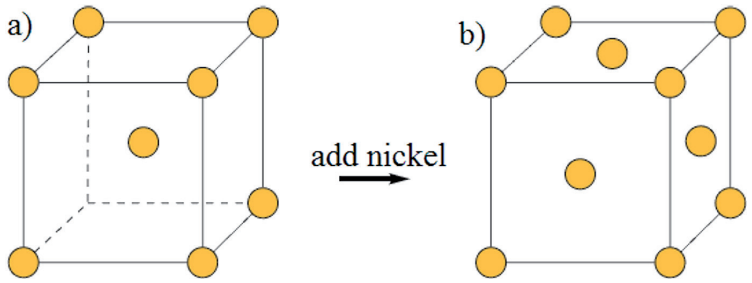

Fig. 4. Iron crystalline structure: a) in ferrite, b) in austenite [12]

The formation of the diphase (austenitic-ferritic) microstructure of stainless steel is the result of appropriate alloy chemical composition, i.e. a balance between ferrite and austenite formers, and steel thermal treatment. Melted steel solidifies to complete ferrite structure and then, at a temperature of about 1000ºC (depending on alloy chemical composition), some ferrite grains transform into austenite, at lower temperatures further changes in the equilibrium ferrite-austenite balance occur. The austenite/ferrite phase balance in stainless steel microstructure can be estimated with multivariable linear regression [12]:

$$\%\text{Ferrite} = -20.93 + 4.01\text{Cr}_{eq} - 5.6\text{Ni}_{eq} + 0.016\text{T}, \tag{3}$$

where

$$\text{Cr}_{eq} = \%\text{Cr} + 1.73\%\text{Si} + 0.88\%\text{Mo}, \tag{4}$$

$$\text{Ni}_{eq} = \%\text{Ni} + 24.55\%\text{C} + 21.75\%\text{N} + 0.4\%\text{Cu}, \tag{5}$$

T – the annealing temperature ranging from 1050°C to 1150°C.

According to EN 10088-1 [7], austenite-ferrite stainless steel contains between 40% and 60% of austenite, usually roughly 50%.

The main alloying element of ferritic stainless steel is chromium (Cr) – Fig.5a, for austenitic stainless steel these are chromium (Cr), nickel (Ni) and molybdenum (Mo) – Fig. 5c, as is the case with austenite-ferrite (duplex) stainless steel – Fig. 5b, however, duplex steel has higher content of chromium (Cr) and lower content of nickel (Ni) than austenitic steel.

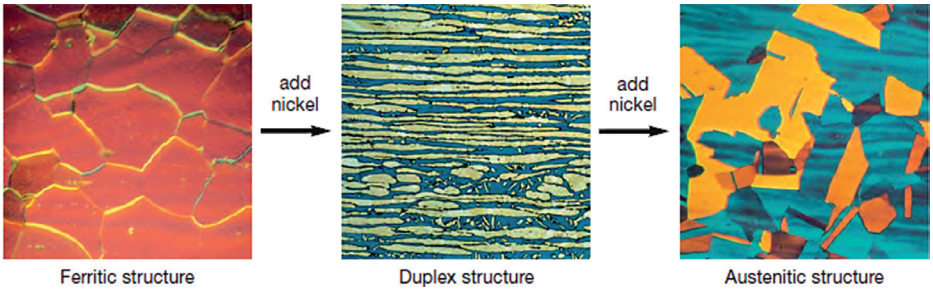

Fig. 5. Changes of stainless steel microstructures due to increasing nickel (Ni) content [12]

Due to having the lowest content of expensive nickel (Ni), ferritic stainless steels are the cheapest of all stainless steel categories. The high content of chromium (Cr) and low content of carbon (C) cause the ferritic microstructure to be stable. In older ferritic steels with a higher content of carbon, some high-temperature austenite formed, this transformed into martensite if quenched [15]. The structural ferritic stainless steels listed in Table 2.1 of EN 1993-1-4 [4] have a chromium (Cr) content in the range of 10.5% to 18.0%. Ferritic stainless steel resistance to corrosion and oxidation is good but steels with a lower (11–12%) content of chromium (Cr), i.e. 1.4003 and 1.4512, are treated as steels with increased resistance to corrosion and

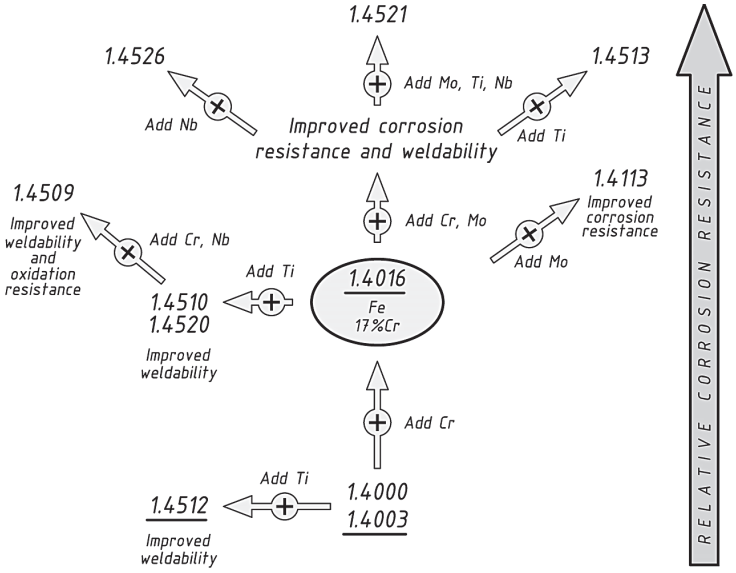

Fig. 6. Influence of alloying components on properties of ferritic stainless steel

should be used only in mildly corrosive environments, because in unfavourable conditions, their corrosion resistance is limited. A particular advantage of ferritic stainless steels is their high resistance to stress corrosion cracking caused by chlorides [19]. The mechanical properties of ferritic steel are moderate. This stainless steel category is characterized by good ductility and high resistance to elevated temperatures, they can only be hardened by cold working. Ferritic stainless steels are often used as light-gauge sheet because their toughness decreases rapidly for heavier sections. Their weldability varies from low to high, depending on the alloy chemical composition. Ferritic steels are magnetic [2, 15, 17, 20].

The most popular grade of ferritic stainless steel is 1.4016 (also in Poland [16]) with a chromium (Cr) content of about 17%. Figure 6 presents the effect of alloying elements on selected properties of ferritic stainless steel [18], structural steel grades listed in Table 2.1 of EN 1993-1-4 [4] are underlined.

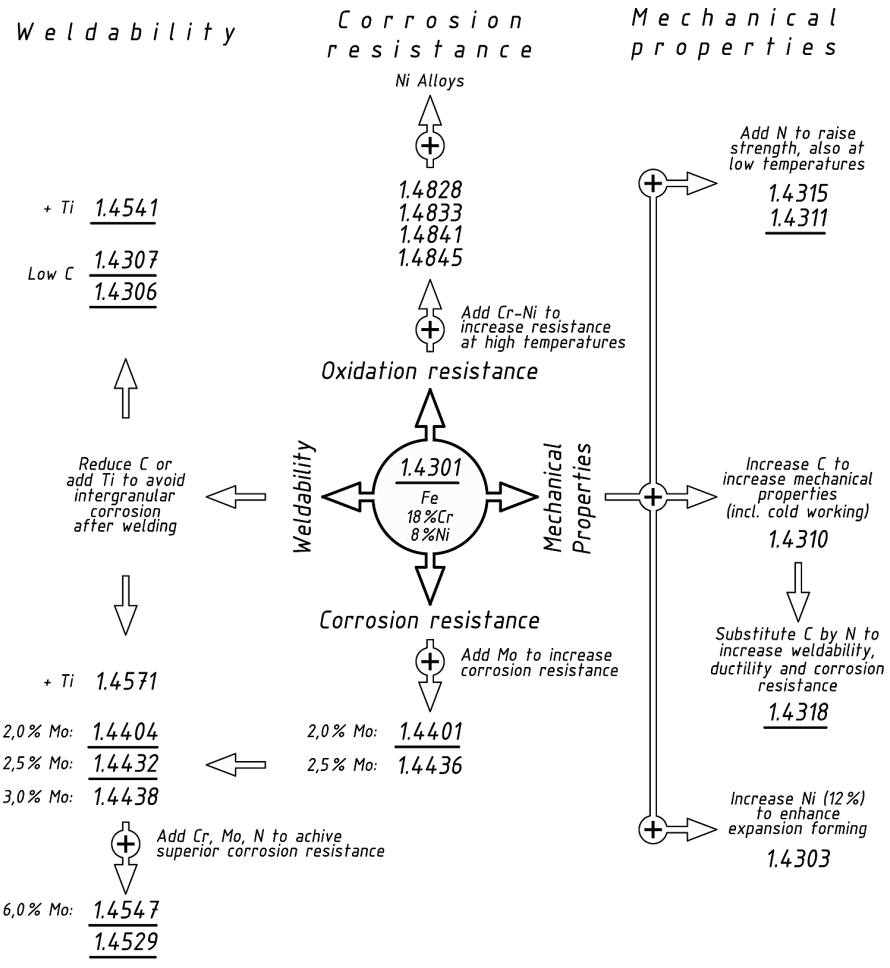

Fig. 7. Influence of alloying components on properties of austenitic stainless steel

Structural austenitic stainless steels, included in Table 2.1 [4], are comprised of at least 16% of chromium (Cr) and 6% of nickel (Ni). Due to their increased chromium (Cr) content, they are more corrosion resistant than ferritic stainless steels, while the high content of nickel (Ni) causes the austenitic microstructure to be stable and makes it resistant to brittleness at low temperatures. Austenitic stainless steels can be used in a wide range of temperatures, from cryogenic to red heat temperatures. They have very good formability and weldability and can be hardened by cold work. In an annealed condition, they are nonmagnetic. Because of their very good mechanical properties, corrosion resistance and weldability, this stainless steel category is the most popular. It should simultaneously be noted that austenitic stainless steels are less resistant to cyclic oxidation than ferritic steels because their greater coefficient of thermal expansion causes possible spalling of the protective oxide coating Additionally, if austenitic stainless steel corrosion resistance is insufficient for application in a particular environment, stress corrosion cracking can occur [1, 15, 19, 20].

Figure 7 shows how, starting form the most popular grade 1.4301 [16], properties of austenitic stainless steel can be modified by changing the alloy composition [18]. Structural steel grades listed in Table 2.1 of EN 1993-1-4 [4] are underlined.

The microstructure of austenitic-ferritic stainless steels consists of austenite and ferrite, usually in the proportion of one to one. The content of chromium (Cr) in structural austenitic--ferritic stainless steel, listed in Table 2.1 [4], is 21–24%, the content of nickel (Ni) – 3.5% to 6.5% [7]. The mixed microstructure causes duplex steels to combine properties of ferritic and austenitic stainless steels, for example, their resistance to stress corrosion cracking (e.g. due to chlorides) is higher than austenitic but not as high as ferritic steel, they have higher toughness than ferritic but not as high as austenitic steel. The toughness of austenitic-

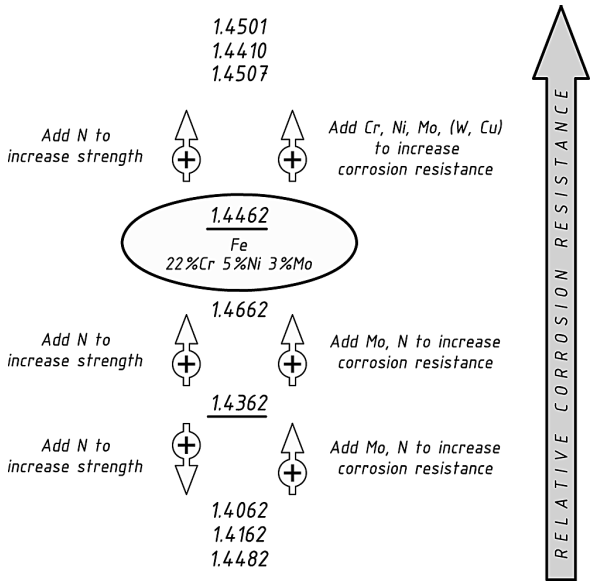

Fig. 8. The influence of alloying components on properties of austenitic-ferritic (duplex) stainless steel

ferritic stainless steel is reduced at temperatures below –50°C and above 300°C, so they should only be used between these temperatures. Duplex steels have a high yield strength, about two times higher than that of comparable austenitic grades, they also have good fatigue parameters, even in corrosive environments. The weldability of austenitic-ferritic stainless steels is good, but there are problems associated with the heat affected zone (HAZ) – loss of corrosion resistance, toughness or post-weld cracking. To avoid these problems, speed and heat input during welding should be diligently controlled. Duplex stainless steels have a lower coefficient of thermal expansion than austenitic stainless steel, so their welding distortions are usually also smaller. Austenitic-ferritic stainless steels can be strengthened by cold working but not by heat treatment. Steels of this category are magnetic. Their lower content of expensive nickel (Ni) makes them more economical than austenitic grades. Furthermore, duplex steels have a higher strength than austenitic steels which results in lower steel consumption. Typical applications of austenitic-ferritic stainless steel are investments where high strength, good corrosion resistance, low susceptibility to stress corrosion cracking or combinations of these requirements are needed [1, 12, 15, 19].

Differences between austenitic-ferritic stainless steel grades, usually showing higher mechanical properties and corrosion resistance than the most popular ferritic and austenitic grades, is shown in Fig. 7 [18], structural steel grades listed in Table 2.1 of EN 1993-1-4 [4] are underlined. According to Euro Inox data [18], the most popular grade of duplex steels is 1.4462.

4. Physical properties of stainless steel

4.1. Density

In contrast to carbon steel, density ρ of stainless steel is not a constant value but changes depending on microstructure and grade, form 7.5 to 8.1 kg/dm^3 [7]. Density of ferritic and austenitic-ferritic stainless steels is a little bit smaller than density of carbon steel (7.7 kg/dm^3 for ferritic grade 1.4016, 7.8 kg/dm^3 for austenitic-ferritic grade 1.4462, in comparison with 7.85 kg/dm^3 for carbon steel). The biggest density have austenitic stainless steels (e.g. 7.9 kg/dm^3 for grade 1.4301 and 8.1 kg/dm^3 for grade 1.4529). In general, within the particular steel category, steel density increases with increasing content of alloying elements, particularly heavy elements (e.g. molybdenum (Mo)) [14].

4.2. Modulus of elasticity

Initial modulus of elasticity E (Young's modulus) of stainless steel is not a constant value but depends on the steel microstructure. Values of Young's modulus taken into account for the design of building structures according to EN 1993-1-4 [4] due to ultimate limit state (ULS) are determined on the basis of EN 10088-1 [7]: 220 kN/mm^2 for ferritic stainless steels, 200 kN/mm^2 for austenitic-ferritic stainless steels and 195-200 kN/mm^2 for austenitic stainless steels. These values were determined at temperature of 20°C. The changeability of Young's modulus with temperature for different steel microstructure is shown in Fig. 9 [7].

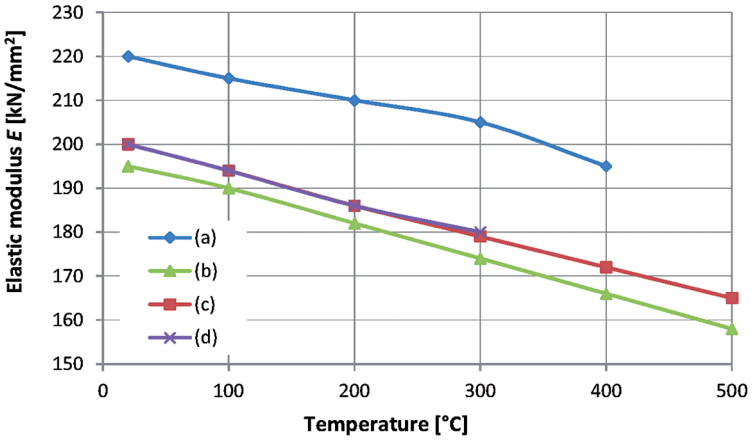

Fig. 9. Elastic modulus E of structural stainless steel: (a) ferritic, (b) austenitic (grades: 1.4539, 1.4547, 1.4529), (c) austenitic (other grades), (d) austenitic-ferritic

The behaviour of stainless steel in the annealed condition can alternatively be described by a nonlinear stress-strain curve according to Annex C of EN 1993-1-4 [4]. Depending on the accuracy required and the maximum strains attained, European Standard [4] specifies three approaches for modelling the material behaviour:

1) stress-strain curve with strain hardening:

$$\varepsilon = \begin{cases} \dfrac{\sigma}{E} + 0.002\left(\dfrac{\sigma}{f_y}\right)^n & \text{for} \quad \sigma \le f_y \\ 0.002 + \dfrac{f_y}{E} + \dfrac{\sigma - f_y}{E_y} + \varepsilon_u\left(\dfrac{\sigma - f_y}{f_u - f_y}\right)^m & \text{for} \quad f_y < \sigma \le f_u \end{cases}, \tag{6}$$

where:

- n – the coefficient depending on rolling direction, defined as $n = \ln(20)/\ln(f_y/R_{p0.01})$; it may be taken from Table 2 or it may be calculated from measured properties,
- $R_{p0.01}$ – the 0.01% proof strength,
- E_y – the tangent modulus of stress-strain curve at the yield strength, defined as $E_y = E/(1 + 0.002n\, E/f_y)$,
- ε_u – the ultimate strain, corresponding to the ultimate strength f_u; it may be obtained from approximation $\varepsilon_u = 1 - f_y/f_u$, but $\varepsilon_u \le A$ where A is the elongation after fracture defined in [8–11],
- m – the coefficient that may be determined as $m = 1 + 3.5\, f_y/f_u$.

2) stress-strain curve calculated as in a) based on experimental data,

3) true stress-strain curve calculated from an engineering stress-strain curve as measured as follows:

$$\begin{aligned} \varepsilon_{\text{true}} &= \sigma(1+\varepsilon) \\ \sigma_{\text{true}} &= \ln(1+\varepsilon) \end{aligned}. \tag{7}$$

Table 2

Values of *n* according to [4]

Steel grade	Coefficient *n*	
	Longitudinal direction	Transverse direction
1.4003	7	11
1.4016	6	14
1.4512	9	16
1.4301	6	8
1.4306		
1.4307		
1.4318		
1.4541		
1.4401	7	9
1.4404		
1.4432		
1.4435		
1.4539		
1.4571		
1.4462	5	5
1.4362		

Nonlinear stress-strain curves for the section made of exemplary stainless steel grade 1.4016, determined form formula (6) for longitudinal ($n = 6$) and transversal ($n = 14$) rolling direction, are shown in Fig. 10.

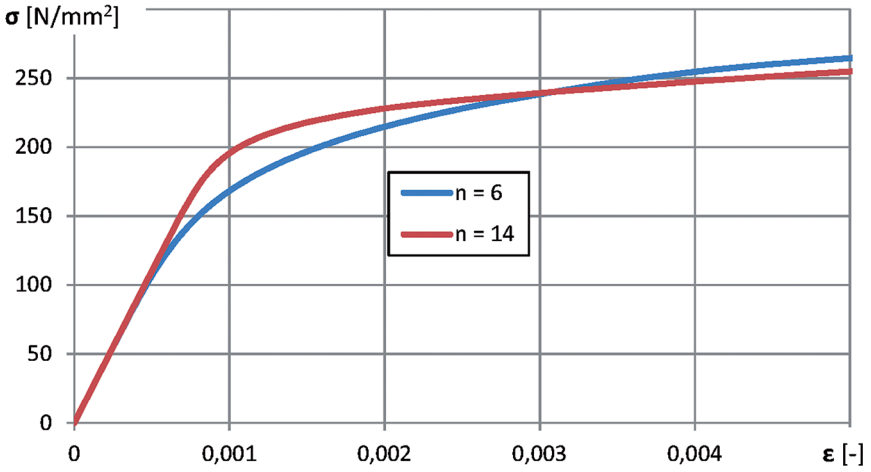

Fig. 10. Influence of the parameter *n* on the nonlinearity of the stress-strain curve

Calculating deflections of structural element European Standard EN 1993-1-4 [4] requires taking stainless steel nonlinear stress-strain behaviour into account; for annealed material guidelines given in Annex C [4] can be used.

Deflections in an individual member may be determined using the secant modulus of elasticity $E_{s,\mathrm{ser}}$ appropriate to the stress level in the member at the serviceability limit state (SLS) and to the rolling direction or, alternatively, using Finite Element Methods (FEM) [5], assuming nonlinear material behaviour according to Annex C [4].

The value of the secant modulus of elasticity $E_{s,\mathrm{ser}}$ may be calculated according to EN 1993-1-4, p.4.2(5) [4] as follows:

$$E_{s,\mathrm{ser}} = \frac{(E_{s,1} + E_{s,2})}{2}, \tag{8}$$

where:

$E_{s,1}$ – the secant modulus corresponding to the stress σ_1 in the tension flange,
$E_{s,2}$ – the secant modulus corresponding to the stress σ_2 in the compression flange.

The values of $E_{s,1}$ and $E_{s,2}$, for the appropriate serviceability design stress $\sigma_{i,Ed,\mathrm{ser}}$ (i = 1 or 2) and rolling direction, may be estimated using:

$$E_{s,i} = \frac{E}{1 + 0.002 \dfrac{E}{\sigma_{i,Ed,\mathrm{ser}}} \left(\dfrac{\sigma_{i,Ed,\mathrm{ser}}}{f_y} \right)^n}. \tag{9}$$

Parameter n may be taken from Table 2 or determined according to Annex C [4].

To simplify calculations, European Standard EN 1993-1-4 [4] allows us to neglect variations of the secant modulus of elasticity $E_{s,\mathrm{ser}}$ along the length of the member and use minimum value of $E_{s,\mathrm{ser}}$, corresponding to the maximum values of the stresses $\sigma_{1,Ed,\mathrm{ser}}$ and $\sigma_{2,Ed,\mathrm{ser}}$ in the member, throughout the member's length.

4.3. Shear modulus

According to EN 1993-1-4 [4], stainless steel shear modulus G is determined depending on Young's modulus value as

$$G = \frac{E}{2(1+\nu)}, \tag{10}$$

where

ν – Poisson's ratio, in elastic stage equal to 0.3.

4.4. Coefficient of thermal expansion, thermal conductivity and specific heat

Coefficients of thermal expansion α and thermal conductivity k are the physical properties that take significantly different values depending on the microstructure of stainless steel, they also distinguish stainless steel from carbon steel. Values of the coefficient of thermal expansion α between 20°C and 100°C are as follows [7]: $12 \cdot 10^{-6}$/K for carbon steel, $10.0 - 10.5 \cdot 10^{-6}$/K for ferritic stainless steel, $13.0 \cdot 10^{-6}$/K for austenitic-ferritic stainless

steel and 15.8 – 16.5·10^{-6}/K for austenitic stainless steel. The values presented above concern stainless steel grades listed in Table 2.1 EN 1993-1-4 [4]. High thermal expansion of austenitic stainless steels is the reason for large thermal stresses and distortions. The thermal elongation ε_T of austenitic stainless steel included in EN 1993-1-4 [4] may be determined according to Annex C of EN 1993-1-2 [3]:

$$\varepsilon_T = \frac{\Delta l}{l} = (16 + 4.79 \cdot 10^{-3}\theta_a - 1.243 \cdot 10^{-6}\theta_a)(\theta_a - 20)10^{-6}, \tag{11}$$

where

Δl – the temperature induced expansion,
l – the length at 20°C,
θ_a – the steel temperature [°C].

According to (11), the thermal elongation $l/\Delta l$ of a 6000 mm long exemplary element made of austenitic stainless steel, heated to 800°C is equal to 15·10^{-3} (see Fig.11), this means that temperature induced expansion Δl is about 90 mm. Figure 11 illustrates how the thermal elongation $l/\Delta l$ of structural austenitic stainless steels, determined according to [3], changes with temperature.

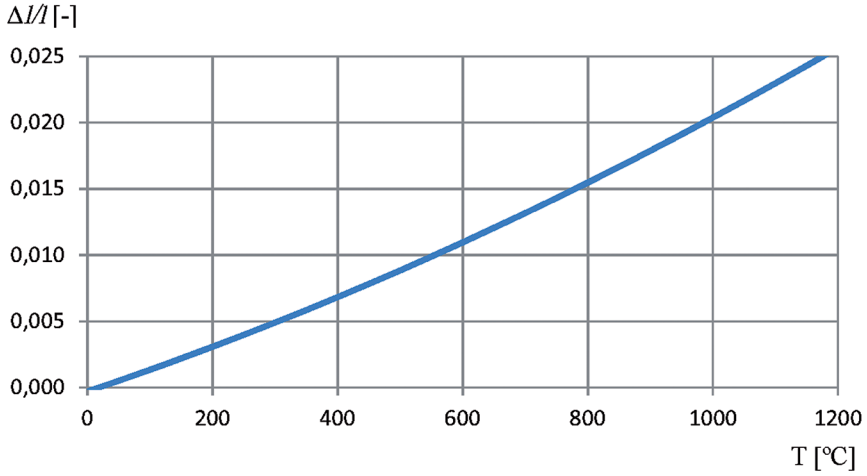

Fig. 11. Thermal elongation $\Delta l/l$ of stainless steel as a function of temperature

Thermal conductivity k of stainless steel is lower than thermal conductivity k of carbon steel, this is related to the high content of chromium in stainless steels. For each stainless steel category, it decreases with increasing the alloying elements content. Austenitic stainless steels have the lowest thermal conductivity k at temperature of 20°C – 12–15 W/m·K, for austenitic-ferritic stainless steels this parameter is equal 15 W/m·K, ferritic stainless steels have the highest thermal conductivity k – 25 W/m·K [7]. The presented values concern stainless steel grades listed in Table 2.1 EN 1993-1-4 [4]. By comparison, carbon steel thermal conductivity k at 20°C is about 53.3 W/m·K. Thermal conductivity k of stainless steel increases with increasing temperature [3] – Fig. 12.

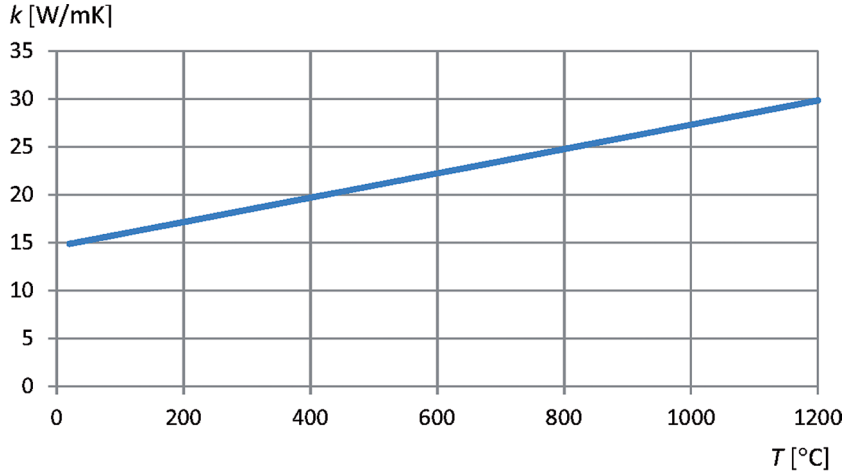

Fig. 12. Thermal conductivity *k* of stainless steel as a function of temperature

The specific heat *c* (unitary thermal capacity at 20°C) of ferritic stainless steels varies in range of 430–460 J/kg·K, so it is of a value similar to specific heat *c* of carbon steels – 440 J/kg·K, most austenitic grades and austenitic-ferritic stainless steels are characterized by greater specific heat *c* = 500 J/kg·K [7]. Stainless steel specific heat *c* is a monotonically increasing function of temperature; its value may be calculated according to Annex C.3 of EN 1993-1-2 [3] – Fig. 13.

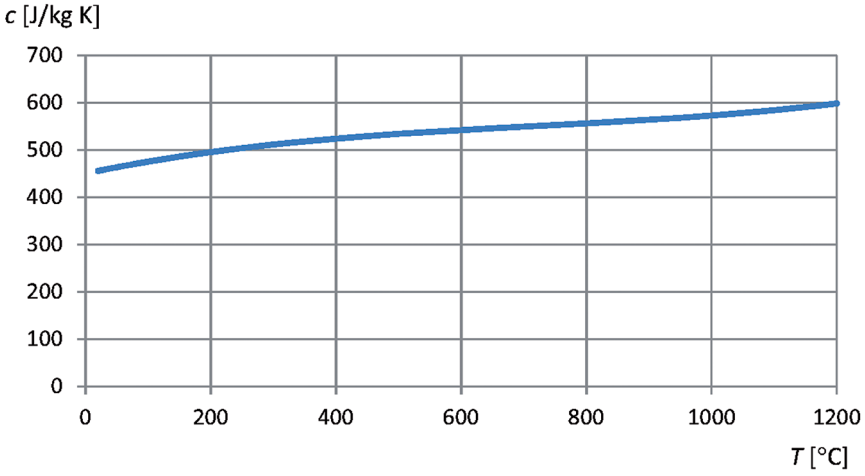

Fig. 13. Specific heat *c* of stainless steel as a function of temperature

5. Technological properties of stainless steel

5.1. Corrosion resistance

The corrosion resistance of stainless steel is connected with its high chromium (Cr) content (min. 10.5% [7]) which supports the forming of a passive film protecting the steel surface against corrosion. A significant distinguishing feature of the passive film is its ability to immediately self-repair in the presence of air or an oxidising environment without any additional treatments. The passive film formed on the stainless steel surface is stable and makes stainless steel resistant to corrosion in normal atmospheric and mild aqueous environments. The main alloying elements that increase corrosion resistance are, apart from chromium (Cr), molybdenum (Mo), nickel (Ni) and nitrogen (N). Chromium (Cr) enhances the stability of the passive film, and with molybdenum (Mo), increases resistance to chloride penetration. Nickel (Ni) improves the resistance of the passive film in some acid environments. Structural austenitic stainless steel grade 1.4401 has a higher corrosion resistance than grade 1.4301 because it contains molybdenum (Mo) and more nickel (Ni). In order to improve corrosion resistance in a particular environment, some other elements may be added to the alloy, e.g. copper (Cu) which enhances corrosion resistance to sulphuric acid [1, 2, 15]. To keep appropriate corrosion resistance of stainless steel, one should pay attention to the fact that during fabrications, the passive film on stainless steel structural components should not be broken down, for example, by using the same tools for the processing of stainless and carbon steels.

The corrosion of stainless steel can occur when the passive film is damaged and, because of environmental conditions (lack of oxygen, strong acid or alkaline environments), is not allowed to re-form. Stainless steel grades may differ in their corrosion resistance depending on the steel chemical composition and the type of corrosive environment. For that reason, the selection of stainless steel grade for a given application should be preceded by an analysis of the corrosion environment effect on the particular grade. Sometimes, the actual durability of the stainless steel structure is lower than assumed. Possible reasons for this situation are: an incorrect selection of stainless steel grade for corrosive environment; exposure to unexpected conditions (e.g. contamination by chloride ions); incorrect treatment of steel components decreasing its corrosion resistance; incorrect detailing of steel structures increasing the possibility of corrosion (dirt entrapments, notch causing stress concentration, etc.).

Corrosion resistance is also dependent on the type of surface finishing – the smoother the surface, the higher the corrosion resistance. The exception is stainless steel susceptible to stress corrosion cracking because stresses caused by surface mechanical polishing can initiate corrosion cracking in the structure elements situated in the environment containing chloride ions.

European Standard EN 1993-1-4 [4] specifies six types of corrosion that may occur in structural elements made of stainless steel: pitting; crevice corrosion; bimetallic corrosion; stress corrosion cracking; general corrosion and inter-granular attack; weld decay. Only pitting, crevice corrosion and bimetallic corrosion are likely to occur in buildings [4].

Corrosion of stainless steel elements causes many problems. The reduction of structural member cross section leads to the reduction of its capacity. The perforation of tanks and pipes causes leakage of fluids or gases. In food industry, products of corrosion can contaminate the material being handled, etc.

5.2. Heat treatment ability

Stainless steels are often subjected to technological processes of heat treatment such as annealing, hardening and stress relieving. The objective of these treatments is to restore the required properties of material (resistance to corrosion, ductility) and to relieve residual stresses caused by the production process or previous technological treatments. They are also used to produce hard structures of stainless steel able to withstand high stresses or abrasion in service. Heat treatment of stainless steel is performed in specific conditions, depending on the steel category and type of treatment.

The annealing of austenitic stainless steel recrystallizes the work hardened grains but also homogenizes dendritic weld metal structures and relieves remnant stresses from cold working. The obtained austenitic microstructure has no carbides precipitation at grain boundaries which prevents chromium (Cr) impoverishment of grain boundary zones and thus prevents inter-granular corrosion. The temperature of this heat treatment is usually above 1040°C, although, if fine size of grain is important, some grades may be annealed at closely controlled temperatures as low as 1010°C. The annealing of austenitic-ferritic stainless steels is generally very similar to austenitic grades. Ferritic stainless steels, depending on their grade, may be annealed at a temperature in the range of 760°C to 955°C. Heat treatment at higher temperatures of stainless steel in this category may cause the formation of austenite that, during cooling, transforms into martensite, thus making steel brittle [1].

Residual stress relieving of austenitic stainless steels at temperatures below 400°C gives a modest result - only after heat treatment at temperatures in the range of 425°C to 925°C, is a significant reduction of residual stresses achieved. It is assumed that one hour treatment at 870°C relieves about 85% of the residual stresses. It should be noted that stress relieving in this higher temperature range can also precipitate grain boundary carbides, resulting in decreasing corrosion resistance. The full annealing process, i.e. heating to about 1080°C followed by rapid cooling, removes all residual stresses in austenitic grades, but is not a practical treatment for most large or complex fabrications [1].

Stainless steel can also be heat treated in order to surface harden but only to a limited extent. As an example, the surface of austenitic stainless steels can be hardened by nitriding, but it should be noted that the hard and thin surface layer obtained during this process, surrounds the underlying stainless steel core which is relatively soft, this excludes the use of this solution in heavily loaded engineering applications. Additionally nitriding decreases the corrosion resistance of stainless steel [1].

Before heat treatment, the surface of stainless steel must be cleaned in order to remove oil, grease and other carbonaceous residues that would otherwise lead to carburization during heat treating which degrades corrosion resistance.

5.3. Cold forming ability

Characteristic of structural stainless steel is that during cold working, it can be hardened, i.e. made stronger. The hardening rate depends on the stainless steel microstructure and the highest is for austenitic grades. Stainless steel work hardening may be the result of cold rolling or the fabrication process of the structural member, or a combination of both. According to EN 1993-1-4 [4], for the design of stainless steel structures, nominal values of yield strength f_y and ultimate tensile strength f_u may only be adopted for material delivered in the cold worked conditions specified in [8–11]. The recommendations given in [4] may be applied if for steel in the worked harden condition yield strength do not exceed 350 MPa or ultimate tensile strength – 700 MPa. These recommendations may also be used for higher grades when local or global instability is not a deciding factor for the bearing capacity of an element or of a whole structure. In cases when the bearing capacity is determined by local or global stability, and steel yield strength is higher than 350 MPa (or ultimate tensile strength exceeds 700 MPa), stainless steel structures should be designed on the basis of full size tests. Stainless steel work hardening from fabrication may be utilized in the design provided that the effect of work hardening has been verified by full size tests [4].

5.4. Weldability

Welding is the most popular technique of connecting metal elements. The weldability of structural stainless steel may vary from low to high, depending on the steel category and grade. Most austenitic and austenitic-ferritic grades are readily welded. Ferritic grades with a very low carbon (C) content are weldable, while grades with a higher content of carbon (C) are not as easily welded and must often be preheated.

The weld metal and the heated affected zone (HAZ) of austenitic stainless steels has a tendency to crack, especially in fully austenitic microstructures. Stainless steel microstructures containing a small amount of ferrite (5–10%) are less susceptible to cracking. Therefore, when austenitic stainless steel is welded, the selection of filler material composition is very important. The main problem of ferritic stainless steel welding is the low toughness of the heat affected zone (HAZ) due to excessive grain coarsening. The preheating of the stainless steel in this category does not reduces the grain size but will reduce the HAZ cooling rate, maintain the weld metal above the ductile-brittle transition temperature, and may reduce residual stresses. The preheat temperature should be within the range 50–250°C, depending on material composition. Modern austenitic-ferritic stainless steels are readily weldable, but obtaining a proper weld requires the maintenance of process parameters, especially the heat input range. In the case of duplex steel, welding an appropriate selection of filler material is very important because the balance between ferrite and austenite in weld microstructure should be close to that in the parent material microstructure [21].

To weld stainless steel, most welding methods can be used, including welding in an inert gas atmosphere with a consumable (MIG) and non-consumable (TIG) electrode, and welding with a coated electrode and resistance welding. During stainless steel welding, one should remember that this kind of steel has a higher coefficient of thermal expansion and lower thermal conductivity than carbon steel, so relevant actions to limit welding distortions should be undertaken.

6. Conclusions

Stainless steels approved for use in building structures by EN 1993-1-4 [4], may have one of following microstructures: ferritic; austenitic; austenitic-ferritic. The type of microstructure (steel category) strongly affects both the physical and technological properties of stainless steel. These properties are quantitatively and qualitatively diverse in comparison with carbon steel as well as between stainless steel grades. In general, structural stainless steel has a higher work hardening rate, higher ductility and strength, higher cryogenic toughness, higher hardness, much lower thermal conductivity and, of course, higher resistance to corrosion than structural carbon steel. The disadvantage of stainless steel is its high price, about four times higher than the price of carbon steel. On the other hand, its advantages include high strength, durability, low maintenance costs, low thermal conductivity. These advantages can favour the growth of stainless steel applications in building structures.

Diversity of chemical compositions, microstructures and surface finishing means that the selection of an appropriate stainless steel grade for structural application is more complicated than in the case of carbon steel. When selecting a carbon steel grade, the designer only usually takes into consideration the mechanical and technological parameters. In most cases, the choice of anticorrosive protection and the surface visual appearance of the carbon steel structure can be considered as independent of steel grade selection. The corrosion resistance of carbon steel is ensured by appropriate anticorrosive coating matched up to environmental corrosive conditions. This coating can be periodically renovated or, in the case of substantial damage or environment corrosiveness change, can be completely removed and replaced. In contrast to carbon steel, corrosion resistance of stainless steel is inextricably linked with properties of steel grade. For this reason, proper selection of structural stainless steel grade is more important than in the case of carbon steel – it affects not only structure load bearing capacity, but also structure corrosion resistance.

References

[1] Atlas Steels Technical Department, *The Atlas Steels Technical Handbook of Stainless Steels*, Melbourne, 2010.

[2] Baddoo N.R., Burgan B.A., *Structural design of stainless steel*, The Steel Construction Institute, Ascot, 2001.

[3] EN 1993-1-2:2005. Eurocode 3 – Design of steel structures – Part 1-1: General rules – structural fire design.

[4] EN 1993-1-4:2006. Eurocode 3 – Design of steel structures – Part 1-4: General rules – Supplementary rules for stainless steels.

[5] EN 1993-1-5:2006. Eurocode 3 – Design of steel structures – Part 1-5: Plated structural elements.

[6] EN 10027-2:1992. Designation systems for steels – Part 2: Numerical system.

[7] EN 10088-1:2005. Stainless steels – Part 1: List of stainless steels.

[8] EN 10088-2:2005. Stainless steels – Part 2: Technical delivery conditions for sheet/plate and strip of corrosion resisting steels for general purposes.

[9] EN 10088-3:2005. Stainless steels – Part 3: Technical delivery conditions for semi-finished products, bars, rods, wire, sections and bright products of corrosion resisting steels for general purposes.

[10] EN 10088-4:2009. Stainless steels – Part 4: Technical delivery conditions for sheet/plate and strip of corrosion resisting steels for construction purposes.
[11] EN 10088-5:2009. Stainless steels – Part 5: Technical delivery conditions for bars, rods, wire, sections and bright products of corrosion resisting steels for construction purposes.
[12] International Molybdenum Association, *Practical guidelines for the fabrication of duplex stainless steels*, London 2009.
[13] International Molybdenum Association, *Practical guidelines for the fabrication of high performance austenitic stainless steels*, London 2010.
[14] Leffler B., *Stainless steel and their properties* (online), homepage: www.hazmetal.com (date of access: 2014-01-30).
[15] McGuire M.F., *Stainless steel for design engineers*, ASM International, Ohio, 1st Edition, 2008.
[16] Nova Trading S.A. *Statystyki sprzedaży stali nierdzewnej* (private communication).
[17] The European Stainless Steel Development Association Euro Inox, *Design manual for structural stainless steel*, 2003.
[18] The European Stainless Steel Development Association Euro Inox, *What is stainless steel?* (brochure).
[19] The European Stainless Steel Development Association Euro Inox, *Własności stali odpornych na korozję*, Luxembourg 2002 (in Polish).
[20] The Specialty Steel Industry of North America (SSINA), *Design guidelines for the selection and use of stainless steel*, Washington 2011.
[21] *The weldability of stainless steel* (www.valve-world.net – date of access: 2013-11-07).

TECHNICAL TRANSACTIONS | CZASOPISMO TECHNICZNE
CIVIL ENGINEERING | BUDOWNICTWO
4-B/2014

PAWEŁ ŻWIREK*

STATISTICAL RESEARCH OF STEEL GRADES: DX51D, DX52D AND DX53D

BADANIA STATYSTYCZNE GATUNKÓW STALI: DX51D, DX52D I DX53D

Abstract

This article presents the results of the statistical research of the mechanical properties of sheets of Polish grades DX51D, DX52D and DX53D, made of low carbon steel for cold forming, continuously hot-dip coated. DX-type sheets, in particular DX51D, produced according to standard EN 10346 [4], can be used, inter alia, to produce corrugated metal sheets and sandwich panels. Standard EN 10346 [4] does not give at all, or gives in the form of very wide intervals, strength parameters for sheets of DX type. Characteristic and design values of yield strength and tensile strength have been presented in the article. Also, the values of partial factors for DX-type steel have been analyzed.

Keywords: *DX51D*, *DX52D*, *DX53D*, *steel sheets*, *statistical research*

Streszczenie

W artykule przedstawiono wyniki badań statystycznych cech wytrzymałościowych dla krajowych blach gatunku DX51D, DX52D i DX53D ze stali niskowęglowych do obróbki plastycznej na zimno powlekanych ogniowo w sposób ciągły. Blachy typu DX wg normy EN 10346 [4], w szczególności DX51D, mogą być stosowane m.in do produkcji blach trapezowych i płyt warstwowych. Norma EN 10346 [4] nie podaje wcale lub podaje w postaci bardzo szerokich przedziałów parametry wytrzymałościowe blach typu DX. W pracy wyznaczono wartości charakterystyczne i obliczeniowe dla granicy plastyczności i wytrzymałości na rozciąganie oraz przeanalizowano wartości częściowych współczynników bezpieczeństwa dla blach typu DX.

Słowa kluczowe: *DX51D*, *DX52D*, *DX53D*, *blachy stalowe*, *badania statystyczne*

* Ph.D. Eng. Paweł Żwirek, Faculty of Civil Engineering, Cracow University of Technology.

1. Introduction

According to standard EN 10346 [4], contemporary corrugated sheets [8] and external layers of sandwich panels [9] are mainly made of thin sheets of the following steel grades – S220GD, S250GD, S280GD, S320GD, S350GD (continuously hot-dip coated strips and sheets of structural steel) or DX51D (continuously hot-dip coated strips and sheets of low carbon steel for cold forming).

The strength parameters for the national continuously hot-dip coated strips and sheets of structural steel manufactured according to [4] have been verified on the basis of a large statistical test in [5]. For DX-type steel, the standard EN 10346 [4] only specifies intervals of its mechanical properties or does not provide the information at all. While comparing the tables contained in standards EN 10346 [4] and EN 1993-1-3 [3], it can be noted that the standard for designing steel structures [3] defines the minimum values of the intervals specified in standard [4] (for transverse direction) – c.f. Table 1. The aim of this paper is to determine the characteristics and design values of the strength parameters and partial safety factors for DX-type sheets on the basis of statistical research. The calculations shall be performed for Polish steel products.

Table 1

Mechanical properties of steel grades: DX51D, DX52D and DX53D

	EN 10346 [4]			EN 1993-1-3 [3]	
Steel grade	Yield strength R_e MPa	Tensile strength R_m MPa	Elongation A_{80} % min	f_{yb} MPa	f_u MPa
DX51D	–	270–500	22	140	270
DX52D	140–300	270–420	26		
DX53D	140–260	270–380	30		

According to [3], properties of the base material, in particular, the nominal yield strength f_{yb} and ultimate tensile strength f_u can be adopted either by assuming values $f_y=R_{eh}$ or $R_{p0.2}$ and $f_u=R_m$ direct from product standards, by using the values given in the tables contained in the standard, or by appropriate tests, according to EN 1990 [1]. This work will use the provisions of Appendix D to the standard EN 1990 [1].

Determining the design values of material properties from statistical research may be carried out in one of the following ways:

– by assessing a characteristic value X_k, which is then divided by a partial factor γ_m and multiplied by an explicit conversion factor η_d (method *a*),
– by direct determination of the design value X_d, implicitly or explicitly accounting for the conversion of results and the total reliability required (method *b*).

The formulas specified in the design standard PN-EN 1990 [1] are based on the assumption that all random variables have normal or log-normal distributions and there is no prior information about their mean values. The estimation of the design values can be performed either when there is no prior information about the dispersion measurement

of the random variable in the form of a coefficient of variation v_x, or when there is full information about a coefficient of variation.

In the case of method *a, the* design value of a property X can be calculated from the formula:

– for the normal distrubution

$$X_d = \eta_d \frac{X_k}{\gamma_m} = \frac{\eta_d}{\gamma_m} m_x (1 - k_n v_x) \tag{1}$$

$$v_x = s_x / m_x \tag{2}$$

$$m_x = \frac{1}{n} \sum_{i=1}^{n} x_i \tag{3}$$

$$s_x^2 = \frac{1}{n-1} \sum_{i=1}^{n} (x_i - m_x)^2 \tag{4}$$

– for the log-normal distribution

$$X_d = \frac{\eta_d}{\gamma_m} \exp(m_y - k_n s_y) \tag{5}$$

$$m_y = \frac{1}{n} \sum_{i=1}^{n} \ln(x_i) \tag{6}$$

$$s_y = \sqrt{\ln(V_x^2 + 1)} = v_x \quad – \quad \text{if } v_s \text{ is known from prior knowledge} \tag{7}$$

$$s_y = \sqrt{\frac{1}{n-1} \sum_{i=1}^{n} (\ln x_i - m_y)^2} \quad – \quad \text{if } v_x \text{ is unknown from prior knowledge} \tag{8}$$

where:

η_d – design value of the conversion coefficient,
γ_m – partial safety factor associated with the uncertainty of material properties,
n – number of test results,
x_i – value of a single result,
k_n – value of statistics, depending on the number of test results according to Table 2.

In the case of method *b,* the design value of X is determined from the following formulas:

– for normal distribution

$$X_d = \eta_d m_x (1 - k_{d,n} v_x) \tag{9}$$

– for log-normal distribution

$$X_d = \eta_d \exp(m_p - k_{d,n} s_y) \tag{10}$$

where:

$k_{d,n}$ – value of statistics according to Table 3.

If the value of the coefficient of variation $v_x \leq 0.1$ (as is usually the case for the strength properties of steel products), the difference between the results of the statistical analysis for normal and log-normal distribution is practically insignificant. While analyzing the values of statistics in each row of Tables 2 and 3, it can be observed that for large sample sizes, the values of statistics tend asymptotically to the same value, irrespective of whether the coefficient of variation is known or estimated from the test.

Table 2

Values of statistics k_n for the 5% characteristic value

n	1	2	3	4	5	6	7	8	9	10	∞
v_x (known)	2.31	2.01	1.89	1.83	1.80	1.77	1.74	1.72	1.68	1.67	1.64
v_x (unknown)	–	–	3.37	2.63	2.33	2.18	2.00	1.92	1.76	1.73	1.64

Table 3

Values of statistics $k_{d,n}$ for the design value

n	1	2	3	4	5	6	7	8	9	10	∞
v_x (known)	4.36	3.77	3.56	3.44	3.37	3.33	3.27	3.23	3.16	3.13	3.04
v_x (unknown)	–	–	–	11.40	7.85	6.36	5.07	4.51	3.64	3.44	3.04

2. Statistical research

In order to determine the mechanical parameters of the DX-type sheets manufactured according to standard EN 10346 [4], the data on the mechanical properties of metal sheets from the years 2005–2010, provided by the Quality Control Department of Arcelor Mittal, have been used by the author. The presented statistical test includes properties of the sheets with a nominal thickness of 0,45–2,00 mm. The results of statistical research for the different grades of steel have been presented in Table 4. The number of the data set for each property was 63292.

Particularly interesting, from a practical point of view, are the results for the DX51D steel grade, which is used in the manufacturing of corrugated sheets, external layers of sandwich panels and cold formed sections. Sheets made of grade DX52 are intended primarily for drawing and DX53D for deep drawing. A large number of the results since 2007 are due to the introduction of the electronic archiving system by the company. The results of earlier years were obtained from the archives stored in the paper version. A small number of the results for the DX52 and DX53 steel grades are caused by a relatively small production volume compared to the DX51D steel.

Verification of a type of probability distribution for random yield strength $\underline{R}_e$ and random ultimate tensile strength $\underline{R}_m$, was performed with a graphical method using probabilistic grids where the statistical results have been applied. Figure 1a presents a verification of the probability distribution of yield strength of the DX51D grade steel sheets on the grid of normal distribution. Linear approximation of empirical data seems reasonable. Similar results were also obtained for the other two analyzed grades of steel.

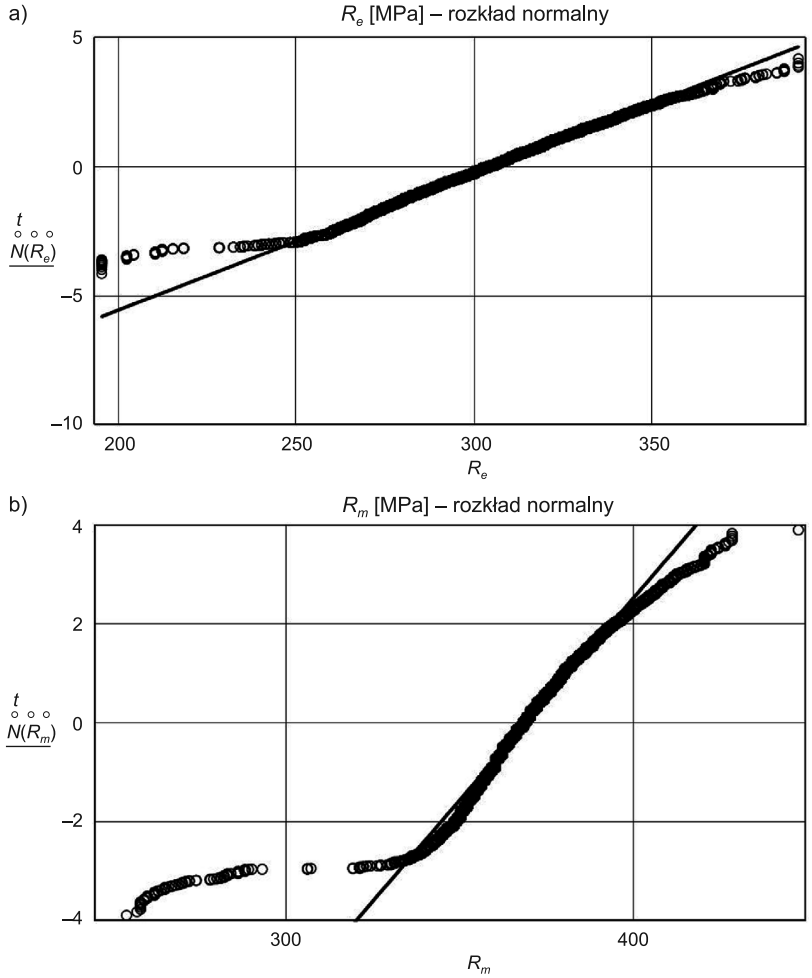

Fig. 1. Statistical test for the DX51D steel (years 2005–2010) on the normal probability grid for: a) yield strength R_e, b) ultimate tensile strength R_m

The results obtained for the ultimate tensile strength R_m (c.f. Fig. 1b) imply a possibility of using linear approximation only for results concentrated around the central values. The assumption of normality of distribution of ultimate tensile strength R_m is therefore satisfied in approximation. Figure 2 depicts sets of implementation on the plane $R_e - R_m$, and linear regression lines for the DX51D grade steel. The values of the correlation coefficients have been included in table 4, column (9). In the case of the DX51D steel of the largest number of data, for the joint test of years 2005 to 2010, a moderate [7] dependence of the correlation $\rho = 0{,}498 \in < 0{,}4;0{,}6)$ was obtained.

Table 4 summarizes the detailed statistical research results both for the annual tests, and for the joint tests of years 2005–2010. Columns (3), (6) and (10) of the table include:

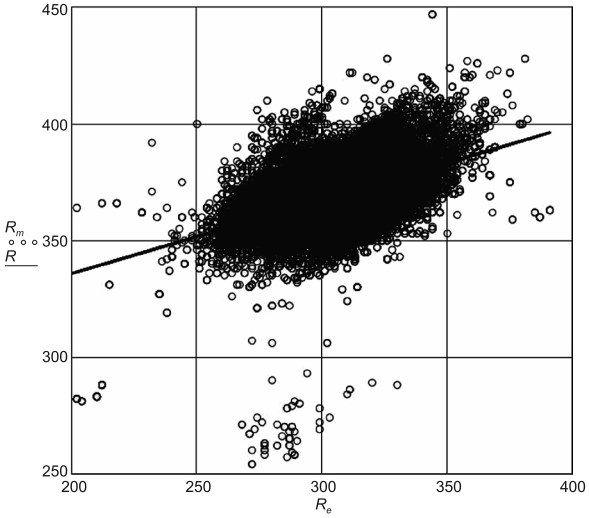

Fig. 2. Linear regression between yield strength R_e and ultimate tensile strength R_m for the DX51D grade steel

Table 4

The results of statistical research of mechanical properties of the following steel grades: DX51D, DX52D and DX53D

Year	Number of results n	$\bar{R}_e$ MPa	μ_{Re} MPa	v_{Re}	$\bar{R}_m$ MPa	μ_{Rm} MPa	v_{Rm}	ρ	$\bar{A}$ %	v_A
(1)	(2)	(3)	(4)	(5)	(6)	(7)	(8)	(9)	(10)	(11)
2005	75	315.92	18.07	0.057	372.27	13.82	0.037	0.783	32.04	0.053
2006	35	307.11	11.91	0.039	368.43	10.71	0.029	0.744	32.17	0.063
2007	6534	314.41	15.25	0.048	368.44	11.12	0.030	0.516	31.33	0.068
2008	12127	316.22	16.62	0.053	367.97	11.12	0.030	0.595	31.98	0.069
2009	27326	299.19	18.28	0.061	367.44	12.07	0.033	0.499	31.02	0.100
2010	18100	300.02	16.56	0.055	371.66	11.89	0.032	0.657	31.39	0.102
DX51D –2005–10										
2005–10	64197	304.21	18.69	0.061	368.84	11.89	0.032	0.498	31.34	0.093
DX52D										
2007–10	156	299.23	13.97	0.047	366.10	9.93	0.027	0.254	31.97	0.087
DX53D										
2007–9	39	248.97	21.62	0.087	336.44	25.49	0.076	0.958	33.64	0.151

mean values $\bar{R}_e$, $\bar{R}_m$ and $\bar{A}$ – respectively for random yield strength $\underline{R}_e$, random ultimate tensile strength $\underline{R}_m$ and random elongation of the tested sample $\underline{A}$ – calculated according to the formula (3). Columns (5), (8) and (11) represent the values of the coefficient of variation determined according to formula (2). Columns (4) and (7) contain the values of standard deviation obtained from formula (4) ($\mu = s$).

3. Characteristic and design values

The next stage of the analysis was to determine the characteristic and design values of the strength properties of the analysed grades of steel. The columns (5) and (10) of Table 5 compare the characteristic values calculated according to formula (1), as the lower 5% quantiles of the normal distribution (assuming the conversion coefficient $\eta_d = 1{,}0$, as in the work in [6]). On the other hand, the columns (6) and (11) contain design values of yield strength R_e and ultimate tensile strength R_m, calculated as 0.1% lower quantiles of a normal distribution.

Table 5

Characteristic and design values of R_e and R_m

No. Year	Number of results n	R_e MPa	v_{Re}	$\boldsymbol{R_{e,k}}$ MPa	$\boldsymbol{R_{e,d}}$ MPa	γ_{m0}	R_m MPa	v_{Rm}	$\boldsymbol{R_{m,k}}$ MPa	$\boldsymbol{R_{m,d}}$ MPa	γ_{m2}
(1)	(2)	(3)	(4)	(6)	(6)	(7)	(8)	(9)	(10)	(11)	(12)
DX51											
2005–10	64197	304.21	0.061	**273.78**	**247.80**	**1.10**	368.84	0.032	**349.48**	**332.96**	**1.05**
DX52											
2007–10	156	299.23	0.047	**276.16**	**256.48**	**1.08**	366.10	0.027	**349.90**	**336.05**	**1.04**
DX53											
2007–9	39	248.97	0.087	**213.45**	**183.12**	**1.16**	336.44	0.076	**294.51**	**258.71**	**1.13**

According to the interpretation presented in standard EN 1990 [1] and the work in [6], a partial safety factor $\gamma_M = \gamma_m \gamma_R$ is a product of the coefficient γ_m describing the uncertainty in assessing material properties, and the coefficient γ_R describing the uncertainty of the adopted model in structural resistance. Comparing formulas (1) and (9), and assuming k_n and $k_{d,n}$ according to the sample size (c.f. Tables 2 and 3), the value of the coefficient γ_m can be calculated from the formula (11):

$$\gamma_m = \frac{1 - 1.64 v_x}{1 - 3.04 v_x} \tag{11}$$

Values of the coefficient γ_m, for the different grades of steel have been summarized in columns (7) and (12) of Table 5 for yield strength R_e and ultimate tensile strength R_m,

respectively. Values of the partial safety factor for the cross-section resistance γ_{M0} have been calculated by multiplying the value of the coefficient γ_{m0} (determined from the tests) by $\gamma_R = 1.0$.

Estimates of the coefficient γ_R value, describing the uncertainty of the model of the cross-section resistance have been obtained making use of the results of similar studies carried out for the thin sheets manufactured according to the standard EN 10346 [4]. For the S280GD and S320GD grades of steel the values of $\gamma_R = \gamma_{M0} / \gamma_{m0} \cong 1.0$ were obtained. Thus, for DX-type sheets, the value of the partial factor is $\gamma_{M0} = 1.0 \cdot \gamma_{m0}$. In the case of partial resistance factor γ_{M2} of the net section at fastener holes, the values of model uncertainty factor in structural resistance are not known to the author. A similar problem is mentioned by the authors of the work in [6].

Starting from the values of the coefficient $\gamma_{M2} = 1.25$ specified in standard EN 1993-1-3 [3], estimation of the model uncertainty in structural resistance coefficient for net sections at fastener holes can be calculated as interval $\gamma_R = 1.25/(1.04 – 1.13) = 1.11 – 1.20$.

4. Conclusions

The statistical data collected by the author allowed for the determination of the characteristic and design values of the strength properties and the values of partial factors for the DX51D, DX52D, DX53D sheets manufactured according to standard EN 10346 [4]. In the case of the Polish steel products, the obtained results allow to adopt for the calculations the significantly higher strength parameters than those specified in the design standard EN 1993-1-3 [3].

References

[1] PN-EN 1990:2004. Eurokod. Podstawy projektowania konstrukcji.

[2] PN-EN 1993-1-1:2005. Eurokod 3. Projektowanie konstrukcji stalowych. Część 1.1: Reguły ogólne i reguły dla budynków.

[3] PN-EN 1993-1-3:2008. Eurokod 3. Projektowanie konstrukcji stalowych. Część 1.3: Regóły ogólne – Reguły uzupełniające dla konstrukcji z kształtowników i blach profilowanych na zimno.

[4] PN-EN 10346:2011. Wyroby płaskie stalowe powlekane ogniowo w sposób ciągły – Warunki techniczne dostawy.

[5] Gwóźdź M., Żwirek P., *Weryfikacja statystyczne współczynników częściowych nośności blach cienkich*, Inżynieria i Budownictwo 9/2011, 492-495.

[6] Mendera Z., Suchodoła M., *Częściowe współczynniki bezpieczeństwa w projektowaniu konstrukcji stalowych według eurokodów*, Inżynieria i Budownictwo 12/2013, 667-671.

[7] Sobczyk M., *Statystyka. Aspekty praktyczne i teoretyczne*, Wydawnictwo UMCS, Lublin 2006.

[8] Technical Approval ITB AT-15-3429/2011, Stalowe blachy profilowane Mauka, Bromo, ACP-, AC-, TR-, V-, TR35, TR40, TS40, TR50, TR60, TR70, TR84, TR94, TR150, TR160, LT40, LT70, EP-, Hacierba-, Haciero-, Frequence-, Floline-, Softline-, Hairbable-, Pampa-, Cofrasol-, PMA-, opracowana dla ArcelorMittal Construction.

[9] Technical Approval ITB AT-15-8519/2010, Ścienne płyty warstwowe PWS-WA Pruszyński z rdzeniem z wełny mineralnej w okładzinach z blachy stalowej pełnej i perforowanej dla firmy Pruszyński Spółka z o.o.

CONTENTS

TREŚĆ